

Государственное образовательное учреждение
высшего профессионального образования
**«Томский государственный университет
систем управления и радиоэлектроники»**

ТЕМАТИЧЕСКИЙ РЕФЕРАТИВНЫЙ СБОРНИК № 45-1

**“СВЧ диагностика”
(«Microwave Diagnostics»)**

Журнальные публикации

Источник: *Digital Library IEEEExplore*

Язык: *английский*

Глубина поиска: *2001 – 2011 гг.*

Дата формирования: *март 2011 г.*

Составитель: *В.И. Карнышев*

Томск – 2011

ТЕМАТИЧЕСКИЙ РЕФЕРАТИВНЫЙ СБОРНИК № 45-1

"Microwave Diagnostics" («СВЧ диагностика»)

Журнальные публикации

"Broadband Reflectometry for Diagnostics and Monitoring Applications"

Reflectometry is a powerful technique that can be effectively employed for a number of practical applications; in particular, the high versatility, the real-time response, and the potential for practical implementation have contributed to the success of microwave reflectometry for monitoring purposes. In this regard, this paper provides a survey of the current state of the art of reflectometry-based methods for diagnostics and monitoring applications. After a brief overview of the theoretical principles at the base of this technique, the different approaches of microwave reflectometry (time domain, frequency domain, and combined approaches) are fully discussed; particular attention is given to the strategies for enhancing measurement accuracy. Finally, the major practical applications of reflectometry and related results are discussed, thus evidencing current achievements, limitations, and potential. [J1]

"Quantitative Microplasma Electron Number Density Measurement by Coherent Microwave Rayleigh Scattering"

In this paper, a method for quantitative measurement of electron number density in a microplasma by coherent microwave Rayleigh scattering is described. Coherent microwave Rayleigh scattering reaches its maximum when the microwave frequency is at its resonance frequency. The resonance frequency depends on the electron number density in the microplasma and the electron-neutral and Coulomb collisional frequencies. When a subnanosecond microwave pulse illuminates the microplasma, the average electron number density can be measured from the frequency analysis of microwave scattering. The technique will be able to quantitatively measure subnanosecond-resolved electron number density evolution in the microplasma. [J2]

"Microwave N₂-Ar plasma torch. II. Experiment and comparison with theory"

Spatially resolved emission spectroscopy techniques have been used to determine the gas temperature, the electron, and N₂⁺ ion densities and the relative emission intensities of radiative species in a microwave (2.45 GHz) plasma torch driven by a surface wave. The experimental results have been analyzed in terms of a two-dimensional theoretical model based on a self-consistent treatment of particles kinetics, gas dynamics, and wave electrodynamics. The measured spatial variations in the various quantities agree well with the model predictions. The radially averaged gas temperature is around 3000 K and varies only slowly along the discharge zone of the source but it drops sharply down to about 400 K in the postdischarge. The experimental wave dispersion characteristics nearly follow the theoretical ones, thus confirming that this plasma source is driven by a surface wave. [J3]

"Registration of Alfvén resonances in TCABR tokamak by the scanning reflectometer at sideband frequencies"

A frequency scanning O-mode reflectometer was used for studies of plasma density oscillations during local Alfvén wave (LAW) excitation in the Tokamak Chauffage Alfvén Brésilien (TCABR) at the frequency $f_A = 5$ MHz. It was found that the spectrum of the reflectometer output signal, which consists mainly of the "beat" frequency f_B , is modified by the LAW excitation, and two additional frequency peaks appear, which are symmetrical in relation to the LAW excitation frequency $f = f_A \pm f_B$. This result opens the possibility to improve the efficiency of studying the LAW induced density oscillations. The symmetry of these frequency peaks yields the possibility of finding the microwave frequency at which the reflectometer cutoff layer coincides with radial position of the LAW resonance zone in the TCABR tokamak. [J4]

"Determination of OH Radicals in an Atmospheric Pressure Helium Microwave Plasma Jet"

A recent study has reported the observation of the OH radicals in the far downstream of an atmospheric argon microwave plasma jet. The far downstream is referred to as the location where the ratio of the distance from the

jet orifice to the length of the jet column is greater than three. In this paper, we report that this phenomenon also exists in a similar plasma jet that is 2.5 mm long, operated in helium gas. A detailed characterization of the helium microwave plasma jet was carried out by using UV-pulsed cavity ringdown spectroscopy and optical emission spectroscopy. The absolute number densities of the OH radicals were measured along the plasma jet column from the jet orifice to the far downstream, and the OH concentrations vary from 9.64×10^{15} near the jet orifice to 7.32×10^{12} molecules/cm³ in the far downstream (16 mm away from the jet orifice, corresponding to a distance ratio of 6.4). The dependence of the OH concentration on plasma power and gas flow rate at different locations along the jet axis is characterized, and the result suggests that the OH concentration increases with an increase in plasma power and gas flow rate in the downstream. [J5]

"Temporary-resolved measurement of electron density in small atmospheric plasmas"

A new method for temporally resolved measurements of absolute values of plasma density applicable for wide spectrum of small-size atmospheric plasmas and utilizing Rayleigh microwave scattering on the tested plasma object is proposed. The absolute electron density measurements in an atmospheric plasma jet revealed presence of two consecutive breakdowns during the half-wave of the discharge-driven high voltage. The ionization mechanisms of both breakdowns are considered. [J6]

"Approach to Spectral Measurements of a Millimeter-Wave-Band Relativistic Magnetron"

Rigorous 3-D finite-difference time-domain computer simulations are used to investigate the electromagnetic characteristics of the diffraction output of a millimeter (mm)-wave-band relativistic magnetron. In the simulations, the diffraction output is outfitted with a dielectric grating that can be tuned in either reflection or transmission mode at definite operation wavelengths. This grating acts as a tunable filter of high-power oscillations generated by the magnetron and is similar to gratings widely used in optics to control ultrashort power optical pulses. Specifically, computer simulations establish a relation between the generation wavelength of the magnetron and the configuration of the grating, as well as predict that the grating provides the field reduction of up to -40 dB. The application of the grating suggests an approach to spectral measurements of mm-wave-band relativistic magnetrons with a measurement accuracy of better than 0.3 mm. The implementation of the approach solves a series of engineering and metrological problems arising during spectral measurements of a variety of high-power vacuum microwave devices. [J7]

"Quasi-Multistatic MIST Beamforming for the Early Detection of Breast Cancer"

Microwave imaging via space-time (MIST) beamforming has been shown to be one of the most promising imaging modalities for detecting small malignant breast tumors. This paper outlines two modifications to the MIST system developed by Hagness for the early detection of breast cancer, resulting in a quasi-multistatic MIST beamformer (multi-MIST). Multistatic MIST beamforming involves illuminating the breast with an ultrawideband (UWB) signal from one antenna while collecting the reflections at an array of antennas, as opposed to traditional monostatic MIST beamforming where only the transmitting antenna records the reflections from the breast. In order to process the multistatic data, traditional data-adaptive artifact removal algorithms have to be modified to accommodate signals from all antennas. Also, the MIST beamforming algorithm, which spatially focuses the signal and compensates for frequency-dependent propagation effects, has to be modified. The algorithms are tested on a 2-D anatomically accurate finite-difference time-domain model of the breast. The multi-MIST beamformer described here is shown to offer an improved signal to clutter ratio when compared to the traditional monostatic MIST beamformer. [J8]

"fewUpconversion of a relativistic Coulomb field terahertz pulse to the near infrared"

We demonstrate the spectral upconversion of a unipolar subpicosecond terahertz (THz) pulse, where the THz pulse is the Coulomb field of a single relativistic electron bunch. The upconversion to the optical allows remotely located detection of long wavelength and nonpropagating components of the THz spectrum, as required for ultrafast electron bunch diagnostics. The upconversion of quasimonochromatic THz radiation has also been demonstrated, allowing the observation of distinct sum- and difference-frequency mixing components in the spectrum. Polarization dependence of first and second order sidebands at $\omega_{\text{opt}} \pm \omega_{\text{THz}}$, and $\omega_{\text{opt}} \pm 2\omega_{\text{THz}}$, respectively, confirms the chi (2) frequency mixing mechanism. [J9]

"Surface loss rates of H and Cl radicals in an inductively coupled plasma etcher derived from time-resolved electron density and optical emission measurements"

A study is undertaken of the loss kinetics of H and Cl atoms in an inductively coupled plasma (ICP) reactor used for the etching of III-V semiconductor materials. A time-resolved optical emission spectroscopy technique, also referred to as pulsed induced fluorescence (PIF), has been combined with time-resolved microwave hairpin

probe measurements of the electron density in a pulsed Cl₂/H₂-based discharge for this purpose. The surface loss rate of H, kwH, was measured in H₂plasma and was found to lie in the 125-500s⁻¹ range (gamma H surface recombination coefficient of 0.006-0.023), depending on the reactor walls conditioning. The PIF technique was then evaluated for the derivation of kwCl, and gamma Cl in Cl₂-based plasmas. In contrast to H₂plasma, significant variations in the electron density may occur over the millisecond time scale corresponding to Cl₂dissociation at the rising edge of the plasma pulse. By comparing the temporal evolution of the electron density and the Ar-line intensity curves with 10% of Ar added in the discharge, the authors show that a time-resolved actinometry procedure using Ar as an actinometer is valid at low to moderate ICP powers to estimate the Cl loss rate. They measured a Cl loss rate of 125-200s⁻¹ (0.03 ≤ gamma Cl ≤ 0.06) at 150 W ICP power for a reactor state close to etching conditions. The Cl surface loss rate was also estimated for high ICP power (800 W) following the same procedure, giving a value of 130-150s⁻¹ (gamma Cl 0.04), which is close to that measured at 150 W ICP power. [J10]

"Time-Frequency Analysis of Virtual-Cathode Oscillator"

Time-frequency analysis has been carried out for microwave radiation from a virtual-cathode oscillator. The objective is to observe and understand the frequency behavior of virtual-cathode oscillation. The diagnostic results have given clear evidence of mode hopping and frequency shifting. The dependence of mode competition on diode operation parameters is also identified. Initial particle-in-cell simulations using "MAGIC" code have been carried out, and the results were in general agreement with those obtained in the experiments. [J11]

"Measurement of radial and axial high energy x-ray spectra in electron cyclotron resonance ion source plasmas"

Radial and axial x-ray measurements of electron cyclotron resonance ion sources operating at microwave frequencies of 6.4 and 14 GHz are presented. Results indicate a greater detected photon energy in the radial direction than the axial direction for both the 6.4 GHz source and the 14 GHz source. It is also seen that the 14 GHz source produces x-rays with higher energies, when compared to the 6.4 GHz source, in both radial and axial directions. [J12]

"Multiple diagnostics in a high-pressure hydrogen microwave plasma torch"

We present an experimental study of a hydrogen plasma produced by a microwave axial injection torch, launching the plasma in a helium-filled chamber. Three different diagnostic methods have been used to obtain the electron density and temperature as follows: The Stark intersection method of Balmer spectral lines (already tested in argon and helium plasmas); the modified Boltzmann-plot showing that the plasma is far from the local thermodynamic equilibrium but ruled by the excitation-saturation balance; and a study by the disturbed bilateral relations theory. All of these diagnostic techniques show a good agreement. [J13]

"Toward Carbon-Nanotube-Based Theranostic Agents for Microwave Detection and Treatment of Breast Cancer: Enhanced Dielectric and Heating Response of Tissue-Mimicking Materials"

The experimental results reported in this paper suggest that single-walled carbon nanotubes (SWCNTs) have the potential to enhance dielectric contrast between malignant and normal tissue for microwave detection of breast cancer and facilitate selective heating of malignant tissue for microwave hyperthermia treatment of breast cancer. In this study, we constructed tissue-mimicking materials with varying concentrations of SWCNTs and characterized their dielectric properties and heating response. At SWCNT concentrations of less than 0.5% by weight, we observed significant increases in the relative permittivity and effective conductivity. In microwave heating experiments, we observed significantly greater temperature increases in mixtures containing SWCNTs. These temperature increases scaled linearly with the effective conductivity of the mixtures. This work is a first step towards the development of functionalized, tumor-targeting SWCNTs as theranostic (integrated therapeutic and diagnostic) agents for microwave breast cancer detection and treatment. [J14]

"Time-resolved imaging of millimeter waves using visible continuum from the positive column of a Cs-Xe dc discharge"

We present a high-sensitivity technique for time-resolved imaging of millimeter waves (MMWs) using the visible continuum (VC) from the positive column (PC) of a medium-pressure Cs-Xe dc discharge. For the MMW imaging application, a uniform plasma slab of the PC of a Cs-Xe discharge with 10.48 cm² aperture and 2 cm in thickness was generated for 45 Torr xenon. The imaging technique is based on the fact that the intensity of the e-Xe bremsstrahlung continuum from the PC increases in the visible region when the electrons in the plasma are heated by MMWs. It is shown that in the MMW intensity range from zero to the threshold of the microwave-

induced plasma breakdown, the intensity of the VC from the PC of a Cs-Xe discharge increases approximately as a second-order polynomial function of the MMW intensity. The obtained experimental data agree well with our calculations of the dependence of the VC intensity on electron temperature. The Ka-band MMW field patterns at the output of conical horn antennas and in the quasioptical beam were imaged using the discharge technique. It is shown that the technique can be used for time-resolved measurement of the profiles of watt- and subwatt-level MMWs. An energy flux sensitivity of the technique of about $10 \mu\text{J}/\text{cm}^2$ in the Ka-band was demonstrated. The temporal resolution of the technique is about $0.8 \mu\text{s}$. Our modeling of the transient behavior of the electron temperature in the PC shows that the time history of the electron temperature variation coincides well with the measured time history of the VC intensity variation. [J15]

"A Phenomenological Investigation of Anomalous Performance in Flex Coaxial Cables"

In this study, we investigate anomalous flex cable performance in a phased-array antenna on advanced EHF. A number of low-gain IF paths were found in one local-oscillator region during thermal cycle testing, subsequently causing an out-of-specification condition. Utilizing advanced diagnostic tools, the contractor determined that the root cause of the gain drop was a failure in a flex coaxial cable. We outline the development of an analytical phenomenology model employed in understanding the failure pathology and verifying the root cause. We have developed 3-D finite-element models using Ansoft High Frequency Structure Simulator (HFSS) that mimic the insertion loss behavior associated with cable failure modes. To synthesize a particular loss characteristic, we use an equivalent circuit model consisting of parallel LC sections. A closed-form analytical expression for resonance frequency was derived, linking the circuit and physical parameters; linear regression is used to fit measured data to the HFSS cable model. Using the phenomenology model, we determined that the root cause of the failures is a delamination of the layered outer sheath of the cable. Two mechanisms were discovered: 1) spurs in the outer layer and 2) complete layer separation over short cable lengths. The first mechanism induces a small frequency-independent increase in the loss and is inversely proportional to the spur delamination angle. This loss is attributable to conventional aging and considered benign. With the second mechanism, the delamination gap induces a sharp resonance in the loss at a discrete frequency and is reminiscent of a low-order filter. This phenomenon is a malignant loss responsible for our anomalous out-of-specification condition. We completed a parametric study using the phenomenology model, and determined that: 1) resonance frequency is inversely proportional to the gap width (W_g); 2) resonance frequency is proportional to the square root of the gap size ($\sqrt{A_g}$); 3) insertion loss amplitude is proportional to the air gap size and width; and 4) the Q of a given delamination region is proportional to the square root of the gap size. [J16]

"Multifrequency channel microwave reflectometer with frequency hopping operation for density fluctuation measurements in Large Helical Device"

In order to measure the internal structure of density fluctuations using a microwave reflectometer, the broadband frequency tunable system, which has the ability of fast and stable hopping operation, has been improved in the Large Helical Device. Simultaneous multipoint measurement is the key issue of this development. For accurate phase measurement, the system utilizes a single sideband modulation technique. Currently, a dual channel heterodyne frequency hopping reflectometer system has been constructed and applied to the Alfvén eigenmode measurements. [J17]

"Characteristics of Microwave Plasma Torch at Atmospheric Pressure"

We studied the characteristics of a microwave argon plasma torch at atmospheric pressure. The electron temperature of the plasma was measured by optical-emission spectroscopy and increases nonlinearly from 3000 to 3800 K with the increase of the microwave power from 1.0 to 4.0 kW. The spatial distribution of the electron density was measured with a Mach-Zehnder interferometer to be on the order of $10^{17}/\text{cm}^3$ and characterized by fluctuating with the time under the same experimental conditions. Based on the plasma parameters measured, it can be concluded that the plasma is in the state of local thermodynamic equilibrium. [J18]

"A synthetic diagnostic for the evaluation of new microwave imaging reflectometry diagnostics for DIII-D and KSTAR"

The first microwave imaging reflectometry (MIR) system for characterization of fluctuating plasma density has been implemented for the TEXTOR tokamak [H. Park et al, Rev. Sci. Instrum. 75, 3787 (2004)]; an improved MIR system will be installed on DIII-D and KSTAR. The central issue remains in preserving phase information by addressing antenna coupling between the reflection layer and the detector array in the presence of plasma turbulence. A synthetic diagnostic making use of coupled full-wave diffractive codes has been developed in geometries and applied to a variety of optical arrangements. The effectiveness of each scheme is quantitatively compared with respect to the fluctuation levels accessible in the simulation. [J19]

"Wireless Implants"

In vivo wireless biomedical microsystems fueled by the continued scaling of electronic components and the development of new micro sensors and micropackaging technologies is rapidly changing the landscape of the electronics and medical industry. These devices can be used for a myriad of monitoring, diagnostic, therapeutic, and interventional applications that range from the well known cardiac pacemakers and defibrillators to emerging applications in visual prosthesis, brain computer interfaces (BCIs), and embedded monitoring of a variety of medical useful variables such as oxygen, glucose, pH level, pressure, and core temperature. This article presents a brief overview of design considerations for implementing wireless power and data interfaces for in vivo biomedical devices. Examples of emerging implantable and ingestible wireless biomedical devices are discussed. [J20]

"On the role of spectral resolution in velocity shear layer measurements by Doppler reflectometry"

The signal quality of a Doppler reflectometer depends strongly on its spectral resolution, which is influenced by the microwave beam properties and the radius of curvature of the cutoff layer in the plasma. If measured close to a strong perpendicular velocity shear layer, the spectrum of the backscattered signal is influenced by different velocities. This can give rise to two Doppler shifted peaks in the spectrum as observed in TJ-II H-mode plasmas. It is shown by two-dimensional full wave simulations that the two peaks are separable provided the spectral resolution of the system is sufficient. However, if the spectral resolution is poor, the two peaks blend into one and yield an intermediate and incorrect velocity. [J21]

"Development of laser induced fluorescence diagnostic for measuring the parameters of plasma containing rare gas species"

Laser induced fluorescence (LIF) technique development activity for measurement of plasma parameters in ITER divertor plasma is described. Helium density is the task of priority, but Doppler measurement of ion (atom) temperatures is also the aim of the program. The concept of ITER scenarios includes injection of "extrinsic" impurities (Ne, Ar, and Kr). It is possible to use the species as tracing elements for measurement of Ti, Ta. The program included modeling experiments on PNX-U (a multicusp trap with microwave argon plasma). Helium was added by puffing into discharge. Temperatures Ti(Ar1+) and Ta(He0) have been measured by scanning laser line across absorption line of species. Summarizing of fluorescence signals provided input data for estimation of Ar1+ and He0 densities via interpretative collisional-radiative models. Besides, the collisional-radiative model has been used for estimation of electron density using the ratio of fluorescence signals at 388.9 and 706.5 nm helium lines. [J22]

"Argon Microplasma Diagnostics by Diode Laser Absorption"

The densities of argon excited states (1s3, 1s4, and 1s5) and the gas temperature of argon microplasma were measured by diode laser absorption. A 900-MHz microstrip split-ring resonator was used to excite the argon microplasma with gas pressures between 1 and 760 torr. The line-integrated excited-state densities and gas temperature of these states were estimated by the integrated absorption and broadening of the measured lineshapes, respectively. The excited-state densities were found to be minimum around 50 torr and increased with either decreasing or increasing pressure. The gas temperature increases from 300 K to 900 K as pressure increases from 1 to 760 torr. [J23]

"Using a priori Information for Regularization in Breast Microwave Image Reconstruction"

Regularization methods are used in microwave image reconstruction problems, which are ill-posed. Traditional regularization methods are usually problem-independent and do not take advantage of a priori information specific to any particular imaging application. In this paper, a novel problem-dependent regularization approach is introduced for the application of breast imaging. A real genetic algorithm (RGA) minimizes a cost function that is the error between the recorded and the simulated data. At each iteration of the RGA, a priori information about the shape of the breast profiles is used by a neural network classifier to reject the solutions that cannot be a map of the dielectric properties of a breast profile. The algorithm was tested against four realistic numerical breast phantoms including a mostly fatty, a scattered fibroglandular, a heterogeneously dense, and a very dense sample. The tests were also repeated where a 4 mm \times 4 mm tumor was inserted in the fibroglandular tissue in each of the four breast types. The results show the effectiveness of the proposed approach, which to the best of our knowledge has the highest resolution amongst the evolutionary algorithms used for the inversion of realistic numerical breast phantoms. [J24]

"Simulations on the Role of the Resonance of the Probing Wave on Reflectometry Measurements"

in Fluctuating Plasmas"

In fusion plasmas for energy, turbulence is clearly associated to the anomalous transport of energy and particles. Diagnostics using electromagnetic waves is usually used to measure the plasma parameters and the turbulence characteristics. One of the diagnostics is reflectometry, which is based on the radar principle and can be used to reach these different goals: density profile, turbulence characterization, plasma positioning, etc. During the plasma probing, fast phase variations called phase jumps have been measured, and part of them can be explained by a local enhancement of the probing field. Using an analytical model to compute the probing electric field amplification, a new expression for the phase variations has been written, taking into account the amplification of the probing electric field. This formula exhibits a good agreement with the full-wave computations. A possible improvement of the reflectometer sensitivity can be done using the local enhancement of the probing electric field induced by Bragg resonant density perturbations, which build resonant cavities. The computed cases show that it is possible to improve the reflectometry measurements when the local enhancement of the probing electric field exists. To illustrate the possible improvements, simulations of the radial wavenumber spectrum reconstruction have been done, and they confirm the possibility to increase the sensitivity and the spatial resolution for a given range of wavenumber. [J25]

"Optimization studies of the ITER low field side reflectometer"

Microwave reflectometry will be used on ITER to measure the electron density profile, density fluctuations due to MHD/turbulence, edge localized mode (ELM) density transients, and as an L-H transition monitor. The ITER low field side reflectometer system will measure both core and edge quantities using multiple antenna arrays spanning frequency ranges of 15-155 GHz for the O-mode system and 55-220 GHz for the X-mode system. Optimization studies using the GENRAY ray-tracing code have been done for edge and core measurements. The reflectometer launchers will utilize the HE₁₁ mode launched from circular corrugated waveguide. The launched beams are assumed to be Gaussian with a beam waist diameter of 0.643 times the waveguide diameter. Optimum launcher size and placement are investigated by computing the antenna coupling between launchers, assuming the launched and received beams have a Gaussian beam pattern. [J26]

"Simultaneous projection and detection system of four different frequencies for microwave imaging reflectometry in Large Helical Device"

A simultaneous projection/detection system of four different frequencies for microwave imaging reflectometry (MIR) was developed for three-dimensional observation of electron density fluctuations in the Large Helical Device (LHD). The microwave with four frequency components at 60.410, 61.808, 63.008, and 64.610 GHz is projected in a continuous-wave mode to illuminate the target LHD plasma. A two-dimensional horn-antenna mixer array (2D HMA) receives the reflected wave from the plasma as well as the wave from the local oscillator operating at 55.800 GHz. The first intermediate frequency (IF) signals at 4.610, 6.008, 7.208, and 8.810 GHz were confirmed to be obtained by downconversion of these microwaves using the 2D HMA. Each of these first IF components is filtered from each other and downconverted again for the superheterodyne detection. It was confirmed that both the amplitudes and the phases of the detected signals reflect the fluctuations in LHD plasmas. [J27]

"A Ka-band tunable direct-conversion correlation reflectometer for NSTX"

The recent availability of broadband microwave quadrature mixers in the Ka-band (28-40 GHz) of frequencies has allowed the fabrication of low-cost direct-conversion detection circuits for use in the variable-frequency correlation reflectometer on the National Spherical Torus eXperiment (NSTX). The quadrature receiver in this case can be implemented as a simple homodyne circuit, without the complication of a single-sideband modulator or a feedforward tracking circuit present in more typical designs. A pair of direct-conversion receivers is coupled with broadband microwave voltage-controlled oscillators to construct a flexible dual-channel radar system with a fast frequency settling time of 160 μ s. A detailed description of the design and a full characterization of the hardware are provided. Examples of turbulence measurements from radial and poloidal correlation reflectometry on NSTX using a poloidal array of antennas (oriented normal to the magnetic flux surfaces for conventional reflectometry) are presented. [J28]

"Microwave imaging reflectometry studies for turbulence diagnostics on KSTAR"

The first prototype microwave imaging reflectometry (MIR) system [H. Park et al, Rev. Sci. Instrum. 74, 4239 (2004)] clearly demonstrated the shortcomings of conventional reflectometry when the probe beam encountered a large amplitude and/or high fluctuation wavenumber at the reflection layer in laboratory tests, the distinctive advantages shown in these tests were not fully realized in the plasma operation. To understand the discrepancies, the MIR system performance has been thoroughly investigated at POSTECH. In this paper, a

possible cause of the MIR performance degradation on TEXTOR will be presented together with a concept of multifrequency MIR system design that will be developed for KSTAR. [J29]

"Design criteria of the bolometer diagnostic for steady-state operation of the W7-X stellarator"

A bolometric diagnostic system with features necessary for steady-state operation in the superconducting stellarator W7-X was designed. During a pulse length of 1800 s with an ECRH (electron cyclotron resonance heating) power of 10 MW, the components suffer not only from a large thermal load but also from stray radiation of the nonabsorbed isotropic microwaves. This paper gives an overview of the technical problems encountered during the design work and the solutions to individual problems to meet the special requirements in W7-X, e.g., component thermal protection, detector offset thermal drift suppression, as well as a microwave shielding technique. [J30]

"A Tesla-pulse forming line-plasma opening switch pulsed power generator"

A pulsed power generator based on a high-voltage Tesla transformer which charges a 3.85Ω/55nswater-filled pulse forming line to 300 kV has been developed at Loughborough University as a training tool for pulsed power students. The generator uses all forms of insulation specific to pulsed power technology, liquid (oil and water), gas (SF₆), and magnetic insulation in vacuum, and a number of fast voltage and current sensors are implemented for diagnostic purposes. A miniature (centimeter-size) plasma opening switch has recently been coupled to the output of the pulse forming line, with the overall system comprising the first phase of a program aimed at the development of a novel repetitive, table-top generator capable of producing 15 GW pulses for high power microwave loads. Technical details of all the generator components and the main experimental results obtained during the program and demonstrations of their performance are presented in the paper, together with a description of the various diagnostic tools involved. In particular, it is shown that the miniature plasma opening switch is capable of reducing the rise time of the input current while significantly increasing the load power. Future plans are outlined in the conclusions. [J31]

"Development of electron cyclotron emission imaging system on Large Helical Device"

A combined system of microwave imaging reflectometry and electron cyclotron emission (ECE) imaging has been developed for the Large Helical Device. This system includes a wide-band two-dimensional horn-antenna mixer array (HMA). The HMA consists of horn antennas, waveguides, mixers, and intermediate frequency circuits. The frequency response of the HMA is between 50 and 110 GHz. The ECE signal is selected using a 95 GHz local oscillator and a 93 GHz high-pass filter. [J32]

"Comparative study between the reflective optics and lens based system for microwave imaging system on KSTAR"

Recently, two-dimensional microwave imaging diagnostics such as the electron cyclotron emission imaging (ECEI) system and microwave imaging reflectometry (MIR) have been developed to study magnetohydrodynamics instabilities and turbulence in magnetically confined plasmas. These imaging systems utilize large optics to collect passive emission or reflected radiation. The design of this optics can be classified into two different types: reflective or refractive optical systems. For instance, an ECEI/MIR system on the TEXTOR tokamak [Park et al, Rev. Sci. Instrum. 75, 3787 (2004)] employed the reflective optics which consisted of two large mirrors, while the TEXTOR ECEI upgrade [B. Tobias et al, Rev. Sci. Instrum. 80, 093502 (2009)] and systems on DIII-D, ASDEX-U, and KSTAR adopted refractive systems. Each system has advantages and disadvantages in the standing wave problem and optical aberrations. In this paper, a comparative study between the two optical systems has been performed in order to design a MIR system for KSTAR. [J33]

"Antenna development for high field plasma imaging"

Electron cyclotron emission imaging (ECEI) and microwave imaging reflectometry (MIR) are two microwave nonperturbing plasma visualization techniques that employ millimeter-wave imaging arrays with lens-coupled planar antennas, yielding time-resolved images of temperature (via ECEI) and electron density (via MIR) fluctuations within high temperature magnetic fusion plasmas. A series of new planar antennas have been developed that extend this technology to frequencies as high as 220 GHz for use on high field plasma devices with toroidal fields in excess of 3 T. Antenna designs are presented together with theoretical calculations, simulations, and experimental measurements. [J34]

"Microwave air plasma source at atmospheric pressure: Experiment and theory"

An experimental and theoretical investigation of the axial structure of a surface wave (2.45 GHz) driven

atmospheric plasma source in air with a small admixture (1%) of water vapor has been performed. Measurements of the gas temperature and of the intensities of the O(777.4 nm), O(844.6 nm), and O(630 nm) atomic lines and the NO(γ) molecular band versus input power and axial position were carried out. Amplitude and phase sensitive measurements have also been performed to derive the surface wave dispersion characteristics. The experimental results are analyzed in terms of a one-dimensional theoretical model based on a self-consistent treatment of particle kinetics, gas dynamics, and wave electrodynamics. The predicted gas temperature and emission line intensities variations with power and axial position are shown to compare well with experiment. "Hot" excited O atoms (with kinetic energy 2eV) have been detected. [J35]

"Strain Imaging of the Breast by Compression Microwave Imaging"

A method that uses microwave pulses to achieve strain imaging of the breast is presented. In the proposed method, the breast is inserted in an enclosure that defines the boundary conditions for the breast deformation under the influence of external pressure. The upper plate of the enclosure, which also includes an antenna array, is attached to a compression tool, whereas the lower and the front plates are fixed. The breast is allowed to extend in the lateral direction when pressed by the top plate. Each of the antennas at the top plate is used to send an ultrawideband pulse to penetrate the breast and measure the backscattered pulse. Two sets of measurements are taken: one pre- and another post-compression of the breast. A sliding window of cross correlation is then performed on the two sets of data to establish the time delay of each segment of the scattered pulse due to compression. That time delay is then employed to get a three-dimensional strain image of the breast. As lesion tissue is typically much stiffer than normal breast tissue, then regions of low or zero strain indicate areas in need of further diagnostic checks. Full-wave simulations are used to validate the presented imaging method. [J36]

"Report on MSMW'2010 and TERATECH'2010"

The International Kharkov Symposium on Physics and Engineering of Microwaves, Millimeter, and Sub-Millimeter Waves (MSMW) is now a well-known event, which is conducted regularly once every three years. This Symposium has a long history. In fact, the MSMW Symposium grew from a series of conferences on millimeter and sub-millimeter waves that were held from time to time in the USSR since 1974 in the Russian language. These conferences played an important role for research and development in these wavelength ranges. At that time, they were the only widely available forum that was attended by the leading scientists and engineers of the involved organizations from all over the USSR. It must be admitted that then, mm-wave research and development was considered a sensitive defense-related area, and the conferences were usually supervised by defense or double-purpose ministries of the USSR. A number of mm-wave radar, propagation, and communication projects were performed for the military. Sub-mm research and development was in fact concentrated around development of multi-channel interferometers-polarimeters, particularly for hot-plasma diagnostics in Tokamak nuclearfusion machines. [J37]

"New frequency translation technique for FM-CW reflectometry"

In broadband microwave reflectometry, coherent detection is widely used to obtain the phase information and to improve the systems sensitivity, both in diagnostics measuring the electronic density profile and plasma fluctuations. Coherent detection uses a translated version of the probing signal to guarantee a stable intermediate frequency. Here, a novel technique to generate the frequency translation by double frequency conversion is presented and its advantages over the commonly used single frequency conversion techniques employing image rejection mixers are discussed. The results obtained with the new frequency translator modules developed for the three JET FM-CW reflectometers, operating successfully at JET since mid-2009, are presented. [J38]

"Correlation reflectometry at TEXTOR"

In high temperature fusion plasmas the transport of energy and particles is commonly believed to be driven by turbulence. Turbulence quantities as correlation length and decorrelation time are important for the confinement properties of a plasma. Besides other diagnostics, correlation reflectometry has proven to be a suitable tool for the measurement of turbulence properties. At the medium sized Toroidal EXperiment for Technical Oriented Research (TEXTOR) the existing correlation reflectometry has been recently upgraded. A new reflectometer based on a microwave synthesizer has been developed and installed for the investigation of turbulence properties in a fusion plasma. Together with the existing reflectometer the measurement of radial correlation length and decorrelation time becomes available. Both reflectometers are computer controlled and allow to program individual frequency sequences and the duration of each frequency step. With the existing poloidal antenna array at $\theta = 0^\circ$ and on top of the vacuum vessel, the system allows the measurement of radial

correlation and poloidal correlations at the same time. First experiments have been performed and the results on the radial correlation length of density fluctuations in a fusion plasma are presented. [J39]

"Electrical double layers at shock fronts in glow discharges and afterglows"

This paper examines the propagation of spark-generated shockwaves ($1.0 < \text{Mach} < 2.0$) into argon and nitrogen glow discharges and their afterglow. Diagnostic methods were employed and expanded in order to capture the dynamics of the shock front in these weakly-ionized, nonmagnetized, collisional plasmas. We used a microwave hairpin resonator to measure the electron number density, and, for all cases, we measured an increase in the electron number density at the shock front. By comparing the increase in electron number density at the shock front in the active discharge and in the afterglow, we conclude that electrons with a temperature much greater than room temperature can be compressed at the shock front. The ratio of electron number density before and after the shock front can be approximately predicted using the Rankine-Hugoniot relationship. The large gradient in electron density, and hence a large gradient in the flux of charged species, created a region of space-charge separation, i.e., a double layer, at the shock front. The double layer balances the flux of charged particles on both sides of the shock front. The double layer voltage drop was measured in the current-carrying discharge using floating probes and compared with previous models. As well, we measured argon 1s5 metastable-state density and demonstrate that metastable-state neutral species can be compressed across a shock front and approximately predicted using the Rankine-Hugoniot relationship. [J40]

"Diagnostics and modeling of CH₄-CO₂ plasmas for nanosmooth diamond deposition: Comparison to experimental data"

Microwave plasma-assisted chemical vapor deposition of very smooth diamond coatings is an important process for various applications including mechanical and micromechanical systems and acoustic wave devices. Nanosmooth coatings have been deposited from CH₄-CO₂ gas mixtures at moderate temperature, the order of 600 °C. In order to increase the knowledge of the process and the control of the final characteristics of the films, a modeling of these plasmas is necessary. This has been carried out here from the prior determination of the plasma parameters. Optical emission spectroscopy was used in order to determine the gas kinetic temperature. Microwave interferometry and Langmuir double probe were used to determine the electron density and the electron temperature, respectively. All these experimental data have been obtained for a wide range of external parameters, such as the inlet composition, the pressure, the gas flow rate, and the power injected in the plasma. Then modeling of CH₄-CO₂ plasmas was developed by coupling chemical kinetics with a two-dimensional description of hydrodynamics and a surface-wall recombination of main radicals. The kinetic description of the CH₄-CO₂ plasmas was done by combining a specific mechanism of dissociation by electrons to a slightly modified version of a combustion mechanism for neutral-neutral interactions. This model has been validated by comparing the calculated species concentrations and the experimental results obtained by molecular beam mass spectrometry as a function of various external parameters. The influence of the inlet composition at three microwave power densities has been especially emphasized here. The calculations are in good agreement with the experimental results. It is shown that among the various parameters that influence the diamond growth from CH₄-CO₂ plasmas, the power density injected in the plasma is very important as it changes strongly the degree of completion of the chemical system and then the deposition conditions. [J41]

"Spectroscopic Analysis of Microwave-Generated Plasmas"

Aiming at understanding and controlling the major mechanisms and processes in microwave-generated plasmas, the ground-state densities of the most relevant atomic species and their spatial distributions were determined in these plasmas. They can be measured by optical emission and absorption spectroscopy. Similar to the determination of the silicon ground-state density from the analysis of the self-absorbed spectral lines of the silicon ground-state multiplet 3p²3P-3p4s3P⁰ in the ultraviolet range at about 251 nm, the neutral concentrations of other species like carbon and titanium were evaluated from further spectroscopic analyses. Furthermore, the spatial distributions were explored in detail. New developments of microwave-generated plasma sources and their optical emission spectroscopy to investigate the kind of species in the plasmas, as well as the gas and excitation temperatures, are also presented. [J42]

"Short-Pulse High-Power Microwave Surface Flashover at 3 GHz"

High-power microwave (HPM)-induced surface flashover is investigated in order to gain a better understanding of this phenomenon and reduce the limitations it imposes on transmitted power levels. This paper builds on previous testing using a magnetron producing 5 MW for 4 μs at 2.85 GHz. Both the previous and current experimental setups are designed to produce a flashover on the high-pressure side of a transmission window without the influence of a triple point. The limitations of the previous experiment included a maximum power of 5

MW and a pulse rise time of 50 ns. The current HPM source is an experimental virtual cathode oscillator (vircator), the output of which has been extensively characterized. The vircator is capable of producing 50-MW peak for 100 ns with an adjustable frequency from 3 to 5 GHz and a rise time of < 4 ns. The dominant modes of the vircator and magnetron are the circular TE₁₁ and rectangular TE₁₀ modes, respectively, with the major electric field component in both setups normal to the direction of propagation, yielding comparable field geometries at the transmission window. The experimental setup permits the study of factors, including gas pressure, composition, temperature, and air speed. Diagnostic equipment allows the analysis of power levels and flashover luminosity with subnanosecond resolution. Additional experimental results, including a detailed analysis of the flashover delay times under various conditions, are compared with data from literature and previous testing. A trend of increasing delay time with pressure is clearly observable, and E_{eff}/p versus $p \cdot r$ data fall within what has been previously observed in literature primarily for HPM volume breakdown. [J43]

"Initiation and propagation of the negative leader in transformer oil under impulse voltage"

The complex experimental studies of the discharge mechanism in transformer oil under negative polarity (NP) of the lightning impulse were carried out using alternative diagnostic methods. Novel data concerning propagation mechanism and parameters of the predischage channels were obtained. The results indicate that oil breakdown both under negative and positive polarities are similar in a number of properties to the breakdown in the long air gaps. [J44]

"Measurement of the electron density in a microwave plasma torch at atmospheric pressure"

The electron density in a microwave plasma torch at atmospheric pressure was measured with a Mach-Zehnder interferometer. The electron density is on the order of $10^{17}/\text{cm}^3$, one order higher than that deduced from the Stark broadening of spectral lines, and increases with the increase in the microwave power. The spatial distribution of the electron density was obtained. The highest electron density locates at the symmetrical axis of the plasma torch and decreases radially. It was found that the electron density fluctuates within a range of 0.3 with the time under the same experimental conditions. [J45]

"Effects of Csl Coating of Carbon Fiber Cathodes on the Microwave Emission From a Triode Virtual Cathode Oscillator"

We discuss the effects of cesium iodide (Csl) coating of carbon fiber cathodes on the microwave emission from a triode virtual cathode oscillator. As compared with the uncoated cathode, the Csl-coated carbon fiber cathode significantly improved the diode performance and, most notably, lengthened the microwave pulse, from 150 to 200 ns. The light emission from the diode, the diode perveance, and the diode gap change were introduced to explain the observed extension of microwave pulse. After Csl coating, the carbon fiber cathode exhibited the absence of strong plasma, a slow plasma expansion velocity, and an almost unchanged diode gap during the main voltage pulse. It was found that heavy plasma ions, slow plasma expansion velocities, and long microwave pulses tend to be closely tied. These results show that, given a proper diode design, the carbon fiber cathodes with Csl coating have great promise for generating long-pulse microwave radiation. [J46]

"Low-Power Microwave Plasma Conductivity"

Plasma conductivity is of general interest for both fundamental research and specific applications. For this purpose, plasma equivalent impedance and complex conductivity are measured at 2.2 GHz, at pressures between 1 and 103 mbar, as a function of microwave power in a slot-type resonator, predominantly capacitively coupled to plasma. The plasma impedance is self-adjusting, maintaining a quasi-constant microwave amplitude. The sign of the imaginary part of the impedance (or conductivity) depends on pressure and, consequently, on electron density. The reactive part becomes significant if the Debye length is comparable with the size of the resonator and the plasma frequency is close to the microwave driving frequency. [J47]

"Diagnostic of phased arrays with faulty elements using the mutual coupling method"

The ability to calibrate phased array antennas by utilising the mutual coupling method (MCM), which takes advantage of the mutual coupling effect between adjacent elements, is addressed. The basic assumption of the method is that the mutual coupling between adjacent elements is equal for all elements in the array and its major deficiency is its failure in the case of faulty elements. A parametric study to identify the effect of faulty elements in the array has been conducted. It has been shown that displacement of one element in the array may cause a significant error in the calibration, which affects its radiation characteristics (increase in the far side lobe level). The main contribution is the presentation of the effect of faulty elements in the calibration process and the proposal of a way to detect and bypass the faulty elements in a phased array calibrated by the MCM. [J48]

"Design of a Microwave Microplasma Source at Atmospheric Pressure"

This paper studies two linear resonator sources, which use a continuous 2.45-GHz microwave excitation to produce stable microplasmas, in air and in argon, at atmospheric pressure. The discharges are produced and sustained within the 50-200- μm gap created between two metal electrodes with either 6 or 14 mm in length. Particular attention is given to the design and optimization of the sources (in terms of frequency tuning and power coupling), following a complementary approach based on simulations and experiments. Optical-emission-spectroscopy diagnostics allow one to deduce the rotational, vibrational, and excitation gas temperatures and the electron density (using Stark broadening measurements of the H β -emission profile). [J49]

"A Cost-Effective UHF RFID Tag for Transmission of Generic Sensor Data in Wireless Sensor Networks"

The use of RF identification (RFID) technology for the automatic transmission of physical parameters in wireless sensor networks paves the way to a large class of attractive applications ranging from healthcare to automotive, diagnostic systems, robotics, and many others. Nevertheless, although some RFID tags capable to transmit sensor-like information are already on the market, only a limited number of sensors, such as those for temperature or pressure measurement, can be easily miniaturized and embedded in the RFID chip. The integration of more complex sensors, in fact, appears to be complicated and extremely expensive. In this paper, a cost-effective general-purpose multi-ID tag is proposed. It can be connected to generic sensors, regardless of the actual measured value, and it is capable to transmit, when interrogated by a standard RFID reader, a proper combination of ID codes that univocally codifies the sensor measured value. The functionalities of this device have been extensively validated under stressing conditions and the capability to transmit whatever kind of sensor data has been demonstrated. [J50]

"Spatial nonuniformity of electron energy in a microwave atmospheric-pressure microplasma"

The characteristics of the electron energy in a microwave atmospheric-pressure argon microplasma are investigated by a spatially resolved optical emission spectroscopy. By adding tiny amount of xenon (1 ppm) as tracer gas into the argon discharge, it is found that the spatial distribution of the electrons with energy 8.3 eV is quite different from that of the electrons with energy 11.5 eV. Spatial distribution of the population ratio between 4p and 5p levels of Ar atom is also determined. Furthermore, with a collisional-radiative model, it is found that the spatial variation of this population ratio is mainly attributed to the spatial nonuniformity of the effective electron temperature. [J51]

"Temporal behavior of cold atmospheric plasma jet"

Temporally resolved evolution of parameters in atmospheric plasma jet is studied by means of microwave scattering, fast photographing, and measuring of jet currents. It is observed that streamer ("plasma bullet") propagating along with gas flow is generated immediately after the breakdown. It is demonstrated that an afterglow plasma column remains on the way of streamer passing. Lifetime of the afterglow plasma column is 3-5 μs , which is longer than that of the streamer. [J52]

"Optical Emission Characteristics of Atmospheric-Pressure Nonequilibrium Microwave Discharge and High-Frequency DC Pulse Discharge Plasma Jets"

With an aim to understand the mechanism of surface processing by atmospheric-pressure nonequilibrium discharge plasma jets, we measured the vibrational and rotational temperatures in the plasmas by means of optical emission spectroscopy (OES) measurement method. This paper focuses on the OES measurement method using a torch-shaped atmospheric-pressure nonequilibrium discharge plasma jet power supply consisting of a microwave (2.45-GHz) generator and a high-frequency (5.0-10-kHz) dc pulse power supply, using a gas mixture of Ar (8.0 L/min) and N₂ (0.1-0.5 L/min) as the discharge plasma gas, and changing the flow rate of N₂ gas at the input power of 100-150 W. Upon comparing vibrational and rotational temperatures (0.18-0.27 eV) determined from the OES measurement method using two types of atmospheric-pressure nonequilibrium discharge plasma jets, results indicate that the microwave discharge plasma jet has considerably low vibrational and rotational temperatures. [J53]

"Development of New X-Ray Source Based on Carbon Nanotube Field Emission and Application to the Non Destructive Imaging Technology"

In the present work, a new concept of X-ray source was developed. The conventional thermionic tungsten filament tube is commonly available in various fields of application, such as, medical diagnostic and therapy

system, microwave amplifier, non-destructive testing (NDT) technology, and so on. However, it has intrinsic problems such as high power consumption, very low X-ray efficiency, and out-gassing problems. Therefore, in the present study a new carbon nanotube (CNT) based X-ray source was developed as a substitute for the conventional one. The new X-ray source consists of three major parts. The CNT electron field emitter was employed as a cathode, a very thin metal mesh as a grid to extract electrons from the CNT, and finally a molybdenum embedded copper target as an anode to accelerate electrons. A supplementary electrostatic focusing lens was employed in the tube to focus the electron beam on the anode target. A detailed description of the tube structure as well as electron beam characteristics is presented in this study. In addition, preliminary X-ray images obtained by using the CNT X-ray tube are presented. [J54]

"Multichannel microwave interferometer for the levitated dipole experiment"

A four-channel microwave interferometer (center frequency: 60 GHz) has been constructed to measure plasma density profiles in the levitated dipole experiment (LDX). The LDX interferometer has a unique design owing to the unique geometry of LDX. The main design features of the interferometer are: (1) the transmitted beam traverses the plasma entirely in O-mode; (2) the interferometer is a heterodyne system employing two free-running oscillators; (3) four signals of data are received from just on transmitted beam; (4) phase shifts are detected in quadrature. Calibration tests demonstrate that the interferometer measures phase shifts with an uncertainty of approximately 5° . Plasma densities in LDX corresponding to phase shifts of up to 5π are routinely and successfully measured. [J55]

"A system to investigate the remediation of organic vapors using microwave-induced plasma with fluidized carbon granules"

This article describes a system to investigate the parameters for the remediation of organic vapors using microwave-induced plasma on fluidized carbon granules. The system is based on a single mode microwave apparatus with a variable power (2.45 GHz) generator. Carbon granules are fluidized in a silica tube situated in the sample section of a waveguide incorporating two additional ports to allow plasma intensity monitoring using a light sensor and imaging with a digital camera. A fluoroptic probe is used for in situ measurement of the carbon granule temperature, while the effluent gas temperature is measured with a thermocouple situated in the silica tube outside the cavity. Data acquisition and control software allow experiments using a variety of microwave power regimes while simultaneously recording the light intensity of any plasma generated within the carbon bed, together with its temperature. Evaluation using two different granular activated carbons and ethyl acetate, introduced as a vapor into the fluidizing air stream at a concentration of 1 ppm, yielded results which indicated that significant destruction of ethyl acetate, as monitored using a mass spectrometer, was achieved only with the carbon granules showing high plasma activity under pulsed microwave conditions. The system is therefore suitable for comparison of the relative microwave activities of various activated carbon granules and their performance in microwave remediation and regeneration. [J56]

"Chromatic-free spatially resolved optical emission spectroscopy diagnostics for microplasma"

A chromatic-free spatially resolved diagnostic system for microplasma measurement is proposed and demonstrated, which consists of an optical chromatic-free microscope mirror system, an electron multiplying charge coupled device (EMCCD), and bandpass filters. The diagnostic system free of chromatic aberrations with a spatial resolution of about $6\mu\text{m}$ is achieved. The factors that limit the resolution of this diagnostic system have been analyzed, which are optical diffraction, the pixel size of the EMCCD, and the thickness of the microplasma. In this paper, the optimal condition for achieving a maximum resolution power has been analyzed. With this diagnostic system, we revealed the spatial nonuniformity of a microwave atmospheric-pressure argon microplasma. Furthermore, the spatial distribution of the time-averaged effective electron temperature has been estimated from the intensity distributions of 750.4 and 415.8 nm emissions. [J57]

"Radio-frequency electromagnetic field measurements for direct detection of electron Bernstein waves in a torus plasma"

To identify the mode-converted electron Bernstein wave (EBW) in a torus plasma directly, we have developed an interferometry system, in which a diagnostic microwave injected outside of the plasma column was directly detected with the probing antenna inserted into the plasma. In this work, plasma production and heating are achieved with 2.45GHz, 2.5kW electron cyclotron heating (ECH), whereas diagnostics are carried out with a lower power (10W) separate frequency (1-2.1GHz) microwave. Three components, i.e., two electromagnetic (toroidal and poloidal directions) and an electrostatic (if refractive index is sufficiently higher than unity, it corresponds to radial component), of ECRF electric field are simultaneously measured with three probing antennas, which are inserted into plasma. Selectivities of each component signal were checked experimentally.

Excitation antennas have quite high selectivity of direction of linear polarization. As probing antennas for detecting electromagnetic components, we employed a monopole antenna with a length of 35mm, and the separation of the poloidal (O-wave) and toroidal (X-wave) components of ECRF electric field could be available with this antenna. To detect EBW, which is an electrostatic wave, a small tip (1mm) antenna was used. As the preliminary results, we detected signals that have three characteristics of EBW, i.e., short wavelength, backward propagation, and electrostatic. [J58]

"Investigation of the Scattering Efficiency in Doppler Reflectometry by Two-Dimensional Full-Wave Simulations"

Two-dimensional full-wave simulations of Doppler reflectometry in slab and curved geometries have been carried out with the finite-difference time-domain code IPF-FD3D. The goal is to find the instrument response function of the reflectometer that allows the recovery of the poloidal plasma-density-fluctuation-wavenumber spectrum by Doppler reflectometry at different angles of incidence. Apart from nonlinearities caused by high fluctuation levels, the scattering process is found to be strongly dependent on the angle of incidence on the cutoff layer, the beam parameters, and the plasma-density gradient length. In addition, the code was applied to the actual geometry of an ASDEX-Upgrade plasma. [J59]

"Electronic paramagnetic resonance power saturation of wooden samples"

The deterioration of wood used for artifacts of artistic interest involves the production of different free radicals from the macromolecules of the wooden matrix (cellulose, lignin, and hemicellulose). Among the techniques able to provide information about these free radicals, the contribution of electronic paramagnetic resonance (EPR) can be very valuable. In this paper, the study of EPR signals (with $g \approx 2$) of both modern and ancient wooden taxa was undertaken in order to analyze some features of the free radicals in natural wood. In particular, we have studied the microwave power saturation behaviors of seasoned wooden samples from ten species, and we have found remarkable differences between softwoods and hardwoods. These differences can be correlated to dissimilarities in the relaxation times T_1 and T_2 attributable to the different microscopic structures of the two trees' categories. The method has been also applied to ancient woods belonging to works of art in order to assess the conservation state of these artifacts. The analysis of the saturation curves has been found to be sensitive to the wood decay state. Indeed the deterioration process of the wooden matrix involves a variation of the relaxation times; this could be ascribed to both possible structure modifications and to concentration increments of the free radicals inside ancient woods due to decay induced by natural (biological, chemical, and physical) agents. This analysis method seems to be promising for the characterization of the wooden decay state and, therefore, it could provide valuable diagnostic indications which are necessary for the restoration and conservation of many artifact of historical-artistic-archaeological interest. [J60]

"Short pulse, high power microwave radiation source with a laser-induced sheet plasma mirror"

We have demonstrated the short pulse, high power microwave radiation source using an ultraviolet laser-induced sheet plasma mirror in a gas-filled x-band rectangular waveguide from the conventional microwave sources and components. A laser-induced sheet plasma with an overdense plasma acts as a plasma mirror. The long pulse propagating in the gas-filled waveguide was sliced by the sheet plasma mirror at two different points along the waveguide. We observed about twice the power of the pulse by adding the two sliced microwave pulses produced by this scheme. A maximum peak power of 200 kW with a pulse duration of 10 ns (full width at half maximum) from the long microwave pulse source with a pulse duration of 0.8 ns was observed. [J61]

"Characterizations of strip-line microwave micro atmospheric plasma and its application to neutralization"

In this work, we estimate the plasma parameters of strip-line microwave micro atmospheric plasma (SMMA) such as rotational temperature (T_r) both from OH and N_2 rotational transitions (610-770 and 770-980 K in Ar, respectively), electron density (N_e) from Stark broadening (about $10^{13}/\text{cm}^3$ in mixture of Ar and H_2), and the distribution of electric field before ignition of SMMA (54104 V/mat maximum, and applied voltage less than 5 V). Since the lower applied voltage of SMMA might enable us to conduct efficient processing without electrostatic damage (ESD), we applied jet-type SMMA to neutralization. The result of neutralization showed that it can reduce surface charge from ± 1000 to ± 100 V for 0.2 s at 10 W with Ar gas flow within 4 V offset voltage, which provides efficient plasma processing without ESD. [J62]

"Doppler reflectometer system in the stellarator TJ-II"

A Doppler reflectometer system has recently been installed in the stellarator TJ-II. The system is optimized for

the Q-band (33-50 GHz) and the high-curvature plasmas produced in TJ-II. The launch angle of the microwave beam can be controlled by a steerable mirror to obtain angles between $\pm 20^\circ$ enabling the measurement of perpendicular wave numbers in the range of 3-15 cm⁻¹. The available angular range allows for comparisons between positive and negative values and additionally for calibration of the system. Localization and k_z - estimation is done via the three-dimensional ray/beam-tracing code TRUBA. First measured spectra and radial profiles of the perpendicular velocity of plasma density fluctuations are presented. [J63]

"Measurements of plasma potential in high-pressure microwave plasmas"

Plasma potential of a high-pressure (1 Torr) microwave-generated argon plasma is measured using a Langmuir probe and a cold emissive probe. The operation of a hot emissive probe in a high-pressure plasma has been very difficult due to frequent burn-outs and significantly reduced lifetime of the probe filament, which, in turn, limits the possibility of collecting a wide range of data. The I-V characteristics from both Langmuir and emissive probes are interpreted using the collisionless probe theory since the collision correction factor is not very significant. The plasma potential determined from both Langmuir and cold emissive probe characteristics agrees well with one another and is observed to be dependent on the operating gas pressure but relatively unchanged as a function of the microwave power. An average plasma potential determined over the operating range of microwave powers varies nonlinearly with the gas pressure. [J64]

"Compact microwave re-entrant cavity applicator for plasma-assisted combustion"

The design and experimental operation of a compact microwave/rf applicator is described. This applicator operates at atmospheric pressure and couples electromagnetic energy into a premixed CH₄/O₂ flame. The addition of only 2-15 W of microwave power to a premixed combustion flame with a flame power of 10-40 W serves to extend the flammability limits for fuel lean conditions, increases the flame length and intensity, and increases the number density and mixture of excited radical species in the flame vicinity. The downstream gas temperature also increases. Optical emission spectroscopy measurements show gas rotational temperatures in the range of 2500-3600 K. At the higher input power of ≥ 10 W microplasma discharges can be produced in the high electric field region of the applicator. [J65]

"Validating optical emission spectroscopy as a diagnostic of microwave activated CH₄/Ar/H₂ plasmas used for diamond chemical vapor deposition"

Spatially resolved optical emission spectroscopy (OES) has been used to investigate the gas phase chemistry and composition in a microwave activated CH₄/Ar/H₂ plasma operating at moderate power densities (≤ 30 W cm⁻³) and pressures (≤ 175 Torr) during chemical vapor deposition of polycrystalline diamond. Several tracer species are monitored in order to gain information about the plasma. Relative concentrations of ground state H ($n=1$) atoms have been determined by actinometry, and the validity of this method have been demonstrated for the present experimental conditions. Electronically excited H ($n=3$ and 4) atoms, Ar (4p) atoms, and C₂ and CH radicals have been studied also, by monitoring their emissions as functions of process parameters (Ar and CH₄ flow rates, input power, and pressure) and of distance above the substrate. These various species exhibit distinctive behaviors, reflecting their different formation mechanisms. Relative trends identified by OES are found to be in very good agreement with those revealed by complementary absolute absorption measurements (using cavity ring down spectroscopy) and with the results of complementary two-dimensional modeling of the plasma chemistry prevailing within this reactor. [J66]

"Measured Antenna Response of a Proposed Microwave Tomography System Using an Efficient 3-D FDTD Model"

This letter presents a detailed study of a microwave tomography system using 3-D finite-difference time-domain methods (FDTDs). The algorithm, which uses a subcell model in form of the thin-wire approximation to model wire antennas, has been validated numerically using published numerical electromagnetic code (NEC) data for dipole antennas, and experimentally by comparing with measurements obtained for a monopole antenna array. The agreement between calculated and measured performances of the monopoles is close. In order to understand the fabrication tolerance, a parametric study was performed with regards to position of ground plane and grid size. It is found that the ground plane plays an important role in the performance of the monopole antennas. The excellent agreement is very promising for future deployment of the algorithm in 3-D microwave tomography applications. [J67]

"Effect of microwave frequency on breakdown and electron energy distribution function using a global model"

Global models (GMs) have proven a key modeling tool for the plasma processing field due to simplicity and speed. However, a GM requires specification of the electron energy distribution function (EEDF). The assumption of a Maxwellian EEDF leads to inaccurate reaction rate coefficients and results in error in plasma parameter prediction in high power microwave (HPM) driven discharges. Recently, a GM was developed with a pressure-independent enhanced EEDF to improve fidelity for modeling HPM breakdown. In this work, the GM is extended to 2 decades in frequency, and the frequency effect on HPM breakdown and the EEDF is investigated. [J68]

"Visual phenomena of surface plasmon polaritons at the dielectric-plasma interface"

Some interesting experiment phenomena of light patterns that appear in microwave plasma have been investigated. The wavelength of surface plasmon polaritons (SPPs) at the dielectric-plasma interface as the functions of incident wave frequency and plasma density has been calculated. The comparison of the experiment results with the calculating results has been carried out. By experimentally and theoretically analyzing, the phenomena are considered to be caused by the surface wave of SPPs at the interface between Pyrex wall and plasma. [J69]

"Materials characteristics and surface morphology of a cesium iodide coated carbon velvet cathode"

Cesium iodide (CsI) coated carbon fiber cathodes have shown promise as a cold cathode for microwave and x-ray devices. In particular, the cathodes have demonstrated over 1 000 000 shots lifetime at operating voltages at or in excess of 165 kV and current densities greater than 25A/cm². While the vacuum emission characteristics have been well studied, the materials characteristics of the cathodes themselves, particularly after operation, have received little attention. Furthermore, while researchers at University of Wisconsin have demonstrated a reduction in work function of carbon due to the CsI coating, the details of the emission mechanism remain poorly understood. This article gives results of a series of materials diagnostics investigating the cathode surface morphology as well as the changes in the carbon fiber structure with cathode shot history. We demonstrate that the cathode surface undergoes several changes in relation to the bond line along the fiber-substrate interface as well as at the fiber tips. While the exact mechanisms leading to these changes have not been determined, we offer several possible explanations for the changes, as well as the means by which these mechanisms can be ascertained. [J70]

"Direct measurement of spatial electron density oscillations in a dual frequency capacitive plasma"

The spatio-temporal electron density oscillation in a narrow gap dual frequency (27.12 and 1.937 MHz) capacitive discharge has been measured for the first time by using a floating microwave hairpin resonance probe. By measuring the probe's resonance frequency in a space and phase-resolved manner, we observe significant oscillation in electron density at both drive frequencies throughout the region between the parallel plate electrodes. The observed phenomenon is attributed to the influence of presheath electric fields of the opposing electrodes in alternate fashion. [J71]

"Probe measurements in a nonstationary plasma"

Single and double probes are simple and common tools for plasma measurements. In the case of nonstationary plasmas, the values of the plasma density obtained with these tools may differ significantly from the correct values measured, e.g., by microwave methods. The reason for such discrepancy could be the Bohm criterion failure during the plasma transition to the steady state. Indeed, the Bohm criterion, which is commonly used as a boundary condition at the plasma-sheath edge, directly determines the ion saturation current to the probe surface. The transition-time duration is studied and explained quantitatively for various plasmas produced by a version of a ferroinductor-coupled plasma source, which has its magnetic core fully immersed in the plasma. Corresponding conversion factors for probe measurements have been evaluated. Also, the influence of a certain amount of "hot" non-Maxwellian electrons on probe characteristics has been investigated. [J72]

"Crystal structure, Raman spectroscopy, far-infrared, and microwave dielectric properties of (1-x)La(MgSn)_{0.5}O₃-xNd(MgSn)_{0.5}O₃ system"

The complex perovskite system (1-x)La(MgSn)_{0.5}O₃-xNd(MgSn)_{0.5}O₃ with the composition (x=0-1) was prepared by the solid state reaction method. Structural and spectroscopic studies were carried out to understand the variation of dielectric properties with x. Rietveld refinement was carried out with the initial model obtained by using the structure prediction and diagnostic software. The symmetry of the compositions was determined to be monoclinic with space group P2₁/n, which corresponds to the a-a-c+tilting system, and the long-range order parameter was found to decrease with an increase in neodymium concentration. Raman spectra were analyzed

by fitting the A1g-like mode to a Lorentzian peak shape. Intrinsic dielectric parameters were estimated by fitting infrared reflectance spectra with the four-parameter semiquantum model. Transverse optic phonon mode strengths and average phonon damping were calculated. The origin of increase in the intrinsic loss with the composition variation is discussed. Microwave measurements were carried out in the frequency range of 9-11 GHz. The dielectric constant decreases and the temperature coefficient of resonant frequency becomes less negative with the increase in neodymium concentration. [J73]

"A microwave-induced plasma source: Characterization and application for the fast deposition of crystalline silicon films"

A microwave-induced plasma source is developed and is applied for the fast deposition of crystalline silicon films. In this paper, the plasma source is diagnosed first. Electron density, electron temperature, and discharge gas temperature of the plasmas generated in ambient air are studied using the optical emission spectroscopy method. The electron density is estimated by analyzing the Stark broadening of the hydrogen H β emission profile and is found to be as high as 10^{15} cm $^{-3}$ over wide conditions. The Boltzmann plot method is used to calculate the electron temperature, which shows a value smaller than 1 eV. Analysis of the rotational structure of OH molecular emission reveals a discharge gas temperature in a range of 400-800 °C. Preliminary efforts of using the plasma source for Si film fast deposition are performed at a reduced pressure by using SiCl $_4$ as the source gas. A fast deposition rate of 150 nm/s has been achieved for Si film with a high Raman crystallinity of 10^{10} even without using substrate heating and under a low H $_2$ dilution condition. Mechanisms for these results are discussed in detail. [J74]

"Attenuation of microwaves propagating through parallel-plate helium glow discharge at atmospheric pressure"

The experimental study of microwave-plasma interaction has been performed to demonstrate the transmission and attenuation of microwaves in atmospheric pressure glow discharge plasma. The cold-collisional plasma produced at atmospheric pressure can absorb the microwave energy because of its complex dielectric constant. The microwave of 10 GHz frequency was launched into the plasma and attenuation was measured as a function of electron plasma density, plasma thickness, electron-neutral collision frequency, etc. It was observed that the attenuation significantly depends on electron plasma density and thickness. The microwave attenuation measurement was also used as a diagnostic to estimate electron plasma density. It was validated by optical emission spectroscopic measurements with helium line intensity ratio method. Both the methods show good agreement. [J75]

"Development of microwave imaging reflectometry in large helical device"

Three key devices of the microwave imaging reflectometry (MIR) are under development in large helical device (LHD). The 2-D mixer array is developed by stacking the one-dimensional array of the planar Yagi-Uda antenna. The new type of the bandpass filter bank is modified to match the requirement of the MIR. The low-cost quadrature demodulator is also developed for the phase detection system. By using the low-price commercial wireless devices, the development cost becomes much lower than the expensive waveguide system. These devices enable the development of 2-D/3-D microwave imaging system for the plasma diagnostics and industrial applications. [J76]

"V-band frequency hopping microwave reflectometer in LHD"

In order to measure the internal structure of fluctuation, the broadband frequency tunable system, which has the ability of fast and stable hopping operation, is applied in the Large Helical Device. One of the important issues of density fluctuation measurements using this reflectometer is the study of energetic particle driven magnetohydrodynamics instability. During one plasma discharge, the launching frequency changes from one frequency to another frequency, which this operation is called as frequency hopping, and the cutoff position can be scanned in the wide area. As a hopping source, a synthesizer is used because it has a quite stable and low phase noise. The frequency component of the source output is multiplied to V-band (50-75 GHz) region for plasma measurements in extraordinary mode polarization. Also this system has a heterodyne detection with single side band frequency modulation for sensitive phase and amplitude measurement. We can obtain the radial profile of Alfvén eigenmode-like oscillation in a neutral beam injected plasma. [J77]

"Application of reflectometry power flow for magnetic field pitch angle measurements in tokamak plasmas (invited)"

Reflectometry has successfully demonstrated measurements of many important parameters in high temperature

tokamak fusion plasmas. However, implementing such capabilities in a high-field, large plasma, such as ITER, will be a significant challenge. In ITER, the ratio of plasma size (meters) to the required reflectometry source wavelength (millimeters) is significantly larger than in existing fusion experiments. This suggests that the flow of the launched reflectometer millimeter-wave power can be realistically analyzed using three-dimensional ray tracing techniques. The analytical and numerical studies presented will highlight the fact that the group velocity (or power flow) of the launched microwaves is dependent on the direction of wave propagation relative to the internal magnetic field. It is shown that this dependence strongly modifies power flow near the cutoff layer in a manner that embeds the local magnetic field direction in the "footprint" of the power returned toward the launch antenna. It will be shown that this can potentially be utilized to locally determine the magnetic field pitch angle at the cutoff location. The resultant beam drift and distortion due to magnetic field and relativistic effects also have significant consequences on the design of reflectometry systems for large, high-field fusion experiments. These effects are discussed in the context of the upcoming ITER burning plasma experiment. [J78]

"Investigation of H-production by surface interaction of the plasma generated in "Camembert III" reactor via distributed electron cyclotron resonance at 2.45 GHz (abstract)"

When considering the state-of-the-art on H-ion sources, ions can be produced either by plasma-surface interaction and/or inside the plasma volume. For the production of negative ions by surface ionization, a low work function material is required. For this purpose, cesium has been used in many cases at LBNL, JAEA, KEK, and in other facilities [M. Bacal, Nucl. Fusion 46, 250 (2006)]. Despite an enhancement in the negative ion production (by a factor of 2.5 in JAEA source), the use of cesium could lead to many drawbacks in the plasma functioning of ITER, for example. An alternative material to cesium could lead to an important improvement for negative ion source. For this purpose, both theoretical and experimental studies must be undertaken. Surface mechanisms have to be taken into account both for creation and loss mechanisms: (i) By recycling the atomic hydrogen into highly vibrationally excited molecular hydrogen via recombinative desorption on specific surfaces (fresh tantalum on surface increases the negative ion density [M. Bacal, A. A. Ivanov, Jr. et al, Rev. Sci. Instrum. 75, 1699 (2004)] by more than 60%). It has been shown for a rigid substrate model that both the recombination cross section and the degree of vibrational excitation are highly sensitive to the nature of the surface [B. Jackson and D. Lemoine, J. Chem. Phys. 114, 474 (2001)]. (ii) By surface passivation, which could lead to a substantial decrease in $H_2(X,v)$ wall losses. In order to understand the fundamental mechanisms of surface production and losses, "Camembert III" experimental setup, recently settled in the LPSC laboratory (Grenoble, France) is used. In this experimental structure, hydrogen multidipolar plasma sustained by microwaves (2.45GHz) presents the potential advantage to operate either in a metallic or a conductive chamber. The inner walls could be then frequently coated, by sputtering or chemical vapor deposition techniques, with no opening of the chamber with various materials. First experiments of H-surface production will be performed on target material. Hence, perfectly knowing the target material (in terms of composition and structural and physical properties), H-ion density production near the target surface will be monitored by laser photodetachment [M. Bacal, Rev. Sci. Instrum. 71, 3981 (2000)]. Even if this diagnostic gives no direct information on high rovibrationally excited level of the H_2 molecule, its implementation and use are far less complicated than vuv LIF. [J79]

"Compact 2.45 GHz microwave ion/atom source"

Characteristics of a microwave driven 3.4cm diameter compact ion/atom source equipped with permanent magnets were tested. The source can be mounted to a standard copper gasket flange, and microwave power is supplied through an N-type microwave connector. The ion source plasma was observed through an ion extraction hole with an optical emission spectrometer. Peak height of an optical line spectrum emission corresponding to atomic nitrogen increased in proportion to the microwave input power. Quadrupole mass spectrometer showed that N^+ and N_2^+ were the dominant species in the extracted ion beam. Nitrogen ion current density of 0.23mA/cm² was obtained with only 10W discharge power and 6410-3Pa source surrounding pressure. [J80]

"Fast visible imaging of turbulent plasma in TORPEX"

Fast framing cameras constitute an important recent diagnostic development aimed at monitoring light emission from magnetically confined plasmas, and are now commonly used to study turbulence in plasmas. In the TORPEX toroidal device [A. Fasoli et al, Phys. Plasmas 13, 055902 (2006)], low frequency electrostatic fluctuations associated with drift-interchange waves are routinely measured by means of extensive sets of Langmuir probes. A Photron Ultima APX-RS fast framing camera has recently been acquired to complement Langmuir probe measurements, which allows comparing statistical and spectral properties of visible light and electrostatic fluctuations. A direct imaging system has been developed, which allows viewing the light, emitted from microwave-produced plasmas tangentially and perpendicularly to the toroidal direction. The comparison of the probability density function, power spectral density, and autoconditional average of the camera data to those

obtained using a multiple head electrostatic probe covering the plasma cross section shows reasonable agreement in the case of perpendicular view and in the plasma region where interchange modes dominate. [J81]

"Development and research of a coaxial microwave plasma thruster"

An overview of the research on a coaxial microwave plasma thruster at Northwestern Polytechnic University is presented. Emphasis is put on the development and research on key components of the thruster system, a microthrust balance, plasma plume diagnostics, and a numerical simulation of the plasma flow field inside the thruster cavity. The developed thruster cavity is chosen from a coaxial resonant cavity with concentrated capacitance, which can operate well in atmosphere and vacuum conditions. The development of a microwave source shows that a magnetron powered by a switch power supply has advantages in the power level and efficiency, but a solid state microwave source synthesized from the arsenide field effect transistor is superior in weight and volume. Through elimination of the effect of large gravity and resistance force induced by a gas pipe line and a microwave transmitting line on the microthrust, 15mN and 340s in the performance of the microwave plasma thruster at 70W and with helium gas are measured. Diagnosing experiment shows that the plasma plume density is in the range of $(1-7.2) \times 10^{16}/\text{m}^3$. Numerical simulation of the plasma flow field inside the coaxial thruster cavity shows that there is a good match between the microwave power and gas flow rate. [J82]

"Dichroic filters to protect milliwatt far-infrared detectors from megawatt ECRH radiation"

Dichroic filters have been used to shield effectively the far infrared (FIR) detectors at the interferometer/polarimeter on TEXTOR. The filters consist of metal foils with regular holes, the hole diameter, the mutual spacing and the thickness of the foils are chosen to transmit radiation at the design frequency with transmission 90%. The attenuation at the low frequency end of the bandpass filter is about 30dB per octave, the high frequency transmission is between 20% and 40%. The filters have been used to block the stray radiation from the megawatt microwave heating beam to the detectors of the FIR interferometer, operating with power on the detector in the milliwatt range. If required, the low frequency attenuation can be still enhanced, without compromising the transmission in the passband. The FIR interferometer used for plasma density and position control is no longer disturbed by electromagnetic waves used for plasma heating. [J83]

"Real-time digital heterodyne interferometer for high resolution plasma density measurements at ISTTOK"

With the implementation of alternating discharges (ac) at the ISTTOK tokamak, the typical duration of the discharges increased from 35 to 250ms. This time increase created the need for a real-time electron density measurement in order to control the plasma fueling. The diagnostic chosen for the real-time calculation was the microwave interferometer. The ISTTOK microwave interferometer is a heterodyne system with quadrature detection and a probing frequency of 100GHz ($\lambda = 3\text{mm}$). In this paper, a low-cost approach for real-time diagnostic using a digital signal programmable intelligent computer embedded system is presented, which allows the measurement of the phase with a 1% fringe accuracy in less than 6 μs . The system increases its accuracy by digitally correcting the offsets of the input signals and making use of a judicious lookup table optimized to improve the nonlinear behavior of the transfer curve. The electron density is determined at a rate of 82kHz (limited by the analog to digital converter), and the data are transmitted for each millisecond although this last parameter could be much lower (around 12 μs - each value calculated is transmitted). In the future, this same system is expected to control plasma actuators, such as the piezoelectric valve of the hydrogen injection system responsible for the plasma fueling. [J84]

"Wide-angle point-to-point x-ray imaging with almost arbitrarily large angles of incidence"

The paper describes a new scheme for wide-angle point-to-point x-ray imaging with almost arbitrarily large angles of incidence by a matched pair of spherically bent crystals to eliminate the astigmatism, which is a well-known imaging error of spherical mirrors. In addition to x rays, the scheme should be applicable to a very broad spectrum of the electromagnetic radiation, including microwaves, infrared and visible light, as well as UV and extreme UV radiation, if the crystals are replaced with appropriate spherical reflectors. The scheme may also be applicable to the imaging with ultrasound. [J85]

"Pulse compression radar reflectometry to measure electron density in plasma with parasitic reflections"

Pulse compression radar reflectometry is used to obtain electron density profile in plasma with parasitic reflections in this article. The pulse compression radar relies on the relation between the temporal width of a pulse and the frequency bandwidth of this pulse: $\Delta t \sim 1/\Delta f$. So a set of sweep-frequency microwaves

within a bandwidth Δf can be introduced sequentially into the plasma to obtain the same information as the one obtained by a real pulse. By applying a Fourier transform to the data of reflectivity array in the frequency domain, the temporal response in the time domain is obtained. The limitation of the parasitic reflections on measurement can be eliminated from the temporal response by the method of time gate. This is a prominent advantage when this method is compared to the traditional reflectometry. For this method, an appropriate compromise between the spatial resolution and the electron density resolution is important. Experimental results show that the profile obtained from pulse compression radar reflectometry is similar to that from a double Langmuir probe. [J86]

"A 280 GHz single-channel millimeter-wave interferometer system for KSTAR"

A 280GHz single-channel horizontal millimeter-wave interferometer system has been fabricated and installed for plasma electron density measurements on the Korea Superconducting Tokamak Advanced Research (KSTAR). A retractable cassette system has been adopted for deep positioning of the interferometer system on large cryostat. The cassette system contains a pneumatic vacuum window shutter and a beam focusing module. The focusing module consists of antennas and aluminum concave mirrors, where an incident beam is reflected on a specially designed carbon inner-wall tile. The module enhances receiving beam power and reduces phase errors due to unexpected beam reflections on a vacuum vessel. Microwave components such as oscillators and mixers are located 2m away from cryostat with a shielding box. Intermediate frequency signals generated by mixers are transmitted to a diagnostics room, and the phase difference between these signals is measured using a multifringe counting phase comparator. A beam path analysis has been performed for a triangular beam path geometry. An effective line-integrated density can be deduced from measured line-integrated density with these results. A beam path length error due to plasma refraction effect has been determined with various plasma conditions. [J87]

"Radial density profile measurement by using the multichannel microwave interferometer in GAMMA 10"

Plasma density radial profile measurements are an important study for fusion plasma researches. We reconstructed a multichannel microwave interferometer for radial plasma electron density and density fluctuation measurements with both changing the transmission horn position and using the Teflon lens by only using this system in a single plasma shot. By using this system, we can successfully measure the radial density and density fluctuation spectra in a single plasma shot. [J88]

"Investigation of helicon ion source extraction systems"

Various versions of an extraction system for a helicon ion source have been investigated in high plasma density (10^{12}cm^{-3}) modes. The measurements of the plasma density were carried out with a microwave interferometer. Experiments were performed with hydrogen and helium gases. The preliminary results indicate that specially designed extractors are very promising for improving ion beam paraxial brightness. [J89]

"Imaging of Atmospheric Air Breakdown Caused by a High-Power 110-GHz Pulsed Gaussian Beam"

We present the images of regular filamentary plasma arrays produced upon the breakdown of air at atmospheric pressure at the focal region of a high-power 110-GHz pulsed Gaussian beam. The source of the millimeter wave beam is a gyrotron that can generate up to 1.5-MW output power with 3-nus pulselength. This unique plasma structure exists only at high pressures. With decreasing pressure, the structure changes into layers of curved plasma sheets and into more familiar diffuse plasma. A main cause of the formation of the regular array structure appears to be the reflection from filaments. The successive generation of conductive filaments modifies the incident field pattern and creates local hot spots upstream of the existing filaments with regular spacing of roughly a quarter wavelength. [J90]

"Atmospheric Pressure Nitrogen Microwave Plasma"

We present nitrogen microwave blown-out plasma at atmospheric pressure and its emission spectra with their spatial distribution. The plasma had a symmetric conical shape until it collapsed to a funnel-like shape at high gas flow rates. We observed the emission of N_2 , N_2^+ , CN and NO : their Abel-inverted emissivity increased with increasing power and decreased with plasma radius. [J91]

"Terahertz Science and Technology Trends"

The recent progress in terahertz science and technology (THz-S&T) opens up a range of potential research

opportunities. Historically, THz technologies were mainly used by the astronomy community for searching far-infrared radiation (cosmic background), and by the laser fusion community for the diagnostics of plasmas. Since the first demonstration of THz wave time-domain spectroscopy in the late 1980s, there has been a series of significant advances (particularly in recent years) as intense THz sources and more sensitive detectors provide new opportunities for understanding the basic science in the THz frequency range. THz radiation can penetrate through many nonpolar dielectric materials and can be used for nondestructive/noninvasive sensing and imaging of targets under nonpolar, nonmetallic covers or containers. An immediate application of THz wave technology is in nondestructive testing or inspection. Short-term applications (within three to five years) are expected in spectroscopic sensing and imaging for homeland security. Biomedical applications are expected in the long term (five to ten years). By comparing the publication record trend of THz-S&T related papers with the publication record of proxy fields (laser, microwave, Raman, and infrared), it is possible to anticipate that the number of publications in the THz-S&T arena will increase and also the impact in other research areas. We compare the publication pattern (number of papers versus time) with searching keywords in title or abstract. We found that all the publication trends share a common pattern with four periods defined by discovery, acceptance, adoption, and maturity. From this pattern trend, THz-S&T seems to be in an acceptance period. The unique properties of THz-S&T suggest that its applications will grow. [J92]

"The Potential of Pulsed Underwater Streamer Discharges as a Disinfection Technique"

In this paper, we investigate the effectiveness of pulsed underwater streamer discharges for water disinfection and its scalability to large throughputs. For this paper, we have built a coaxial streamer reactor containing a central cylindrical anode covered by a thin porous layer of almandine. The reactor was supplied by electric pulses with amplitudes of up to 100 kV and pulse durations between 200 and 400 ns at a repetition rate of up to 20 Hz. Different chemical probes have been used as the main diagnostic to determine the production rates and the accumulation of oxidants in the bulk water. It has been found that the number and the length of streamers scaled linearly with the applied voltage amplitude, whereas the pulse duration only affected the streamer length. All oxidant production rates scaled linearly with the number-length product of streamers. OH-radical concentrations of up to 100 mM appear at the streamer-water-boundary. However, because of the limited volume of streamers and the limited range of OH radicals, the most important oxidant with respect to decontamination is H₂O₂ which accumulates in the water and, by interacting with the intense UV radiation and the shock waves from the streamers, produces OH radicals in the bulk water. Placing water-filled cuvettes from different materials in the reactor, we found that the contribution of shock waves to the production of oxidants in the bulk water seems more important than the contribution of UV radiation. The production of oxidants can be enhanced by percolating suitable gases through the active zone of the reactor. Most effective is the use of oxygen. About 20 J/cm³ of electrical energy was required to reduce the concentration of *Pseudomonas putida* bacteria by six orders of magnitude. However, up to 180 J/cm³ of specific energy input was necessary to reduce the bacterial freight in waste water from a municipal sewage plant by just two orders of magnitude. This has been explained by the high conductivity of waste water which drastically reduces the length of streamers for the same electrical parameters. Therefore, it seems unlikely that underwater streamer discharges alone can become competitive with other advanced oxidation processes like ozonation, UV irradiation, or irradiation with megaelectronvolt electron beams. However, it seems conceivable that a combination of underwater streamer discharges with ozonation or other processes can lead to a more effective and economic decontamination technique. [J93]

"3-D-Microwave Breast Tumor Detection: Study of System Performance"

This paper presents a study of performance for a 3-D breast tumor detection system. The system is based on processing the scattered signals when a narrow pulse is transmitted from a set of antennas placed surrounding the breast. The 3-D system performance is evaluated by placing the tumor at any breast position, even at locations near the breast muscle where detection is more difficult. Results are obtained for different sizes and positions of the abnormalities that are defined as spherical and bunch-shaped geometries, which approach the well-known breast tumors morphology. These results show that the array distribution considered will have a high impact on detection. [J94]

"Experimental Investigation of 193-nm Laser Breakdown in Air"

We present the measurements and analysis of laser-induced breakdown processes in dry air at a wavelength of 193 nm by focusing 180-mJ 10-MW high-power 193-nm UV ArF laser radiation onto a 30-μm-radius spot size. We examine pressures ranging from 40 torr to 5 atm, for laser power densities of 1 TW/cm², well above the threshold power flux for air ionization. The breakdown threshold electric field is measured and compared with classical and quantum theoretical ionization models at this short wavelength. A universal scaling analysis of these results allows one to predict aspects of high-power microwave breakdown based on measured laser breakdown observations. Comparison of 193-nm laser-induced effective field intensities for air breakdown data calculated

based on the collisional cascade and multiphoton breakdown theories is used successfully to determine the collisional microwave scaled portion with good agreement regarding both pressure dependence and breakdown threshold electric fields. Using a laser shadowgraphy diagnostic technique, the plasma and shock-wave dynamics are analyzed. Blast shock-wave expansion of the plasma and laser-heated neutral gas is observed with average velocities of 47 km/s, and the temporal shock-wave velocity variation is used to determine electron temperature evolution just behind the shock wave. [J95]

"Development and Laboratory Testing of a Noninvasive Intracranial Focused Hyperthermia System"

During the past two decades, a great deal of research has been carried out with the aim of developing effective techniques for hyperthermia treatment, primarily using RF, microwave, and ultrasound energy. A system for deep brain hyperthermia treatment, designed to also provide passive measurements of temperature and/or conductivity variations inside the human body, is presented in this paper. The proposed system comprises both therapeutic and diagnostic modules, operating in a totally contactless way, based on the use of an ellipsoidal beamformer to achieve focusing on the areas under treatment and monitoring. In previous publications, the performance of the system's diagnostic module in phantom, animal, and human studies has been reported. In the current research, new theoretical and experimental results using the therapeutic hyperthermia module of the system are presented. The main scope of the theoretical analysis is the improvement of the system's focusing attributes. Moreover, phantom experimental results verify the proof of concept. Both computation and phantom measurement results show that deep focused brain hyperthermia may be achievable with adequate spatial resolution and sensitivity using the proposed methodology, subject to the appropriate combination of operation frequency and low-loss dielectric material used as filling in the ellipsoidal. [J96]

"Studies on x-ray and UV emissions in electron cyclotron resonance x-ray source"

A novel electron cyclotron resonance x-ray source is constructed based on the ECR technique. In this paper, the possibility of using the ECR x-ray source for producing UV rays by optimizing the plasma parameters is explored. X-ray and UV emissions from the ECR x-ray source are carried out for argon, nitrogen, and CO₂ plasma. The x-ray spectral and dose measurements are carried with NaI(Tl) based spectrometer and dosimeter, respectively. For UV measurement, a quartz window arrangement is made at the exit port and the UV intensity is measured at 5cm from the quartz plate using UV meter. The x-ray and UV emissions are carried out for different microwave power levels and gas pressures. The x-ray emission is observed in the pressure range $\leq 10^{-5}$ Torr, whereas the UV emission is found to be negligible for the gas pressures 10^{-5} Torr and it starts increasing in the pressure range between 10^{-5} and 10^{-3} Torr. At high-pressure range, collision frequency of electron-atom is large which leads to the higher UV flux. At low pressure, the electron-atom collision frequency is low and hence the electrons reach high energy and by hitting the cavity wall produces higher x-ray flux. By choosing proper experimental conditions and plasma gas species, the same source can be used as either an x-ray source or an UV source. [J97]

"Stable microwave coaxial cavity plasma system at atmospheric pressure"

We present a systematic study of the development of a novel atmospheric microwave plasma system for material processing in the pressure range up to 760 Torr and the microwave input power up to 6 kW. Atmospheric microwave plasma was reliably produced and sustained by using a cylindrical resonator with the TM₀₁₁ cavity mode. The applicator and the microwave cavity, which is a cylindrical resonator, are carefully designed and optimized with the time dependent finite element Maxwell equation solver. The azimuthal apertures are placed at the maximum magnetic field positions between the cavity and the applicator to maximize the coupling efficiency into the microwave plasma at a resonant frequency of 2.45 GHz. The system consists of a magnetron power supply, a circulator, a directional coupler, a three-stub tuner, a dummy load, a coaxial cavity, and a central cavity. Design and construction of the resonant structures and diagnostics of atmospheric plasma using optical experiments are discussed in various ranges of pressure and microwave input power for different types of gases. [J98]

"Modeling the Visibility of Breast Malignancy by a Microwave Radiometer"

A breast tumor is visible by a passive microwave radiometer if it changes the radiometric output of a healthy breast to an extent that overcomes the radiometric resolution for the given sensing antenna and integration time. We modeled breast temperature by the standard Pennes equation using thermal parameters found in the literature for normal and cancerous breast tissue. An apparent thermal volume and its dependence on blood perfusion have been estimated. The radiometric weighting function has been evaluated as a function of the size of a contacting antenna modeled as an aperture antenna. For comparison with the radiometric resolution, the

difference signal between the outputs in the presence of a lesion and in its absence has been evaluated for different tumor sizes and depths. The results of the numerical analysis show that this difference signal depends on the average over-temperature in the lesion times the heating efficiency, given by the fraction of power delivered to the tumor when the antenna radiates onto the breast in active modality. A tumor of 6 mm (10 mm) diameter is visible by a 0.1 K radiometer and a 3 cm aperture antenna when it is not deeper than 1.2 cm (2.8 cm) under the assumption of ideal radiometer and antenna. [J99]

"A Computational Investigation of Microwave Breast Imaging Using Deformable Reflector"

In recent years, active microwave breast imaging is increasingly being viewed as a promising complementary imaging modality for cancer detection. In this paper, we present a novel deformable reflector microwave tomography technique for noninvasive characterization of the breast tissue. In contrast to conventional multitransceiver designs, the proposed technique utilizes a continuously deformable reflector with metallic coating to acquire field measurements for imaging. Computational feasibility of the proposed technique to image heterogeneous dielectric tissue property is evaluated using simplified 2-D breast models. The robustness of the deformable reflector-based tomography technique in imaging the spatial distribution of the tissue dielectric property in the presence of measurement noise is investigated using first-order Tikhonov regularization. Preliminary results obtained for the 2-D breast models appear promising and indicate further investigation of the new microwave tomography technique for breast imaging. [J100]

"Measurement of edge density profiles of Large Helical Device plasmas using an ultrashort-pulse reflectometer"

We report here on the application of an ultrashort-pulse reflectometer (USPR) to Large Helical Device in National Institute for Fusion Science. An impulse with picosecond pulse width is used as a source in an USPR. Since the bandwidth of a source is inversely related to the pulse width, we can utilize the frequency range of microwave to millimeter-wave by using wide band transmission lines. The density profiles can be reconstructed by collecting time-of-flight signal of each frequency component of an impulse reflected from each cutoff layer. Remote control system using super science information network has been introduced to the present USPR system. [J101]

"Analysis of the Special Sensor Microwave Imager/Sounder (SSMIS) Fields-of-View on DMSP F16"

The Special Sensor Microwave Imager/Sounder (SSMIS) calibration and Earth scene fields-of-view (FOV) are examined using sensor diagnostic modes, a graphic simulation of the SSMIS and spacecraft vehicle, and an electromagnetic analysis of the SSMIS antenna. The on-orbit FOV for each calibration target was found to be larger than the sample locations utilized by the flight software for calibration suggesting that additional observing time for the each target is available. The optimum calibration sampling location appears to be slightly offset from the current sampling. However, it is not expected that this will result in degraded performance. The SSMIS Earth scene FOV was found to have noticeable edge-of-scan biases for several channels. The biases were examined and determined to be due to intrusions of the antenna feed FOVs of the main reflector antenna caused by the SSMIS calibration targets and their associated multilayer insulation (MLI) blanketing in the final flight configuration. A simple algorithm to address the edge-of-scan biases is applied and found to correct the biases to within ~ 0.1 - 0.2 K. [J102]

"Mitigation of electron attachment to oxygen in high pressure air plasmas by vibrational excitation"

A series of time resolved microwave attenuation measurements are performed of the electron number density of an electron beam generated, CO laser excited nonequilibrium O₂/N₂ plasma. Resonant absorption of infrared radiation from the CO laser produces the nonequilibrium state, in which the heavy species vibrational modes are disproportionately excited, compared to the rotational and translational modes ($T_{vib} \approx 2000$ - 3000 K vs $T_{R/T} \approx 300$ K). It is shown that this results in an increase in the plasma free electron lifetime by two orders of magnitude compared to the unexcited cold gas, an effect which is ascribed to complete mitigation of rapid three-body electron attachment to molecular oxygen. A series of heavy species filtered pure rotational Raman scattering measurements are also presented, which exhibit minimal temperature change ($+50$ K), indicating that the observed lifetime increase cannot be due to heavy-species thermal effects. Finally, computational modeling results infer an increase in the rate of O₂-detachment by four to five orders of magnitude, compared to the equilibrium value. [J103]

"Spectroscopic study on the vibrational populations of N 2 C 3 Pi and B 3 Pi states in a microwave nitrogen discharge"

We measured the band spectra (first and second positive systems) of the nitrogen molecule to examine the vibrational and rotational temperatures of the C3Pi and B3Pi states by optical emission spectroscopy. We compared the experimentally measured and the calculated spectra to determine those temperatures of the generated plasma. We generated a microwave discharge nitrogen plasma in a cylindrical quartz tube (26mm inside diameter) with a discharge pressure of 0.5-1.0 Torr. The microwave frequency was 2.45 GHz and the output power was set at 600 W. It was found that $T_v \approx 0.5-0.7$ eV and $T_r \approx 0.07-0.15$ eV at B3Pi ($v=7, 8$, and 9), whereas $T_v \approx 0.65-0.9$ eV and $T_r \approx 0.06-0.16$ eV at C3Pi ($v=0$ and 1). Both rotational temperatures obtained from first and second positive systems were in good agreement. We also compared the measured vibrational populations with theoretical calculations, in which vibrational distribution function at N2X and electron energy distribution function are calculated self-consistently. [J104]

"Spectroscopic determination of H, He, and H₂ temperatures in a large-scale microwave plasma source"

Emission spectroscopy was used for the diagnostic of a large-scale, slot antenna excited microwave plasma source operating in pure hydrogen and in helium-hydrogen and argon-hydrogen mixtures at low pressures ($p=0.3$ mbar) and microwave power ranging from 600 to 900 W. No evidence was found for excessive broadening of the H α line under the present operating conditions, even though this line was found to be broader than the helium singlet line at 667.8 nm. The Doppler temperatures corresponding to this helium line (400-900 K) are close to the rotational temperatures (300-800 K) determined from the Q branch of the Fulcher- α band under the same conditions. The kinetic temperature of H atoms corresponding to the Doppler broadening of the H α line varies spatially between 3100 and 3400 K (95% He-5% H₂, $p=0.3$ mbar, and $P=900$ W) and between 3350 and 3900 K (95% Ar-5% H₂, $p=0.3$ mbar, and $P=600$ W) keeping constant the mixture composition, pressure, and microwave power. The rotational H₂ temperature in argon-hydrogen mixtures varies from 330 to 400 K under the same conditions. Therefore, the results presented here indicate that the kinetic temperature of H atoms is higher than the background gas temperature. [J105]

"Underwater streamer propagation analyzed from detailed measurements of pressure release"

In this paper we describe experimental observations connected with the propagation of primary and secondary streamers in water. Using a Mach-Zehnder interferometer we determined the pressure field surrounding the streamer channel at a given instant in time with high temporal and spatial resolution. This pressure field contains information on the time evolution of the pressure pulse inside the discharge channel. The pressure history in the channel has been reconstructed by comparing the experimentally obtained fringe shifts in the interferograms with those derived from one-dimensional hydrodynamic calculations in cylindrical geometry. Assuming different trial pressure pulses, it has been possible to establish the channel pressure iteratively. A reproduction of the experimental data from secondary streamers requires short (2-3 ns) pressure pulses with amplitudes of 2-3 GPa. These findings are inconsistent with the assumption of bubble-initiated propagation of secondary streamers. It has also been inferred from estimates of the channel diameter that self-propagation of secondary streamers occurs at field strengths at the streamer tip of more than 2 GV/m. We can therefore conclude that field induced dissociation and ionization of molecules in the bulk liquid are the most likely mechanism for secondary streamer propagation. Rather high electrical conductivity (~ 0.2 S/m) is achieved at fields of 2 GV/m and an ionization wave is launched from the streamer tip into the liquid. To advance the streamer the electric field must be expelled from the newly generated section. This occurs with the Maxwellian relaxation time of a few nanoseconds. During this time the region of high conductivity is transformed into a plasma channel of lower density and a pressure wave is launched into the liquid. A different mechanism is suggested for primary streamer formation. Because of the low conductivity in the channels it is more likely that gas bubbles or phase instabilities are involved in this case. [J106]

"Diagnostics of surface wave excited Kr/O₂ plasma for low-temperature oxidation processes"

The characteristics of species in Kr/O₂ mixture surface wave excited plasmas have been studied for clarifying the mechanism of plasma oxidation process. The absolute densities of the ground-state oxygen atom ($3P_j=0,1,2$) and the metastable oxygen atom ($1D_2$) were measured by using vacuum ultraviolet absorption spectroscopy. Under a microwave power of 1 kW and a total pressure of 90 Pa, the absolute density of O($3P_j$) atom decreased from 2.4×10^{14} to 3.4×10^{13} cm⁻³ with increasing Kr dilution ratio from 80 to 99%. However, the absolute density of O($1D_2$) atom increased with the increase of Kr dilution ratio and had a peak at a high Kr dilution condition of 97%. The production mechanisms of O($3P_j$) and O($1D_2$) atoms have been discussed on the results of the metastable Kr atom density, the electron density, and electron temperature measured by near-infrared absorption spectroscopy and Langmuir single probe, respectively. Moreover, we have measured the characteristics of positive ions by using quadrupole mass spectroscopy. From these results, the bombardments of O₂⁺ ions with low energy seem to affect the Si oxidation with oxygen atoms. [J107]

"Three-dimensional analysis of microwave generated plasmas with extended planar laser-induced fluorescence"

We present the development and application of a diagnostic system for the analysis of microwave generated low-pressure plasmas, which might also be used for the investigation of the edge regions in magnetically confined fusion plasmas. Our method uses planar laser-induced fluorescence, which is produced by excitation of neutral metastable atoms through a short, intense, pulsed laser. The beam expansion optics consist of an uncommon setup of four lenses. By controlled shifting of an element of the optics sideways, the location of the laser sheet in the plasma is scanned perpendicular to the excitation plane. Together with a spectrometer observing different observation volumes along the beam path, we are able to map absolute three-dimensional (3D) population density distributions of the metastable $(2P_{1/2o})3s[1/2]0$ state of Ne I in an electron cyclotron resonance heating (ECRH) plasma. This optical tomography system was used to study the influence of the microwave power and mode on the spatial structure of the plasma. The results show that the population density of the neutral neon in this metastable state is found to be in the range of 10^{16} m^{-3} , and that its spatial distribution is associated with the 3D structure of the magnetic field. We also report that the spatial distribution strongly varies with the mode structure, which depends on the microwave power. [J108]

"Electron density modulation in an asymmetric bipolar pulsed dc magnetron discharge"

This paper investigates the spatial and temporal variation in plasma electron density over a region between 5 and 10 cm above the race-track region of a pulsed magnetron sputtering target. The pulse operation is performed using an asymmetric bipolar pulsed dc power supply, which provides a sequence of large negative "on-phase" voltage (-350V) and a small positive "reverse-phase" voltage (+10V) for 55% of the pulse duration (10 μ s). The electron density is measured using a floating microwave hairpin resonance probe. The results show electron expulsion from the target in the initial on phase, which propagates with a characteristic speed exceeding the ion thermal speed. In the steady state on phase, a consistent higher density is observed. A quantitative model has been developed to explain the resultant density drops in the initial on phase. While in the reverse phase, we observed an anomalous growth in density at a specific location from the target ($d = 7 \text{ cm}$). The mechanism behind the increase in electron density has been attributed to the modulation in spatial plasma potential, which was measured earlier in the same apparatus using a floating emissive probe [J. W. Bradley et al, Plasma Sources Sci. Technol. 13, 189 (2004)]. [J109]

"Plasma induced by resonance enhanced multiphoton ionization in inert gas"

We present a detailed model for the evolution of resonance enhanced multiphoton ionization (REMPI) produced plasma during and after the ionizing laser pulse in inert gas (argon, as an example) at arbitrary pressures. Our theory includes the complete process of the REMPI plasma generation and losses, together with the changing gas thermodynamic parameters. The model shows that the plasma expansion follows a classical ambipolar diffusion and that gas heating results in a weak shock or acoustic wave. The gas becomes involved in the motion not only from the pressure gradient due to the heating, but also from the momentum transfer from the charged particles to gas atoms. The time dependence of the total number of electrons computed in theory matches closely with the results of coherent microwave scattering experiments. [J110]

"Direct measurement of density oscillation induced by a radio-frequency wave"

An O-mode reflectometer at a frequency of 25.85 GHz was applied to plasmas heated by the high harmonic fast wave (21 MHz) in the TST-2 spherical tokamak. An oscillation in the phase of the reflected microwave in the rf range was observed directly for the first time. In TST-2, the rf (250 kW) induced density oscillation depends mainly on the poloidal rf electric field, which is estimated to be about 0.2 kV/mrms by the reflectometer measurement. Sideband peaks separated in frequency by ion cyclotron harmonics from 21 MHz, and peaks at ion cyclotron harmonics which are suggested to be quasimodes generated by parametric decay, were detected. [J111]

"Reduction of the Coupling to External Sources and Modes of Propagation by a Nearly Confocal Resonator"

This paper presents a numerical and experimental study of a nearly confocal resonator with spherical mirrors at 12 GHz. The geometry was chosen in order to have a large quality factor for the diffraction losses, and thereby a weak coupling to external parasitic TE and TM modes, that propagate in a pipe on which the resonator may be installed. In turn, this allows a significant improvement of its signal-to-noise ratio, e.g., when used as a beam monitor. [J112]

"Phaseless characterisation of compact antenna test ranges"

Antenna characterisation and radar cross section measurements can be conveniently and successfully carried out by means of a compact antenna test range (CATR), whose performance is primarily assessed in terms of quiet zone size and field uniformity. CATR characterisation and diagnostics are usually performed by means of (amplitude and phase) field measurements in the quiet zone and are of timely interest either on CATR installation or on its periodic reassessments performed by manufacturers and/or users. This paper addresses CATR characterisation from amplitude-only data, an attractive topic because of the application of CATRs to the millimetre or sub-millimetre wave ranges. The approach is based on an appropriate strategy retrieving the missing quiet zone phase and facing the issue of the large electrical dimensions of the CATR. To take into account the characteristics of the collimating system as well as to keep as low as possible the number of unknowns to be sought for, it exploits the Jacobi-Bessel expansion of the aperture field. The performance of the algorithm has been tested through a wide numerical analysis against synthetic data generated by GRASP8-SE whose full version is routinely employed for CATR design. The main results related to a Gregorian dual offset reflector CATR, modelled on that proposed in the literature by Pistorius et al, and to a single offset reflector CATR, inspired by the one available at the Queen Mary & Westfield College, London (UK), are reported. [J113]

"Advances in Ground Transmitters for the NASA Deep Space Network"

The Deep Space Network (DSN), managed by the Jet Propulsion Laboratory for NASA, is equipped with multiple microwave transmitters ranging in average radiated power from 200 W to 400 kW. The transmitters are used for routine or emergency communication with spacecraft, for navigation, and for radio science tasks. The latest advances in transmitter engineering were implemented in a new generation of 20-kW dual-band transmitters developed for the DSN 34-m beam waveguide antennas. Innovations include additional X-band communication capability for near Earth missions, new c, automated calibration, improved and expanded computerized monitoring and diagnostics, reduced cabling, and improved maintainability. The innovations were very beneficial for the DSN during the Mars 2003/2004 missions and will benefit other missions throughout the next decade. This paper describes the current design of the new transmitters and possible future developments. [J114]

"Microwave surfing-Channeling the voice within"

{no data available} [J115]

"Broadband Dielectric Characterization of Tumorous and Nontumorous Breast Tissues"

The broadband dielectric properties of tumorous and nontumorous tissues were analyzed at the millimeter-wave and terahertz frequencies. Ex-vivo measurements were obtained using the backward-wave oscillator-based free-space quasi-optical spectroscopy and dispersive Fourier transform spectroscopy methods. Both techniques were modified to yield the real and imaginary parts of permittivity, absorption coefficient, refractive index, and transmission data over an extended frequency range from 30 to 900 GHz. Results reveal characteristic signatures of breast tissues and display a significant difference in the electromagnetic response of tumorous and nontumorous tissues. The techniques employed in this study provide prospects for extending ex-vivo measurements to in-vivo breast cancer detection and diagnostics. [J116]

"EU Megawatt-Class 140-GHz CW Gyrotron"

The first series tube of the gyrotrons for the 10-MW electron cyclotron resonance heating system of the stellarator W7-X was tested at Forschungszentrum Karlsruhe (FZK) and yielded a total output power of 0.98 MW, with an efficiency of 31% (without a single-stage depressed collector) in short-pulse operation and of 0.92 MW in pulses of 180 s (efficiency of almost 45% at a depression voltage of 29 kV). The Gaussian mode output power was 0.91 MW. The pulselength at full power (1 MW) is limited at FZK by the available power supply. At a reduced electron beam current, it is possible to operate at longer pulselengths. At an output power of 0.57 MW (electron beam current of 29 A), the pulselength was increased to 1893 s. There was no physical reason for a limitation of this pulse: The pressure increase during the pulse was less than a factor of two and ended up at a very low value in the 10-9mbar range. The tube was delivered to Max-Planck-Institut fuer Plasmaphysik Greifswald for tests at full power and up to 30-min pulselength. The Gaussian mode RF output power, measured in a calorimetric load after a 25-m-long quasi-optical transmission line (seven mirrors), was 0.87 MW at a total output power of 0.92 MW in 30-min pulses. Again, no indications for a limitation in pulselength were found. The second series tube was tested in short-pulse operation and showed a strange behavior concerning a mode hopping which has not yet been understood. The third series gyrotron delivers up to now 0.65 MW at a pulse duration of 180 s. Preliminary operation of the prototype tube as a two-frequency gyrotron delivered 0.41 MW in

10-s pulses at 103.8 GHz (TE_{21,6}mode) [J117]

"Atmospheric-Pressure PECVD Coating and Plasma Chemical Etching for Continuous Processing"

Plasma processing at atmospheric pressure (APPlasmas) has attractions for both economic and technological reasons. Potential costs-saving factors are associated with online-processing capability and increase throughput due to high deposition rates. Capital cost savings for both equipment and line space (foot print), and relative ease of integration, are further benefits in comparison to low-pressure-technology approaches. Three types of APPlasmas are considered for coating: microwave chemical vapor deposition (CVD), dc ArcJet-CVD based on a linearly extended plasma source, and dielectric barrier glow discharge plasma CVD. Spectroscopic plasma characterization has shown that high fluxes of activated species are available in the plasma downstream region and can be used for deep fragmentation of even stable molecules. After precursor injection, a range of atomic and molecular intermediates, precursor fragments, and reaction products were identified leading to a conclusion that a complete conversion of the element-organic precursors into an inorganic materials take place. Alternatively, the dc ArcJet source is used for plasma chemical etching. All AP-plasma-enhanced chemical vapor deposition (PECVD), reactors are designed for continuous air-to-air processing on flat or slightly shaped substrates and allow deposition of nonoxide films. Reactor design is supported by fluid-dynamic modeling. Typical thin-film growth rates for PECVD are in the range of 5-100 nm/s (static) and up to 2 nm²/m/s (dynamic). The rates for plasma chemical etching are typically ten times higher. Plasma activation substantially widens the range of potential applications, e.g., coating on steel, lightweight metals, preshaped glass, and plastics. Developments are underway to explore the use of the coating technologies in areas such as scratch-resistant coatings on metals, barrier layers, self-clean coatings, biocidal functional surfaces, and antireflective coatings. The coating materials range explored - , so far, includes: silica, titania, carbon, silicon nitride/carbide, and metal oxides [J118]

"Arctangent Demodulation With DC Offset Compensation in Quadrature Doppler Radar Receiver Systems"

Direct-conversion microwave Doppler radar can be used to detect cardiopulmonary activity at a distance. One challenge for such detection in single channel receivers is demodulation sensitivity to target position, which can be overcome by using a quadrature receiver. This paper presents a mathematical analysis and experimental results demonstrating the effectiveness of arctangent demodulation in quadrature receivers. A particular challenge in this technique is the presence of dc offset resulting from receiver imperfections and clutter reflections, in addition to dc information related to target position and associated phase. These dc components can be large compared to the ac motion-related signal, and thus, cannot simply be included in digitization without adversely affecting resolution. Presented here is a method for calibrating the dc offset while preserving the dc information and capturing the motion-related signal with maximum resolution. Experimental results demonstrate that arctangent demodulation with dc offset compensation results in a significant improvement in heart rate measurement accuracy over quadrature channel selection, with a standard deviation of less than 1 beat/min [J119]

"Fabrication of a Nb-Based 180-Degree IF Hybrid for Balanced SIS Mixers"

180-degree IF hybrids are potentially useful for balanced superconductor-insulator-superconductor (SIS) mixers. We have developed a compact Nb-based 180-degree hybrid for 4-12 GHz which addresses concerns of element size, ohmic loss, and IF bandwidth. The fabrication scheme developed for these elements will be discussed, including the use of a thin overlayer Au process for via contacts, RF diode sputtered SiO_x in lieu of sublimated SiO_x films in order to improve the wafer yield, and diagnostic Nb capacitors to evaluate these SiO_x films. Experimental results will be presented and compared with simulations of these lumped element transmission line "rat-race" hybrids. It should be noted that the hybrids can be used in cryogenic balanced mixers for any RF band. [J120]

"Active antennas in medical microwave radiometry"

The use of active antennas in microwave radiometric thermometry is investigated, where prospective applications are within biomedical diagnostics. By incorporating a tiny low-noise amplifier, with only marginal self-heating, in the antenna probe, it is shown that the temperature accuracy of a broadband radiometer can be improved as a consequence of a smaller overall system noise figure. Proof of concept is verified experimentally through increased detectability of a hot object within a lossy medium. [J121]

"Detection of foreign body using fast thermoacoustic tomography with a multielement linear transducer array"

Current imaging modalities face challenges in clinical applications due to limitations in resolution or contrast. Microwave-induced thermoacoustic imaging may provide a complementary modality for medical imaging, particularly for detecting foreign objects due to their different absorption of electromagnetic radiation at specific frequencies. A thermoacoustic tomography system with a multielement linear transducer array was developed and used to detect foreign objects in tissue. Radiography and thermoacoustic images of objects with different electromagnetic properties, including glass, sand, and iron, were compared. The authors' results demonstrate that thermoacoustic imaging has the potential to become a fast method for surgical localization of occult foreign objects. [J122]

"Performance and analysis of an electron cyclotron resonance plasma cathode"

A scalable electron cyclotron resonance (ECR) plasma source was investigated for plasma cathode applications. The rectangular source utilized permanent magnets to establish the ECR condition. The microwave applicator region was windowless, making the source applicable to sputtering environment applications. The source was characterized using primarily two diagnostics: (1) a near-field and far-field Langmuir probe and (2) a downstream electron extraction electrode. Source operation and plasma properties were characterized at low pressures ranging from 0.2 to 5 mTorr and power levels up to 250 W. Evidence of grad-B drift in the plane of the source was observed. Extracted currents agreed well with predictions. [J123]

"Simulated experiment for elimination of air contaminated with odorous chemical agents by microwave plasma burner"

An experimental study on elimination of odorous chemical agent was carried out by making use of a microwave plasma burner, which consists of a microwave plasma torch and a reaction chamber with a fuel injector. Injection of hydrocarbon fuels into a high-temperature microwave torch plasma generates a plasma flame. The plasma flame can eliminate the odorous chemical agent diluted in air or purify the interior air of a large volume in isolated spaces. The specially designed reaction chamber eliminated H₂S and NH₃ diluted in airflow rate of 5000 lpm (liters per minute), showing beta values of 46.52 and 39.69 J/l, respectively. [J124]

"Upgrade of the data acquisition and control system of the ASDEX upgrade microwave reflectometer"

Microwave reflectometry is an important diagnostic to characterize the plasma electron density in fusion experiments. The broadband frequency swept microwave reflectometry system of the ASDEX Upgrade tokamak covers the frequency range of 16 to 100 GHz. In order to fully exploit the diagnostic capabilities it is mandatory to upgrade the data acquisition and control system. It should comply with shorter frequency sweep times and improved time resolution as well as accuracy allowing, for example, plasma position and shape measurements for control purposes, as it is foreseen for ITER. A new PCI-based system is under development based on a digitizer card with two channels, 12-bit resolution, and a waveform generator with one channel, 16-bit resolution. Both cards have 512 Mbytes of memory, a digital signal processor (DSP) for advanced processing modes, and a field programmable gate array (FPGA) for real-time algorithms and complex trigger managing modes. The system is able to support multiple cards (digitizers and signal generators) operating synchronously at a maximum rate of 210 MSamples/second. [J125]

"Microwave reflectometry as a novel diagnostic tool for detection of skin cancers"

More than 1 000 000 people are diagnosed with skin cancer each year in the United States, and more than 10 000 people die from the disease. Methods such as visual inspection and dermoscopy are available for early detection of skin cancers, but improvement in accuracy is needed. This paper investigates the use of microwave reflectometry as a potential diagnostic tool for detection of skin cancers. Open-ended coaxial probes were used to measure microwave properties of skin. The influences of measurement parameters such as probe application pressure, power level, and variation in reflection properties of skin with location and hydration were investigated. Using an available electromagnetic formulation, providing for the reflection properties of a layered dielectric structure irradiated by a coaxial probe, measurement and simulation results were compared. The results of the measurements and simulations for normal and moistened skin show that the water content of normal skin and benign and malignant lesions may cause significant differences among their reflection properties and subsequently render a malignant lesion detectable. The results of microwave measurements performed on human subjects are also presented, which show the potential of this technique to distinguish between cancerous and benign lesions. [J126]

"Guest Editorial Special Issue on Plenary and Invited Papers From ICOPS 2005"

{no data available} [J127]

"Microwave diagnostics of a repetitive, short-pulse-sustained, weakly ionized, air plasma under the influence of a magnetic field"

A microwave-transmission-based diagnostic method is presented here, applicable to plasmas having electron collision frequencies up to about twice their electron plasma frequency, and under the influence of an applied magnetic field. This technique is capable of measuring both electron number density and collision frequency. By varying the intensity of the applied magnetic field, the frequency of the upper hybrid resonance for transmission of extraordinary waves, as predicted by the Asher-Appleton-Hartree dispersion relation, is scanned through the microwave diagnostic frequency. Qualitatively, the zero transmission location of the resonant band depends on the electron number density, and the existence of the band depends on the collision frequency. Because there is essentially zero transmission through the resonant band, the measurement is accomplished by determining the ranges of microwave frequencies and magnetic field intensities that yield no transmission. In contrast to more standard techniques, the results presented here do not rely on accurate measurement of the transmission fraction or phase shift. The technique relies instead on measuring the applied field strengths and diagnostic frequencies that yield an opaque plasma. The opacity of the plasma can be robust with respect to the refraction, diffraction, multiple reflections, and impedance matching that can plague accurate measurements of microwave transmission fraction and phase shift, particularly in the case of small plasmas with near field geometries [J128]

"Beam Line Design, Beam Alignment Procedure, and Initial Results for the -Band Gain Experiment at Los Alamos"

A gain experiment was performed at Los Alamos using a 120-keV 2-A cylindrical electron beam with a ridged waveguide slow-wave structure at 94 GHz, demonstrating 22 dB of amplification through a traveling-wave interaction. The structure was planar with a gap of 0.75 mm and a length of 5 cm. The 2-A electron beam was confined in a 3.2-kG axial magnetic field, with roughly a 0.5-mm diameter. The electron beam was aligned along the magnetic axis of the solenoid by scribing out its cyclotron motion on a novel optical diagnostic using a procedure that depends on varying the solenoidal field strength. The transport through the structure was verified by letting the beam drill holes in a series of thin metallic foils before insertion of the structure [J129]

"Assessment of EOS Aqua AMSR-E Arctic Sea Ice Concentrations Using Landsat-7 and Airborne Microwave Imagery"

An assessment of Advanced Microwave Scanning Radiometer Earth Observing System (AMSR-E) sea ice concentrations under winter conditions using ice concentrations derived from Landsat-7 Enhanced Thematic Mapper Plus (ETM+) imagery obtained during the March 2003 Arctic sea ice validation field campaign is presented. The National Oceanic and Atmospheric Administration Environmental Technology Laboratory's Airborne Polarimetric Scanning Radiometer Measurements, which were made from the National Aeronautics and Space Administration P 3B aircraft during the campaign, were used primarily as a diagnostic tool to understand the comparative results and to suggest improvements to the AMSR-E ice concentration algorithm. Based on the AMSR-E/ETM+ comparisons, a good overall agreement with little bias (~1%) for areas of first year and young sea ice was found. Areas of new ice production result in a negative bias of about 5% in the AMSR-E ice concentration retrievals, with a root mean square error of 8%. Some areas of deep snow also resulted in an underestimate of the ice concentration (~10%). For all ice types combined and for the full range of ice concentrations, the bias ranged from 0% to 3%, and the rms errors ranged from 1% to 7%, depending on the region. The new-ice and deep-snow biases are expected to be reduced through an adjustment of the new-ice and ice-type C algorithm tie points [J130]

"High-Power Microwave Surface Flashover of a Gas–Dielectric Interface at 90–760 torr"

The major limiting factor in the transmission of high-power microwave (HPM) has been the interface between dielectric-vacuum or, even more severely, between dielectric-air, if HPM is to be radiated into the atmosphere. Extensive studies have identified the physical mechanisms associated with vacuum-dielectric flashover, as opposed to the mechanisms associated with air-dielectric flashover, which are not as well known. Surface-flashover tests involving high field enhancement due to the presence of a triple point have shown that volume breakdown threshold (dielectric removed) is approximately 50% higher than the flashover threshold with a dielectric interface over the 90-760 torr range. In order to quantify the role of field enhancement in the flashover process independent of electron injection from metallic surfaces, the effects of the triple point are minimized by carefully choosing the geometry, and in some cases, the triple point is "removed" from the flashover location. Experimental results were presented, including the impact of gas pressure and the presence of UV illumination, along with temperature analysis of the developing discharge plasma and temporally resolved images of the

flashover formation. These results are compared with literature data for volume breakdown in air, with discussion on the similarities and differences between the data [J131]

"Diagnostics of Collisionless Processes in Plasma"

The importance of phase-space resolving diagnostics for understanding collisionless and weakly collisional plasma is illustrated with three examples. The first example is the problem of understanding the plasma ion response to an external periodic excitation. The second example is the description of the ion density two-point correlation function. The final example is a new technique for measuring the electron velocity distribution function in low-temperature plasmas [J132]

"Methane-Augmented Microwave Plasma Burner"

In this paper, a microwave plasma burner for generating an enlarged high-temperature and large-volume plasma flame by injecting methane gas into the microwave plasma torch was presented. The air microwave plasma torch explosively burned out the hydrocarbon fuel by high atomic oxygen density. It was observed that the volume of the plasma-burner flame was more about ten times than that of the plasma-torch flame, showing an expanded burner flame. In the comparison of flames, while a conventional CH₄ burner reveals the flame of blue color, the CH₄ microwave plasma burner shows milky white flame. Also, preliminary experiments were carried out by measuring the temperature profiles of flames along axial and radial directions. Also, we measured the combustion efficiency and reduction rate of NO₂ for CH₄ plasma burner by employing gas chromatography and Fourier transform infrared [J133]

"Measurements of bremsstrahlung spectra of Lanzhou ECR Ion Source No. 3 (LECR3)"

In order to diagnose the electron cyclotron resonance (ECR) plasma, electron bremsstrahlung spectra were measured by a HPGe detector on Lanzhou ECR Ion Source No. 3 at IMP. The ion source was operated with argon under various working conditions, including different microwave power, mixing gas, extraction high voltage (HV), and so on. Some of the measured spectra are presented in this article. The dependence of energetic electron population on mixing gas and extraction HV is also described. Additionally, we are looking forward to further measurements on SECAL (Superconducting ECR Ion Source with Advanced design at Lanzhou). [J134]

"Electron cyclotron resonance ion source DECRIS-4 for the U400 cyclotron"

The electron cyclotron resonance ion source DECRIS-4 has been designed and constructed at the FLNR to be used as a second injector of heavy multiply charged ions for the U-400 cyclotron. After the modification of the injection side this source can be also used as a "charge breeder" (the "1+→n+" method) for the second phase of the Dubna radioactive ion beams project. The main feature of the ion source design is the creation of the extended resonance zone in a comparatively compact electron cyclotron resonance ion source. For this purpose the axial magnetic field is formed with a flat minimum. In this case the superposition of the axial magnetic field and the radial field of the permanent-magnet hexapole, made from NdFeB, allows one to create a larger resonance volume. For the plasma heating a microwave frequency of 14 GHz is used. In this paper we will present the basic design features of the ion source, including the results of the magnetic-field measurements. Some preliminary results of ion source tests are also reported. [J135]

"Extraction of single-ion beams from helicon ion source in high plasma density operation mode: Experiment and simulation"

Tests of a high plasma density high-brightness helicon ion source for nuclear microscopy applications are underway. Experiments were performed with hydrogen, helium, and argon. Different extraction structures of the helicon rf ion source were investigated with an imposed external magnetic field. We present measurements of the extracted current as a function of the extraction voltage and rf power. The source has been diagnosed by a microwave interferometer. Plasma densities in the vicinity of the emission hole of up to $7.24 \times 10^{12} \text{ cm}^{-3}$ (for argon), $1.64 \times 10^{12} \text{ cm}^{-3}$ (for helium), and $6.04 \times 10^{11} \text{ cm}^{-3}$ (for hydrogen) were obtained for working gas pressure of 5 mTorr and rf power 350 W ($f_{rf} = 27.12 \text{ MHz}$). The ion current density was 80 mA/cm^2 with high percentage of protons in the beam (80%). In the extraction structure, the cathode channel has a 3 mm length and a 0.6 mm diameter. The phase set degradation due to aberrations in the extraction structure of the helicon rf ion source was simulated for a fourth-order approximation in series expansion of the electrostatic potential and third-order approximation in series of the magnetic fields, by the matrix method. The calculations were performed involving experimental data on ion energy spread, average ion energy, and plasma density of the helicon rf ion source with permanent magnets. [J136]

"Technique for measuring D 2 pellet mass loss through a curved guide tube using two microwave cavity detectors"

Two microwave cavity mass detectors have been used to measure the mass loss of deuterium (D₂) pellets transported through a curved guide tube. The test tube was a mock-up of the pellet injection guide tube for the proposed ITER experiment, which will be used to transport pellets, including deuterium-tritium (D-T), from the pellet acceleration device to the inner wall (or magnetic high-field side) of the large tokamak for pellet injection and core fueling of plasmas. An accurate estimate of the mass loss is particularly important for D-T injection, because the inventory of the radioactive isotope (T) for ITER is limited and accountability and recycling will be crucial issues. In the laboratory, frozen cylindrical D₂ pellets of nominal 5.3-mm diameter were shot through the stainless steel test tube (≈ 10 m length and 10-mm inside diameter), with each end equipped with a microwave cavity. As the pellet passes through each tuned microwave cavity, the peak output signal from the electronics is directly proportional to the pellet mass. An absolute calibration of the cavities, which can be problematic, is not needed for the nondestructive technique described here. Instead, a cross calibration of the two cavities with pellets of varying masses provides the relationship to determine mass loss more precisely than any other technique previously reported. In addition, the individual output signals from the cavities can be used to identify intact pellets (a single signal peak) or broken pellets (multiple signal peaks). For the pellet speed range tested in this study (100-500 m/s), the mass loss for intact pellets was directly dependent on the pellet speed, with $\approx 10\%$ mass loss at 300 m/s. The microwave cavities and the associated electronics, as well as some basic theory, are described; calibration and experimental data are presented and discussed. [J137]

"In situ frequency calibration technique of FM reflectometer"

A frequency modulation (FM) reflectometer is designed to linearly sweep the microwave frequency in order to diagnose the plasma density profile. The static characteristic curve of the frequency versus the control voltage can be easily measured by using a spectrum analyzer. However, it is not guaranteed that the characteristic curve will be the same when the frequency is swept. A technique is devised which measures the dynamic characteristics by using the reflectometer itself. The results show that the shape of the characteristic curve does not depend on the sweep rate but on the time delay between the control voltage of the function generator and the microwave frequency at the detector input. This time delay should be compensated. Based on this measured characteristic curve, the frequency sweep rate and the distance between the antenna and the vacuum chamber are experimentally determined. [J138]

"Application of differential phase method to interferometry"

The differential phase (DP) method was applied to microwave interferometry for the first time. Its advantage over standard interferometry is that the greatly reduced phase shift enables the unique determination of phase. Such a system was implemented on the Tokyo Spherical Tokamak-2 (TST-2), and demonstrated that the correct phase shift can be obtained even when the probing frequency is close to the cutoff density, and that very fast time evolutions of the line-integrated density can be measured. [J139]

"Recent improvements of the broadband FMCW reflectometry system for density profile measurements on ASDEX Upgrade"

The broadband FMCW reflectometry system on ASDEX Upgrade has had significant improvements extending its measuring capabilities both on high and low density plasmas: (i) the upgrade of the Wband to probe electron densities up to $12.4 \times 10^{19} \text{ m}^{-3}$ with Omode, (ii) Q and V frequency bands operating in Xmode to probe the edge plasma and to provide information for O-mode profile initialization, and (iii) a new dynamic frequency calibration method to take into account all existing delays in the hyperabrupt varactor-tuned oscillator (HTO) tuning port and driver electronics. These improvements are particularly important to measure accurately the edge pedestal region of high density ITER relevant discharges. Density profiles obtained in high density discharges are presented and compared with results from both Li-beam and Thomson scattering diagnostics. [J140]

"Characterization of modes in coaxial vircator"

Modes' character of high-power microwave (HPM) pulses generated in coaxial vircator is discussed. The electromagnetic (EM) field gains due to beam-wave interaction for TM₀₁ and TE₁₁ modes are derived according to the E-field distribution pattern inside the anode cavity. Two-and-a-half dimensional (2.5-D) and three-dimensional (3-D) computer simulations are carried out to determine the main mode under different numerical simulation coordinate systems. Finally, the experimental verification is obtained by two different diagnostic methods. The results indicate that for most cases, the TE₁₁ mode dominates the output power in the coaxial vircator studied. [J141]

"Reflectometer sensing of rf waves in front of the high harmonic fast wave antenna on NSTX"

The ability to measure rf driven waves in the edge of the plasma can help to elucidate the role that surface waves and parametric decay instabilities (PDIs) play in rf power losses on NSTX. A microwave reflectometer has recently been modified to monitor rf plasma waves in the scrape-off layer in front of the 30MHz high harmonic fast wave antenna array on NSTX. In rf heated plasmas, the plasma-reflected microwave signal exhibits 30MHz sidebands, due primarily to the modulation of the cutoff layer by the electrostatic component of the heating wave. Similarly, electrostatic parametric decay waves (when present) are detected at frequencies below the heating frequency, near 28, 26,...MHz, separated from the heating frequency by harmonics of the local ion cyclotron frequency of about 2MHz. In addition, a corresponding frequency matched set of decay waves is also detected near the ion cyclotron harmonics at 2, 4,...MHz. The rf plasma-wave sensing capability is useful for determination of the PDI power threshold as a function of antenna array phasing (including toroidal wavelength), outer gap spacing, and various plasma parameters such as the magnetic field and the plasma current. [J142]

"New diagnostic techniques and technologies at JET (invited)"

The European Fusion Development Agreement's mission for JET is the development of ITER scenarios exploiting the specific properties of the device. This task requires significant improvements in the measuring techniques. The most innovative diagnostic upgrades are in the fields of edge measurements, detection of fast magnetohydrodynamics modes and "burning plasma" diagnostics. The importance of plasma-wall interactions, and, in particular, the issue of tritium inventory promoted the development of the quartz microbalance, a detector with improved time resolution to measure material redeposition in the remote areas of the inner divertor. Measurement of Alfvén cascades with unprecedented spectral resolution, reaching a toroidal number of up to 16, was obtained using an O-mode microwave reflectometer as an interferometer. For the diagnosis of the fusion products, a new approach is being developed to measure the He ash based on double charge exchange between thermalized particles and neutrals from JET beams. There have been several upgrades of the neutron diagnostic systems, one of which, the new time of flight neutron spectrometer designed for high counting rates is described. [J143]

"New diagnostic systems on HL-2A"

Three new diagnostic systems have been presented in this article: (1) the pulse molecular beam injection as a modulated particle source and microwave reflectometry for investigation of the particle transport, (2) a new three-step electrostatic probe array for zonal flow studying, and (3) eight-channel laser interferometer with 6mHCN laser for electron density profile measurement with good spatial resolution. The main experimental results have also been shown briefly. [J144]

"Role of neutral molecule chemistry in electron cyclotron resonance microwave plasmas capable of diamond deposition"

The chemical compositions of 4% carbon in hydrogen/deuterium electron cyclotron resonance (ECR) microwave plasmas based on ethane, ethylene, acetylene, and methane, as determined by supersonic pulse, plasma sampling mass spectrometry, have been kinetically modeled using only a steady-state concentration of hydrogen to represent the role of the plasma. Using 375 isotopically labeled chemical steps based on 54 reversible neutral molecule chemical reactions, simulated spectra were generated that matched all eight experimental spectra using only literature values of the kinetic and energetic constants and three physically reasonable fitted parameters that were held constant for all eight simulations. The success of the modeling provides strong evidence that the chemistry of ECR-microwave plasmas is dominated by neutral molecule reactions. [J145]

"Microwave plasma burner and temperature measurements in its flames"

An apparatus for generating flames and more particularly the microwave plasma burner for generating high-temperature large-volume plasma flame was presented. The plasma burner is operated by injecting liquid hydrocarbon fuels into a microwave plasma torch in air discharge and by mixing the resultant gaseous hydrogen and carbon compounds with air or oxygen gas. The microwave plasma torch can instantaneously vaporize and decompose the hydrogen and carbon containing fuels. It was observed that the flame volume of the burner was more than 50 times that of the torch plasma. While the temperature of the torch plasma flame was only 550K at a measurement point, that of the plasma-burner flame with the addition of 0.025lpm (liters per minute) kerosene and 20lpm oxygen drastically increased to about 1850K. A preliminary experiment was carried out, measuring the temperature profiles of flames along the radial and axial directions. [J146]

"Searching for O-X-B mode-conversion window with monitoring of stray microwave radiation in

LHD"

In the Large Helical Device, the stray microwave radiation is monitored by using so-called sniffer probes during electron cyclotron heating. In monitoring the stray radiation, we changed the microwave beam injection angle and search the O-X-Bmode-conversion window to excite electron Bernstein waves (EBWs). When the microwave beam is injected toward the vicinity of the predicted O-X-Bmode-conversion window, the electron temperature rises in the central part of overdense plasmas. In that case, the stray radiation level near the injection antenna becomes low. These results indicate that monitoring the stray radiation near the injection antenna is helpful in confirming the effectiveness of excitation of EBWs simply without precise analysis. [J147]

"Microwave imaging reflectometry in LHD"

A multichannel reflectometry with an imaging optical system is under development for the measurement of the electron density fluctuations in the Large Helical Device (LHD). The right-hand cutoff layer is utilized as a reflection surface. The angle of an ellipsoidal mirror installed inside the vacuum chamber is remotely adjustable with the ultrasonic motor in order to optimize the illumination angle for the wider range of the plasma parameters. An oscillation due to density fluctuation was observed using the microwave imaging reflectometry for the first time in LHD plasma experiment. [J148]

"Fast gas injection as a diagnostic technique for particle confinement time measurements"

The determination of the effective particle confinement time (τ_p^*), i.e., the particle confinement time normalized to recycling coefficient, is difficult when its value is long compared to the discharge duration in magnetically confined plasmas. Recent experiments on the current drive experiment upgrade (CDX-U) spherical torus have successfully achieved a significant reduction in recycling with large-area liquid lithium plasma-facing surfaces. The low recycling walls result in an increase in particle pumping and make it possible to measure τ_p^* in short duration plasmas. Measurements of τ_p^* are made using a supersonic gas injector which is closely coupled to plasma. A fast gas pulse is emitted from the supersonic gas injector, after which the density decay is measured using a microwave interferometer. The design of the supersonic gas injector and its configuration on CDX-U will be presented. The results of this technique will be shown as applied to the study of the effects of a liquid lithium toroidal limiter and evaporative lithium coatings on overall plasma density and τ_p^* . [J149]

"Electron and metastable state interactions in two-step ionization waves"

We demonstrate the use of a microwave hairpin resonator to measure the time-dependent, phase-resolved electron number density in ionization waves. Under our argon glow discharge conditions, the instability was caused by two-step ionization; and the wave frequency depended on the volume quenching rate of the metastable states. We measured the 1s5 metastable state density using diode laser absorption. The peak electron number density lagged behind the peak metastable state density by 60°. This phase shift reveals the nonlocal nature of the electron kinetics due to two-step ionization. [J150]

"Atmospheric-pressure hybrid plasma with combination of ac and microwave"

A hybrid plasma system with combination of ac and microwave at atmospheric pressure was developed. The hybrid plasma is initiated by ac capillary plasma, is stabilized by a flowing channel of working gas through common electrodes, and is expanded by the dissipation of microwave energy, revealing two distinguishable plasma columns of about 1 mm length and a transition point. The capillary in the hybrid plasma system is working as a common electrode for the microwave and ac plasmas. Optical emission spectroscopy is used to characterize and monitor the argon and nitrogen excited species produced in different plasma columns. [J151]

"Multichannel ultrashort pulsed radar reflectometer on LHD"

An ultrashort pulsed radar reflectometer with 24 channels in the K band and four channels in the X band is used for the electron density profile measurements in the Large Helical Device. An ultrashort pulse has broadband frequency components. However, we have usually utilized the discrete frequency components because we apply a filter bank system in a time-of-flight measurement. To utilize the whole frequency spectrum of the impulse we apply the switching technique of the intermediate frequency signal and the frequency modulation of the local oscillator. A more detailed reconstructed electron density profile, compared to that of the previous system, is obtained by using an Abel inversion method from the profile of the delay time as a function of the probing frequency. [J152]

"Electron density fluctuation measurements using a multichannel microwave interferometer in GAMMA 10"

Measurement of fluctuation in plasma is important for studying the improvement in plasma confinement by the formation of the plasma confinement potential. The density fluctuation is observed by microwaves by methods such as interferometry, reflectometry and Fraunhofer diffraction method. We have constructed a new multichannel microwave interferometer to measure the plasma density and fluctuation radial profiles in a single plasma shot. We successfully measured the time-dependent density and line-integrated density fluctuation radial profiles in a single plasma shot using the multichannel microwave interferometer. Thus, we have developed a useful tool for studying the improvement in plasma confinement by the formation of plasma confinement potential. [J153]

"Ultrafast millimeter-wave frequency-modulated continuous-wave reflectometry for NSTX"

The millimeter-wave frequency-modulated continuous-wave (FM-CW) reflectometer on NSTX is a multichannel system providing electron density profile measurements with a frequency coverage of 13-53GHz[corresponding O-mode density range of (0.21-3.5) $\times 10^{13}\text{cm}^{-3}$]. Recently, this system has been modified to allow ultrafast full-band sweeps for repetition intervals down to 10 μs . For this system to function as a fluctuation diagnostic it is crucial to eliminate artifacts in the phase derivative caused by nonlinearities in the frequency sweep; we introduce a simple hardware technique for reducing these artifacts to 0.3%. For NSTX, the additional bandwidth ($\leq 100\text{kHz}$) greatly enhances the capability of the FM-CW reflectometer as a diagnostic for low frequency magnetohydrodynamics instabilities (e.g., internal kinks, resistive wall modes, neoclassical tearing modes, as well as fast-particle driven fishbones and low frequency toroidal Alfvén eigenmodes). [J154]

"X -mode reflectometry measurements in the JET plasma core region"

The X-mode radial correlation reflectometry diagnostic on JET has long suffered from strong signal attenuation in the original transmission lines. To reach higher performances, new low-attenuation corrugated circular waveguides and a new cluster of six antennas have been successfully installed in Autumn 2005. The increase of the signal-to-noise ratio using these new transmission lines is found to be on the order of magnitude of 20dB, thus enabling good quality of reflectometry measurement. With the benefit of this improvement, first X-mode reflectometry measurements of density fluctuations in the core region of the JET plasma are reported in this article. [J155]

"Cold atmospheric plasma in nitrogen and air generated by the hybrid plasma source"

Generation of long plumes of cold atmospheric plasma in nitrogen and air has been successfully performed by the hybrid hollow electrode activated discharge (H-HEAD) source. The source with a simple cylindrical electrode terminated by a gas nozzle combines the microwave antenna plasma with the hollow cathode plasma generated inside the gas nozzle by pulsed dc power. The H-HEAD source is capable of generating up to 10 cm long plumes in air at microwave powers below 500 W and at air flow rates as low as 100 sccm (standard cubic centimeter per minute). The corresponding flow rates in the nitrogen plasma are even less than 80 sccm. The discharges in air and nitrogen have similar shapes and are comparable with the corresponding plasma columns in argon. A comparison of the optical emission spectra of the plasma in nitrogen and air is presented. The temperatures generated on steel substrates by interaction with nitrogen and air plasma columns at different microwaves and dc powers are compared with the corresponding effects in argon plasma. [J156]

"Characteristic Study of a Portable Arc Microwave Plasma Torch"

The development of a plasma torch, which carries desirable features to be an ignition aide within a supersonic combustor, is studied. The desirable features include: 1) a microwave adaptor arrangement to couple additional power (from microwave as well as arc discharge) to the plasma torch; 2) an additional port for fuel injection; and 3) compactness (including the power supply), portability, and light weight. The plasma jet generated by this torch is described by the cycle energy of the discharge and by the imaging of its plume under various conditions, supply air pressures, and microwave (on or off) to the torch. This torch system, with its high-voltage discharge, is operated in periodic (60-Hz) mode. The capacitors in the circuit of the power supply are charged at a line frequency of 60 Hz, resulting in a cyclical discharge. The cycle energy reaches up to 12 J. The microwave electric field has a profound effect on the arc discharge. It intensifies the emission and increases the volume of the arc loop region. It also enhances the electron temperature significantly, as shown by the emission spectroscopy of the torch. The spatial distribution of the microwave electric field outside the nozzle of the torch module is not affected by the supersonic crossflow, which is a favorable feature for increasing the penetration depth of the torch plume into the supersonic crossflow in the combustor [J157]

"Microwave diagnostics of laser-induced avalanche ionization in air"

This work presents a simplified model of microwave scattering during the avalanche ionization stage of laser breakdown and corresponding experimental results of microwave scattering from laser breakdown in room air. The model assumes and measurements confirm that the breakdown regime can be viewed as a point dipole scatterer of the microwave radiation and thus directly related to the time evolving number of electrons. The delay between the laser pulse and the rise of the microwave scattering signal is a direct measure of the avalanche ionization process. [J158]

"Remote experiment of ultrashort-pulse reflectometry for large helical device plasmas"

An ultrashort-pulse reflectometer (USPR) has been applied to the large helical device plasmas in National Institute for Fusion Science for edge density profile measurement. Remote control system using super science information network has been introduced to the USPR system. The remote console at Kyushu University having graphical user interface is prepared to control the instruments of the USPR via the general-purpose interface bus. The operations such as the adjustment of supply voltage fed to amplifiers and the frequency doubler, timing control of the impulse, data acquisition, and monitoring can be performed from the remote site. The position of transmitter and receiver antennas can also be controlled remotely in order to observe the cutoff layer depending on various plasma conditions. The directly recorded signal by a sampling scope is analyzed and reconstructed by means of the signal record analysis method. [J159]

"Analysis of multifrequency interferometry in a cylindrical plasma"

A microwave interferometer operating simultaneously at 70, 90, and 110GHz is used to measure line integrated electron density in a plasma column in the VX-20 experiment. Interferometer beam sizes are a significant part of the plasma radius at some locations. We model the wave propagation through the plasma using a scalar wave approximation with assumptions of a Gaussian beam profile and plasma spatial profile. The phase shifts obtained from this model are compared with standard thin beam calculations and experimental data. [J160]

"Homodyne reflectometer for neutral beam injection interlock on large helical device"

Neutral beam injection (NBI) into low-density plasmas can cause serious damage to the vacuum vessel wall. It is necessary to stop the NBI when the plasma terminates. This needs a reliable density monitor for NBI interlock. A three-channel homodyne reflectometer, installed on a large helical device was used for an NBI interlock. Microwaves of 28.5, 34.9, and 40.2GHz were injected with Omode polarization. At present, a simple homodyne detection scheme is used. The reflected signal consists of a dc component due to local and reflected power and an ac component due to fluctuations in the position of the cutoff layer. Since the change in dc signal was very small, the root mean square value of the ac signal was used as the interlock signal. At present the 34.9GHz Omode channel, whose Omode cutoff density is $1.54 \times 10^{19} \text{m}^{-3}$, is used for the interlock. The system has been working since the first NBI experiments on LHD in 1999. [J161]

"Multilayer vacuum window for wide-band microwave plasma diagnostic systems"

Microwave diagnostics, e.g., reflectometry and electron cyclotron emission in plasma machines, often require large windows displaying low attenuation and reflection on a wide band, in addition to some basic features such as vacuum tightness and mechanical robustness. Wide-band matching is usually achieved by coating the window with dielectric layers of suitable permittivity and thickness. On the vacuum side the coating must also be vacuum compatible and resistant to the thermal radiation coming from plasma. On the RFX machine, to satisfy these requirements, a boron nitride disk properly machined on the surface facing the plasma has been clamped to the existing fused silica window. The addition of a Teflon layer on the air side allowed to attain power reflection coefficients as low as 0.025 in the frequency ranges of 26.5-40, 40-56, and 56-75GHz and as low as 0.01 in the frequency ranges of 75-92 and 92-110GHz. [J162]

"Retrieval of information about turbulence in rain by using Doppler-polarimetric Radar"

This paper considers new possibilities of turbulence intensity retrieval by using Doppler and Doppler-polarimetric radar sounding. Peculiarities of microwave scattering on moving droplets of different size and shape underlie new methods that are introduced, discussed, and checked by using radar data [J163]

"Resonant reradiation of electromagnetic waves by thin conductors with transverse gaps"

Transverse gaps are introduced in thin-wire conductors to extend the region of phase variations of currents that are induced on them by an incident electromagnetic wave. Periodically placed gaps lead to qualitative changes in the properties of reradiated waves, such as the appearance of resonances corresponding to total reflection and total transmission of the incident wave. It is shown that total reflection occurs in a narrow band and depends very

weakly on the incident angle of the illuminating radiation. This idea leads to novel filters and switches, whose operation is practically independent of the structure of the incident wave. Total resonant reflection can occur for conductors with high optical transparency, a property that is useful for various microwave diagnostic devices. Because of the increased radiation resistance of such structures, the resonant effects under consideration depend weakly on conductivity. For gratings made using these conductors with gaps stacked above a metal ground plane, it is possible to controllably collimate the rays. Expansion of the scattered fields in terms of Rayleigh's series, together with Poisson's summation formula, are used for numerical simulations of such structures. [J164]

"A 5-by-5 element coupled oscillator-based phased array"

Design, fabrication, and test of a 25-element planar coupled oscillator based phased array is described. The array operates at S-band and is shown to produce an agile beam which is steerable via adjustment of the perimeter oscillator tuning biases only. A phase diagnostic system is described which displays the aperture phase distribution during the far field measurements of the radiated beam. Measured results are presented both with and without the diagnostic system present. Without the diagnostic system, the beam pointing was achieved by setting the perimeter oscillator biases to be values previously used in the measurements with the diagnostic system present. The far field was then measured without the benefit of a knowledge of the aperture phase distribution. Finally, the results of far field measurements are described in which the beam position was incremented from a position previously measured with the diagnostic system in place to a new position by incrementing the perimeter oscillator biases by a fixed amount. [J165]

"Real time polarization monitor developed for high power electron cyclotron resonance heating and current drive experiments in large helical device"

The polarization state of a wave is an important factor in electron cyclotron resonance heating (ECRH) and current drive (ECCD), for it strongly affects the propagation and absorption of the wave in the plasma. A real-time monitor of the polarization of the EC beam has been developed for use in ECRH/ECCD experiments in large helical device (LHD). Two orthogonal components of the wave field are measured in one of the miter-bends by use of a specially designed coupler and a waveguide circuit with a 0° - 90° phase switch to deduce the polarization parameters: the polarization angle α and the ellipticity β . Since fast-response pin diodes are used for the switches, the polarization is determined every 3 ms, facilitating real time acquisition of the polarization. This article reports on the design and the principle of this monitor as well as on the algorithm used to calculate α and β . This article also reports on the method of calibration, for the accuracy of this measurement depends on it. Finally, a comparison is made between polarization parameters measured by a monitor actually installed on one of the ECRH transmission lines on LHD and the value set by the polarizer in ECRH experiments. [J166]

"Phase measurement algorithm without phase jump"

A phase comparator provides two outputs proportional to the cosine and sine of the input phase difference. A new algorithm is devised which calculates the phase from the comparator outputs without a phase jump and without the limit of 2π . Instead of calculating the absolute phase at a given time, it calculates the relative phase differences between two subsequent measurements and accumulates them to get the absolute phase. The phase jump can be avoided if the sampling time is selected fast enough that the phase variation does not exceed 2π during the sampling period. [J167]

"The effect of the gas flow-rate on the radial structure of a torch-like helium plasma"

The effect of the gas flow-rate on the radial structure of a torch-like helium microwave plasma has been studied by measuring the radial distributions of emission intensity of spectral lines from helium and from the air that surrounds the discharge. It has been found that increasing the gas flow-rate leads to an increase of the maximum of the spectral lines and a shift of these emission peaks toward the plasma edge. Apart from that, it is found that the entrainment of air into the plasma increases with the flow-rate. [J168]

"Pulsed microwave discharges sustained at atmospheric pressure: study of the contraction and filamentation phenomena"

Contraction and filamentation phenomena are studied in a neon atmospheric-pressure microwave discharge sustained in a pulsed-power regime. The time evolution of the discharge is observed by means of an intensified charge coupled device (ICCD) and analyzed in terms of nonuniform gas heating and electromagnetic skin effect. [J169]

"Electron and ion sheath effects on a microwave "hairpin" probe"

A microwave measurement of electron density in low-pressure plasmas can be based on a hairpin probe. The hairpin forms a transmission line that supports a quarter-wavelength standing wave. The resonance is related to the relative permittivity of the surroundings, and hence, in a plasma, electron density can be evaluated. For improved fidelity, a general model is developed to include the effects of positive and negative space-charge sheaths formed around the hairpin wires. The former tends to lower the resonance, whereas the latter tends to raise it initially. This is qualitatively in agreement with experiments in dc argon plasmas. [J170]

"Magnetic pull: biological effects or medical applications?"

One of the questions on the IMS 2005 Quiz, is related to the magnetic fields used in magnetic resonance imaging (MRI) machines. In particular, it asked: an MRI (magnetic resonance imaging) machine uses: a) high-intensity static magnetic fields; b) time-varying magnetic fields in the kHz range; c) radio-frequency (RF) fields in the MHz range; and d) All of the above. The correct answer, d) All of the above, highlights the fact that an MRI machine employs all three types of fields in order to accomplish three-dimensional imaging for medical diagnostics. Therefore, in terms of safety, electromagnetic field exposure to patients and medical personnel needs to be assessed for all three types of fields. This is a much greater concern for open MRI systems, where the magnet surrounds the patient only partially in order to allow the medical personnel to perform procedures on the patient, guided by the MRI images. The IEEE Committee on Man and Radiation (COMAR) is in the final stages of preparing a technical information statement (TIS) on the subject. [J171]

"Thermal inequilibrium of atmospheric helium microwave plasma produced by an axial injection torch"

The population density of several excited states has been obtained spectroscopically in a helium plasma sustained by a torch device at atmospheric pressure as a function of the radius in the plasma for different conditions of microwave power and plasma gas flow. The ground-state atom density is determined from the gas temperature, which is deduced from the rotational temperature of the molecular nitrogen ions. The population distribution is fitted to the theoretical results of a collisional-radiative model that includes particle transport. A large deviation of the measured populations is found from the theoretical populations for local thermodynamic equilibrium. The plasma at any radial position is far from local thermodynamic equilibrium; the equilibrium deviation parameter of the ground state is larger than 10 000. The equilibrium deviation parameters of the measured excited-state populations obey the theoretical $\ln N$ -exponential law. [J172]

"Transition from diffuse to filamentary domain in a 9.5 GHz microwave-induced surface discharge"

The transition from the low-pressure diffuse to the high-pressure filamentary domain of a 9.5GHzmicrowave-induced surface discharge in air is recorded. The discharge employs several half-wavelength initiators that locally enhance the electric field to achieve breakdown in the higher-pressure subcritical region. Visible light imaging illustrates the qualitative changes in discharge morphology over the pressure range 4.5to760Torr(0.6to100kPa). [J173]

"Microwave-tomographic imaging of the high dielectric-contrast objects using different image-reconstruction approaches"

Microwave tomography is an imaging modality based on differentiation of dielectric properties of an object. The dielectric properties of biological tissues and its functional changes have high medical significance. Biomedical applications of microwave tomography are a very complicated and challenging problem, from both technical and image reconstruction point-of-views. The high contrast in tissue dielectric properties presenting significant advantage for diagnostic purposes possesses a very challenging problem from an image-reconstruction prospective. Different imaging approaches have been developed to attack the problem, such as two-dimensional (2-D) and three-dimensional (3-D), minimization, and iteration schemes. The goal of this research is to study imaging performance of the Newton and the multiplicative regularized contrast source inversion (MR-CSI) methods in 2-D geometry and gradient and MR-CSI methods in 3-D geometry using high-contrast, medium-size phantoms, and biological objects. Experiments were conducted on phantoms and excised segment of a pig hind-leg using a 3-D microwave-tomographic system operating at frequencies of 0.9 and 2.05 GHz. Both objects being of medium size (10-15 cm) possess high dielectric contrasts. Reconstructed images were obtained using all imaging approaches. Different approaches are evaluated and discussed based on its performance and quality of reconstructed images. [J174]

"Time-resolved measurements of electron number density and collision frequency for a fluorescent

lamp plasma using microwave diagnostics"

Microwave interferometry is an established nonperturbing plasma diagnostic technique to measure plasma number density that is simple, accurate, robust, and reliable. This paper reports a related microwave diagnostic method that measures both the electron number density and the electron-neutral collision frequency, which are crucial to understanding the behavior and transport coefficients of plasma. This method measures the attenuation and phase shift of a microwave signal propagating through a plasma with a network analyzer. These measured quantities are related to the real and imaginary parts of the plasma index of refraction by Appleton's equations, which contain the electron number density and collision frequency. Since the electron number density and collision frequency can be obtained directly from measured quantities, one need not know the electron energy distribution function, the electron kinetic temperature, or the electron energy-dependent cross section for the collision process to determine the electron collision frequency. The experimental measurements used to illustrate the method are a paired comparison of the time-resolved electron number density and collision frequency of two types of commercial fluorescent lamps: the "standard" mercury-based lamp, and the recently introduced "green" low mercury lamp. Since the plasma properties are periodic at 60 Hz, time-resolved measurements could be made by using the external triggering feature of the network analyzer. Data were taken to illustrate the variation of electron number density and collision frequency during one 60-Hz cycle of the fluorescent lamp plasmas. [J175]

"Negative hydrogen ion sources for accelerators"

A variety of H-ion sources are in use at accelerator laboratories around the world. A list of these ion sources includes surface plasma sources with magnetron, Penning and surface converter geometries as well as magnetic-multipole volume sources with and without cesium. Just as varied is the means of igniting and maintaining magnetically confined plasmas. Hot and cold cathodes, radio frequency, and microwave power are all in use, as well as electron tandem source ignition. The extraction systems of accelerator H-ion sources are highly specialized utilizing magnetic and electric fields in their low energy beam transport systems to produce direct current, as well as pulsed and/or chopped beams with a variety of time structures. Within this paper, specific ion sources utilized at accelerator laboratories shall be reviewed along with the physics of surface and volume H-production in regard to source emittance. Current research trends including aperture modeling, thermal modeling, surface conditioning, and laser diagnostics will also be discussed. [J176]

"Microwave Measurement of Decaying Plasma in Liquid Helium"

Decaying plasma in a microwave cavity filled with liquid helium (LHe, hereafter) is studied. An X-band TE₁₁₃ mode cylindrical cavity is filled with LHe, and a high-voltage pulse with duration 7 μ s, voltage 20 kV, and current 360 A is applied between a tungsten needle electrode and a thin stainless-steel mesh which separates an adjacent small discharge space from the cavity. The transmission signals through the cavity show the presence of decaying plasma in LHe with decay time on the order of 200 ms for a temperature range from 4.2 to 2.3 K at saturating vapor pressure. The response signals are suppressed in the pressurized LHe, as well as in superfluid LHe below 2.17 K. Our estimated mass of the charged carriers just after the pulsed discharge, assuming a diffusion loss mechanism, is much less than the value known as an effective mass of heavy ions which were produced by a steady-state ion source in LHe measured by Poitrenaud and Williams (1972). Our experimental observation suggests that the heavy effective mass of ions in LHe might take time to develop to its full extent. [J177]

"Observations of gain on the I (2 P_{1/2} → 2 P_{3/2}) transition by energy transfer from O (2 Δ g) generated by a microwave discharge in a subsonic-flow reactor"

The excitation of I(2P_{1/2}) in the reactions of discharge-generated O₂(a¹ Δ g) and O(3P) with I₂ has been investigated in a microwave discharge-flow reactor at 1.5 Torr and 350 K using a suite of optical absorption and emission diagnostics to detect O₂(a¹ Δ g), O, I(2P_{1/2}), and I(2P_{3/2}) with high sensitivity. For O₂(a¹ Δ g) yields of 0.20-0.25 generated by the microwave discharge, positive gain on the I(2P_{1/2} → 2P_{3/2}) transition at 1.315 μ m was observed when O concentrations were reduced by reaction with added NO₂. The results imply quenching mechanisms for I(2P_{1/2}) which are much faster than direct collisional deactivation by O. [J178]

"2.45 GHz microwave-excited atmospheric pressure air microplasmas based on microstrip technology"

A plasma system based on microstrip technology was developed for the generation of atmospheric pressure microplasmas. A discharge gap was placed between the striplines and the ground plane on the transverse cross section in the direction of microwave propagation. This microstrip structure permits the concentration of electric fields at the discharge gap, which is confirmed by a computer simulation using the three-dimensional simulation

code based on the finite-difference time-domain method, and can produce atmospheric pressure plasmas even in air. The microplasmas were sustained in the discharge gap (width: 0.2 mm, length: 6 mm) at a microwave power of 1 W. The experimentally measured rotational temperature of nitrogen molecules was 800 K, indicating these plasmas to be nonthermal plasmas. This plasma system will provide a portable microplasma system utilizing a small semiconductor microwave source and a large-scale atmospheric pressure nonthermal plasma using the array configuration. [J179]

"Characterization of the cold atmospheric plasma hybrid source"

Parameters of the hybrid hollow electrode activated discharge (H-HEAD) source for cold atmospheric plasma applications are described. The source with a simple cylindrical electrode terminated by a gas nozzle combines the microwave antenna plasma with the hollow cathode plasma generated inside the nozzle by a pulsed dc power. The source can produce over 15 cm long plasma plumes at less than 200 sccm of argon and 100 sccm of neon flowing in open air at the microwave power of 400 W (2.4 GHz). Parameters of the hybrid plasma are controlled by both the microwave power and the power delivered to the hollow cathode. An anomalous effect of a sharp increase in the length of the plasma plume at low gas flows is discussed. Results of the optical emission spectroscopy in argon and neon are presented. Optical spectra confirmed the presence of Ti and Fe from the hollow cathode in the plasma. The production of metal increases with the power applied to the hollow cathode. Traces of Ti from the hollow cathode have been found at substrates positioned as far as 2 cm from the cathode. This finding confirms the possibility to use the H-HEAD source for atmospheric physical vapor deposition (PVD) and hybrid PVD and plasma-enhanced chemical-vapor deposition of composite films. [J180]

"Properties of atmospheric pressure plasmas with microwave excitations for plasma processing"

Atmospheric pressure plasmas with microwave excitations were successfully produced in dielectric barrier micro plasmas employing N₂, Ar, or He gas. N₂ optical emissions of the second positive system were measured for evaluating the gas temperature. The gas temperatures of the plasmas could be much less than 1000 K. Blackbody emissions were measured by Fourier transform infrared spectrometer for evaluating the electrode temperature. Temperatures of both the gas and electrode were evaluated by fitting the experimental results with calculations. The gas temperature in the N₂ plasma was notably increased with the discharge time as compared with those in Ar and He plasmas. It was found that the pulsed discharge and the water-cooled electrode were effective for reducing the gas temperature. The pulsed discharge decreased the gas temperature from 900 to 600 K, and the water-cooled electrode decreased the gas temperature by more than 200 K. Controlling the temperature of the electrodes was the most effective technique to reduce the gas temperature, because the gas temperature was in equilibrium with the electrode temperature. [J181]

"Microwave diagnostics of small plasma objects"

We suggest an approach for using microwave radiation in collisional, weakly ionized plasma diagnostics when plasma dimensions are relatively small compared with the microwave wavelength. We show that in this case the microwave diagnostics can be based on the measurement of the radiation scattered by an oscillating plasma dipole, similar to the Rayleigh scattering of an atom in light. Examples considered show possibilities of obtaining the decaying plasma parameters (time dependence of charge density and information about loss rates, for instance) from the measured scattered signal. [J182]

"Ultrahigh-speed etching of organic films using microwave-excited nonequilibrium atmospheric-pressure plasma"

An ultrahigh etch rate (24 μm/min at 155°C and 0.3 μm/min at 325°C) of an organic film was successfully achieved using a microwave-excited nonequilibrium atmospheric-pressure plasma source employing He and O₂ gases. This has the potential to be applied to various kinds of fabrication of structures for microelectromechanical systems and bionanotechnology. A stable glow discharge was realized between the narrow gap (200 μm) electrodes covered with a dielectric film in atmospheric pressure. The etching characteristics were investigated by changing the O₂ flow rate and the distance of the substrate from the electrode. In order to clarify the ultrahigh etching mechanism, in situ diagnostic methods, including two-dimensional imaging of optical emissions in the plasma with an intensified charge-coupled device camera, electron-density evaluation using the Stark-broadened profile of the hydrogen Balmer beta line in optical emission spectroscopy, and two dimensional spatial distribution of ozone density measured with ultraviolet absorption spectroscopy, have been performed. It was found that O atoms were the dominant etching species for ultrahigh-speed etching of the organic film, and the effect of ozone on the etching process was negligible. [J183]

"Etching process of silicon dioxide with nonequilibrium atmospheric pressure plasma"

An ultrahigh etch rate (14mcm/min) of SiO₂ and a high selectivity of SiO₂/Si over 200 were achieved using a microwave-excited nonequilibrium atmospheric pressure plasma source employing He, NF₃, and H₂O gases, which have been developed for application to microelectromechanical systems and other bionanotechnology fields. In order to clarify the etching mechanism, two diagnostic methods have been performed: (1) imaging of plasma emission with an intensified charge-coupled device camera, and (2) absorption measurements using Fourier transform infrared spectroscopy. The etching characteristics are discussed in relation to the spatial distributions of the species involved. The etch rate depended considerably on the distance between the plasma and the substrate. Some radicals generated from the feed gases reached the substrate directly, while other radicals recombined into different species, which reached the substrate. An abundance of HF molecules were produced through a reaction between radicals generated by the atmospheric pressure discharge of NF₃ and H₂O. From these measurements, it has been found that the HF molecules generated played a role in producing the high etch rate of SiO₂ and high etch selectivity of SiO₂/Si. [J184]

"Electrodynamics of microwave near-field probing: Application to medical diagnostics"

A theory for the near-field (NF) microwave diagnostics of planar-stratified media is developed based on the design of an equivalent NF probe circuit and the solution of the electrodynamical problem for the electromagnetic field of antenna in an inhomogeneous ambient medium. The theory has been verified experimentally by probing into water with controllable dielectric permittivity. A theoretical and experimental study into a possibility to locate contrast structures (malignant growths) within biological media by means of NF probing has been carried out. Detectable contrasts of a growth have been calculated depending on its dimensions and depth of occurrence. Two-dimensional images of a tumorlike contrast object have been obtained for different depths of the object submersion in water. A measurement technique reducing the masking effect of background fluctuations arising by probe contact with a pliant surface is proposed. [J185]

"2-D imaging of electron temperature in Tokamak plasmas"

By taking advantage of recent developments in millimeter wave imaging technology, an electron cyclotron emission imaging (ECEI) instrument, capable of simultaneously measuring 128 channels of localized electron temperature over a two-dimensional (2-D) map in the poloidal plane, has been developed for the TEXTOR tokamak. Data from the new instrument, detailing the magnetohydrodynamic (MHD) activity associated with a sawtooth crash, is presented. [J186]

"On line-ratio analysis for helium-argon microwave discharges"

Regarding spectroscopy diagnostics via line-intensity ratio of high-density diffusion-controlled discharges in helium-argon gas mixtures, the study presents a collisional-radiative model of the discharge. In order to show variations of excited-state population densities and line-intensity ratios related to changes of plasma density and electron temperature, the model is applied to surface-wave-sustained discharges, since the axial structure of these discharges displays self-consistent variations of the discharge characteristics. The comparison with the corona model shows the necessity of developing a collisional-radiative model. Possibilities for simultaneous determination based on the collisional-radiative model of electron temperature and plasma density from measurements of line-intensity ratios are outlined. [J187]

"Control of uniformity of plasma-surface modification inside of small-diameter polyethylene tubing using microplasma diagnostics"

A hollow-cathode microplasma was used to modify the luminal surface of small-diameter polyethylene (PE). We make use of two microplasma diagnostics to monitor the plasma properties during the treatment process. A microwave cavity was used to measure the density of the microplasma. Emitted light from the microplasma was fed into a monochromator at various positions along the PE tube to assess uniformity of the microplasma. Effectiveness of plasma treatments were evaluated using the capillary-rise method at various positions along the tubing. We show a correlation between the properties of the inner surface of the PE tubing and the light emitted from the plasma. A Poly(ethylene oxide) (PEO) surfactant was immobilized to the luminal surface of the PE tubing using the microplasma discharge. An in vitro blood-circulation loop was constructed to test the hemato-compatibility of the PE tubes. After blood exposure, scanning electron microscope images were taken to assess the density of adhering platelets along the length of the tubes. The plasma-treated tubing showed fewer blood adherents than the untreated tubing. By suitably controlling the pressure drop along the tube, the uniformity of the microplasma treatment along the tubing can be optimized. [J188]

"Microstrip microwave induced plasma on a chip for atomic emission spectral analysis"

A stable microstrip microwave plasma (MSP) operated at atmospheric pressure with a power of some 10-20 W and at a gas flow of 0.2-0.8 L/min of argon in a resonant structure produced with the aid of microstructuring technology on a 545 cm² quartz wafer provided with a 0.6-mm diameter plasma channel is described. The device is shown to be useful for the excitation of atomic and molecular species and for the atomic emission spectrometric determination of metals and of nonmetals in gases at the trace level, down to the ng/L-level, as shown for the case of sulfur. [J189]

"Characteristics of an arc-seeded microwave plasma torch"

The design and operation of a portable microwave plasma torch is presented. An arc plasma torch running at 60 Hz and generated by a torch module is installed on the bottom wall in the narrow section of a tapered S-band rectangular cavity, and is used to seed the microwave discharge at the location where the microwave electric field is at a maximum. This tapered cavity is designed to support the TE₁₀₃ mode. With seeding, only low Q cavity and moderate microwave power (time average power of 700 W) are needed. The microwave-enhanced discharge increases the size, cycle energy, and duty cycle of the torch plasma considerably. This torch can be run without introducing gas flow to stabilize the arc and microwave discharges. Adding gas flow can increase not only the size of the torch plasma, but also its cycle energy which reaches a plateau of about 12 J/per cycle for a gas flow rate exceeding 0.393 l/s. The electron density and excitation temperature, and the composition of torch species are determined by emission spectroscopy. It is shown that, at the bottom of the torch close to the cavity wall, electrons distribute quite uniformly across the core of the torch with density and excitation temperature determined to be about $7.4 \times 10^{13} \text{ cm}^{-3}$ and 8000 K, respectively. It is also found that this torch produces an abundance of reactive atomic oxygen. [J190]

"Terahertz technology in biology and medicine"

Terahertz irradiation and sensing is being applied for the first time to a wide range of fields outside the traditional niches of space science, molecular line spectroscopy, and plasma diagnostics. This paper surveys some of the terahertz measurements and applications of interest in the biological and medical sciences. [J191]

"New tools and series for forward and inverse scattering problems in lossy media"

A convenient rewriting of the pertinent integral equation is exploited to introduce a new model for two-dimensional electromagnetic scattering by dielectric objects in lossy media. Exploiting this latter, a new series expansion is introduced to solve the forward problem accurately and effectively. The first term of such a series coincides, in particular situations, with the well-known extended Born approximation. Theoretical tools and results are given on the range of applicability and rate of convergence of the series, which favorably compares with the traditional Born one. These tools allow noticing that the new model exhibits a lower "degree of nonlinearity" with respect to parameters embedding dielectric characteristics as compared to the traditional model, thus suggesting its exploitation in the solution of the inverse problem. Numerical examples assessing effectiveness and convenience of the proposed models, tools and inversion methods are presented. [J192]

"Biomedical engineering's contribution to defending the homeland"

Reports on technological and biomedical initiatives being taken in Japan to counter bioterrorism. These include: telemedicine; noncontact vital sign monitoring using microwave radar; biomedical optical imaging of trauma diagnostics; antimicrobial photodynamic therapy; and biological weapon response. [J193]

"Millimeter-wave-induced hypoalgesia in mice: dependence on type of experimental pain"

Millimeter-wave therapy (MWT) is based on the systemic biological effects resulting from local exposure of skin to low-power electromagnetic waves of millimeter wavelength. The aims of the present study are to quantitatively evaluate hypoalgesic effects of MWT in murine experimental models of acute and chronic neuropathic pain, and to compare them with the previously determined MWT-induced hypoalgesia in an experimental model of chronic nonneuropathic pain, and also to assess the ability of local heating with a Holmium YAG laser to produce hypoalgesia in mice. The cold and hot water tail-flick tests and the unilateral chronic constriction injury (CCI) to the sciatic nerve were used as pain models. The MWT characteristics were: frequency = 61.22 GHz; average power density = 13.3 mW/cm²; duration of exposure = 15 min; and area of exposure = nose. This study demonstrated that a single MWT most effectively suppressed chronic nonneuropathic pain. Less effectively, a single MWT reduced pain sensitivity in the murine model of acute pain, and was ineffective in the model of chronic neuropathic pain. However, multiple MWT reduced the symptoms that developed following CCI. The local heating of the exposed area did not produce hypoalgesia. The findings support the use of MWT in chronic pain

states. [J194]

"Electron Cyclotron emission diagnostics for helical plasma in the large helical device"

Electron cyclotron emission (ECE) diagnostics have been developed in the large helical device (LHD). The ECE is transmitted over 80 m from the antenna to the spectrometer with the corrugated waveguide system, which has a low transmission loss ($\sim 30\%$). The polarization of ECE is identical for all frequencies, while the field angle varies from -40° to $+30^\circ$ on the ECE sight line. The ECE temperature measured by the Michelson, which is calibrated with a hot source, agrees well with Thomson scattering measurement in a wide range of the electron density. Magnetic island formation is investigated using the electron temperature profile measured with the Michelson. The radiometer is cross-calibrated to the Michelson and is employed for the study of fast phenomena, such as the sawtooth oscillation. Besides the normal ECE, tangential ECE is investigated in LHD in order to explore the potential of ECE diagnostics. [J195]

"Three-dimensional nonlinear image reconstruction for microwave biomedical imaging"

Active microwave imaging has attracted significant interests in biomedical applications, in particular for breast imaging. However, the high electrical contrasts in breast tissue also increases the difficulty of forming an accurate image because of the increased multiple scattering. To model such strong three-dimensional (3-D) multiple scattering effects in biomedical imaging applications, we develop a full 3-D inverse scattering algorithm based on the combination of the contrast source inversion and the fast Fourier transform algorithm. Numerical results show that our algorithm can accurately invert for the high-contrast media in breast tissue. [J196]

"A reconstruction procedure for microwave nondestructive evaluation based on a numerically computed Green's function"

This paper describes a new microwave diagnostic tool for nondestructive evaluation. The approach, developed in the spatial domain, is based on the numerical computation of the inhomogeneous Green's function in order to fully exploit all the available a priori information of the domain under test. The heavy reduction of the computational complexity of the proposed procedure (with respect to standard procedures based on the free-space Green's function) is also achieved by means of a customized hybrid-coded genetic algorithm. In order to assess the effectiveness of the method, the results of several simulations are presented and discussed. [J197]

"Rotational, vibrational, and excitation temperatures of a microwave-frequency microplasma"

Integration of microplasma sources in portable systems sets constraints in the amount of power and vacuum levels employed in these plasma sources. Moreover, in order to achieve good power efficiency and prevent physical deterioration of the source, it is desirable to keep the discharge temperature low. In this paper, the thermal characteristics of an atmospheric argon discharge generated with a low-power microwave plasma source are investigated to determine its possible integration in portable systems. The source is based on a microstrip split-ring resonator and is similar to the one reported by Iza and Hopwood, 2003. Rotational, vibrational, and excitation temperatures are measured by means of optical emission spectroscopy. It is found that the discharge at atmospheric pressure presents a rotational temperature of ~ 300 K, while the excitation temperature is ~ 0.3 eV (~ 3500 K). Therefore, the discharge is clearly not in thermal equilibrium. The low rotational temperature allows for efficient air-cooled operation and makes this device suitable for portable applications including those with tight thermal specifications such as treatment of biological materials. [J198]

"Modeling of noninvasive microwave characterization of breast tumors"

This paper describes an approach for the noninvasive microwave characterization of tumors in breast tissue. Tumors are modeled as lossy dielectric targets. Their complex natural resonances (CNR) can be extracted from the time-domain response and correlated with diagnostically useful properties. Finite-difference time-domain simulation is used to obtain the time-domain response from a tumor with a short electromagnetic pulse as an input. The normal breast tissue and tumor are modeled as dispersive media using the Debye model and CNRs are extracted using Prony's method. It is shown that the locations of the dominant CNRs are separated in the complex frequency plane as functions of the tumor dielectric properties. The technique has potential as a diagnostic tool to characterize breast lesions in conjunction with other imaging modalities such as ultrasound for detection. [J199]

"Microwave image reconstruction of tissue property dispersion characteristics utilizing multiple-frequency information"

A multiple-frequency-dispersion reconstruction algorithm utilizing a Gauss-Newton iterative strategy is presented

for microwave imaging. This algorithm facilitates the simultaneous use of multiple-frequency measurement data in a single image reconstruction. Using the stabilizing effects of the low-frequency measurement data, higher frequency data can be included to reconstruct images with improved resolution. The parameters reconstructed in this implementation are now frequency-independent dispersion coefficients instead of the actual properties and may provide new diagnostic information. In this paper, large high-contrast objects are successfully constructed utilizing assumed simple dispersion models for both simulation and phantom cases for which the traditional single-frequency algorithm previously failed. Consistent improvement in image quality can be observed by involving more frequencies in the reconstruction; however, there appears to be a limit to how closely spaced the frequencies can be chosen while still providing independent new information. Possibilities for fine-tuning the image reconstruction performance in this context include: 1) variations of the assumed dispersion model and 2) Jacobian matrix column and row weighting schemes. Techniques for further reducing the forward solution computation time using time-domain solvers are also briefly discussed. The proposed dispersion reconstruction technique is quite general and can also be utilized in conjunction with other Gauss-Newton-based algorithms including the log-magnitude phase-form algorithm. [J200]

"A novel method to prevent secondary exposure of medical and rescue personnel to toxic materials under biochemical hazard conditions using microwave radar and infrared thermography"

In order to prevent secondary exposure of medical personnel to toxic materials under biochemical hazard conditions, we performed a noncontact determination of exposure to toxic conditions via 1215-MHz microwave radar and thermography. A toxic condition was induced by intravenous administration of lipopolysaccharide (LPS) in rabbits. The exposure to LPS was determined by linear discriminant analysis using noncontact derived variables. [J201]

"Emission uniformity and shot-to-shot variation in cold field emission cathodes"

High-power microwave tubes require currents and voltages generally in excess of 1 kA and 100 kV. In the past, these system requirements led to the use of single shot machines, with repetition rates well under 1 Hz. With advances in pulsed power, the Air Force Research Laboratory recently began to investigate the performance of field emission diodes at repetition rate operation. Greater numbers of shots allowed better accuracy in measurements and the application of better statistics to experimental data. In this paper, we report on new measurements that, with better experimental accuracy, show the statistical correlation between emission uniformity and the shot-to-shot variation in diode current. We report on a comparison to particle-in-cell simulations. These comparisons show the importance of randomly occurring nonemission regions on the cathode surface in dictating the spread in current data. These results imply that uniformity, in addition to playing an important role in any electron interaction with radiation, also affects the current stability for any device using these cathodes. Finally, these experiments show that for repetition rate machines, shot-to-shot variation quantified in terms of Gaussian distributions characterized by a standard deviation and skewness, provide a diagnostic capable of inferring beam uniformity in situations where direct uniformity diagnostics prove extremely difficult or impractical. [J202]

"Characterization of relaxation-oscillation noise in continuous-wave traveling wave tubes"

Extremely low noise levels are frequently required in radar and communication systems that utilize microwave tubes. A noise waveform frequently found in continuous-wave (CW) linear-beam microwave tubes is a relaxation-type oscillation that has a period typically on the order of several milliseconds. This paper provides an extensive experimental characterization of this relaxation-oscillation phenomenon by recording the corresponding signal modulations on the output of several solenoid-focused CW traveling wave tubes. The characteristics of these amplitude and phase modulations were studied during systematic variations of tube operating parameters that included magnetic field, cathode voltage, depressed collector voltage, heater filament voltage, and input drive level. A measurement technique was also developed with the capability to obtain detailed information on the growth of the relaxation-oscillation noise waveforms along the beam interaction region by comparing reflected and output noise waveforms. [J203]

"Upgrade to the control system of the reflectometry diagnostic of ASDEX upgrade"

The broadband frequency modulation-continuous wave microwave/millimeter wave reflectometer of ASDEX upgrade tokamak (Institut für Plasma Physik (IPP), Garching, Germany) developed by Centro de Fusão Nuclear (Lisboa, Portugal) with the collaboration of IPP, is a complex system with 13 channels (O and X modes) and two types of operation modes (swept and fixed frequency). The control system that ensures remote operation of the diagnostic incorporates VME and CAMAC bus based acquisition/timing systems. Microprocessor input/output boards are used to control and monitor the microwave circuitry and associated electronic devices. The

implementation of the control system is based on an object-oriented client/server model: a centralized server manages the hardware and receives input from remote clients. Communication is handled through transmission control protocol/internet protocol sockets. Here we describe recent upgrades of the control system aiming to: (i) accommodate new channels; (ii) adapt to the heterogeneity of computing platforms and operating systems; and (iii) overcome remote access restrictions. Platform and operating system independence was achieved by redesigning the graphical user interface in JAVA. As secure shell is the standard remote access protocol adopted in major fusion laboratories, secure shell tunneling was implemented to allow remote operation of the diagnostic through the existing firewalls. [J204]

"Frequency modulation continuous wave reflectometry measurements of plasma position in ASDEX Upgrade ELMy H-mode regimes"

Plasma position measurements of frequency modulation continuous wave reflectometry are analyzed in ASDEX Upgrade ELMy H-mode regimes [International Thermonuclear Energy Reactor (ITER) reference scenario], to assess the viability of using reflectometry for position and shape control purposes in ITER. Plasma separatrix position is estimated both at the low and high field sides of the tokamak. A scaling factor applied to the linear average density (an ITER online measurement) is used to estimate the separatrix density, whose position is then tracked using reflectometry profile measurements. Edge localized mode (ELM) activity effects are overcome by disregarding measurements performed during the onset and magnetohydrodynamic phases of the ELMs. Position data is compared, with data derived from the magnetics and its quality is assessed using one dimensional full-wave numerical simulations, taking into account the influence of the nonprobed edge plasma region (O-mode operation) and of the plasma turbulence. Results indicate that selecting an adequate scaling to the linear average density leads to a good estimate of the separatrix position, even when the pedestal is out of the measuring range, which will be the case of ITER position reflectometer. [J205]

"Frequency hopping millimeter wave reflectometer"

Reflectometry techniques are employed to study density fluctuations in fusion plasmas either using one channel or two channels with slightly different frequencies, to probe simultaneously closely spaced plasma layers (for radial correlation studies). The present article describes a novel system with increasing measuring capability utilizing only one single frequency that can be hopped during the discharge. This broadband fast hopping mm-wave reflectometer (BFHR) has been developed for both ASDEX upgrade (Max Planck Institute-Garching-Germany) and TJ-II stellarator (CIEMAT-Spain). The BFHR incorporates frequency synthesizers at microwave frequencies multiplied into the millimeter-wave range and uses heterodyne detection for sensitive phase and amplitude measurements. [J206]

"Effects of asymmetry and target location on microwave imaging reflectometry"

In this article we perform a numerical study of microwave imaging reflectometry (MIR) and compare it with conventional reflectometry system. As an approximation to the reflections by real plasma fluctuations, a corrugated wheel is used. As far as general performance is concerned, our simulations confirm the results by Munsat et al [Plasma Phys. Controlled Fusion 45, 469 (2003)] that the MIR system reproduces shape of corrugation far from the wheel while conventional systems fail to do so. We addressed the effects of asymmetry and defocusing of the wheel-reflectometer system as well as spectral sensitivity of the imaging reflectometer. For a particular geometry we estimated the deterioration of the MIR performance due to misalignments and existence of broadband fluctuations. [J207]

"Microwave scattering system design for rho e scale turbulence measurements on NSTX"

Despite suppression of rho iscale turbulent fluctuations, electron thermal transport remains anomalous in NSTX. For this reason, a microwave scattering system will be deployed to directly observe the omega and k spectra of rho escale turbulent fluctuations and characterize the effect on electron thermal transport. The scattering system will employ a Gaussian probe beam produced by a high power 280GHzmicrowave source. A five-channel heterodyne detection system will measure radial turbulent spectra in the range $kr=0-20\text{cm}^{-1}$. Inboard and outboard launch configurations cover most of the normalized minor radius. Improved spatial localization of measurements is achieved with low aspect ratio and high magnetic shear configurations. This article will address the global design of the scattering system, such as choice of frequency, size, launching system, and detection system. [J208]

"Evaluation of tapered slot antennas for use in multichannel reflectometers"

We have evaluated a Fermi antenna newly designed in Xband for use in a multichannel reflectometer. The Fermi antenna is a tapered slot antenna provided with both a Fermi-Dirac-function-type tapered slot structure

and a corrugated structure along the antenna edge in order to improve radiation patterns of the linearly tapered slot antenna. We attained a 3dB beam width of 32° in the Eplane and 37° in the Hplane at 12GHz. By optimizing the stripline dimensions according to an equivalent circuit model, a bandwidth of 8-18GHz with a voltage standing-wave ratio less than 2 is obtained. In the mockup experiments using a rotating metal cylinder, the experimental results are in good agreement with the predicted ones. [J209]

"Doppler backscattering system for measuring fluctuations and their perpendicular velocity on Tore Supra"

Backscattering of a microwave beam launched in oblique incidence makes possible measurement of density fluctuations close to the cut-off with a selected wave number $k = -2k_i$, where k_i is the beam wave vector at the reflection layer. On the system installed on Tore Supra, the incidence of the Gaussian beam is controlled thanks to a tiltable monostatic antenna. The microwave part of the system is based on a fluctuation reflectometer scheme with heterodyne detection, and the choice of a Vband (50-75GHz) microwave source and Omode polarization is appropriate for typical enhanced plasma regimes ($n_0 = 3-7 \times 10^{19} \text{ m}^{-3}$). Both the scattering wave number k and the scattering localization r/a can be changed during a shot, owing to the steppable probing frequency and the motorized antenna (tilt angle $0-10^\circ$). The wave-number range k is $4-15 \text{ cm}^{-1}$, with a wave-number resolution around 2 cm^{-1} , and the localization r/a 0.3-0.85. The Doppler effect also provides the perpendicular velocity profile for the same position range. Experiments confirm the diagnostic capabilities. [J210]

"Reduced adhesion of human blood platelets to polyethylene tubing by microplasma surface modification"

A hollow-cathode microplasma modified the luminal surface of small-diameter polyethylene (PE) tubing. A microwave cavity diagnostic was used to measure the density of the microplasma. Plasma light output was observed with a monochromator at various positions along the PE tube to assess uniformity. Treatment effectiveness was evaluated by measuring the variation in capillary rise at various positions along the tubing. A correlation between the properties of the inner surface of the PE tubing and the emitted light intensity was found. A poly(ethylene oxide) surfactant was immobilized to the luminal surface of the PE tubing with an argon microplasma discharge. To test hemocompatibility, an in vitro blood-flow loop circulated heparinized human blood through both a plasma-treated and -untreated PE tubes, simultaneously. After blood exposure, the tubes were examined with a scanning electron microscope to assess the density of adhering platelets along the length of the tubes. By modifying the plasma parameters, the uniformity of the microplasma treatment along the tubing can be optimized. [J211]

"Determination of titanium temperature and density in a magnetron vapor sputtering device assisted by two microwave coaxial excitation systems"

We present an optical absorption diagnostic technique devoted to the simultaneous determination of titanium density and temperature during sputtering of Ti. These measurements were performed in a type of ionized physical vapor deposition reactor, consisting of a magnetron sputtering device assisted by two microwave systems for the ionization of the sputtered vapor of the magnetron. Our goal is to optimize the ionization in this reactor in order to improve the deposition process (film quality, recovery of the layers, etc.) compared to standard magnetron sputtering systems. In order to determine both titanium neutral and ion densities, we have used a titanium hollow cathode vapor lamp powered with pulsed power supply. Measurements were carried out at different positions in the reactor at different pressures (1-15 Pa). We have studied the effect of magnetron current from 100 mA to 2 A and of microwave power from 100 W to 1 kW. At lower pressures, we have shown that the titanium is not thermalized close to the magnetron, whereas it is thermalized at 10 Pa at all positions. The neutral titanium density is typically between 10^{10} and $3 \times 10^{11} \text{ cm}^{-3}$, and the ion density is 10^9 cm^{-3} . The effect of microwave power is the decrease of neutral titanium density and the increase of its temperature. At a position located 1 cm after the crossing of the microwave plasma area, we showed that the illumination of the microwave plasma increases the degree of ionization of Ti from 2% to 10%. copyright 2004 American Vacuum Society. [J212]

"Investigation and modeling of plasma-wall interactions in inductively coupled fluorocarbon plasmas"

Plasma-wall interactions in fluorocarbon based feedgas chemistries, namely CF_4 , are examined in a standard inductively coupled Gaseous Electronics Conference reference cell using in situ Fourier-transform infrared spectroscopy and microwave interferometry. Measurements show the dissociation of the CF_4 feedgas into radical CF_x species, as has been observed elsewhere [M. J. Goeckner and R. A. Breun, J. Vac. Sci. Technol. A 11, 3 (1993)], and qualitatively reveal a decrease in plasma-wall interactions as wall temperature is increased.

Experimental results such as plasma density, 10^{11} cm^{-3} , and CF_4 density 10^{13} cm^{-3} , are further compared to results from the hybrid plasma equipment model [R. Kinder and M. J. Kushner, J. Vac. Sci. Technol. A 19, 76 (2001)] to better elucidate the influence of wall temperature on plasma exposed surfaces and sticking coefficients. Last, CF_4 vibrational temperatures were also measured, revealing that the line-averaged vibrational temperature remains at a constant 40-60 K above the chamber wall temperature while the vibrational temperature in the center of the discharge is significantly higher. Moreover, the vibrational temperatures are further compared to results from a global thermal model and are in good agreement. copyright 2004 American Vacuum Society. [J213]

"Development of an integrated pellet diagnostic system for fueling pellets"

We developed a new diagnostic system of the hydrogen ice pellets for fueling into plasma devices. The system consists of three parts. They are: a light gate system, a microwave mass detector, and a shadowgraph system. This system provides the pellet velocity, mass and shape, simultaneously. In particular, by using multiple mirror system, the light gate system can achieve high detective probability with high signal to noise ratio for submillimeter pellets. At the results of the bench tests carried out on GAMMA 10 and the Large Helical Device, the light gate system completely detected the pellets used in the bench tests and the pellet velocity was estimated by using this system. Similarly, the shadowgraph system was available for the pellet. The microwave mass detector was found to be applicable. These results show the capability of simultaneous measurement of the pellet parameters using this diagnostic system. [J214]

"Excessive Balmer line broadening in microwave-induced discharges"

Results of a hydrogen Balmer line-shape study on microwave-induced plasma discharges operated with pure hydrogen and with argon-hydrogen or helium-hydrogen mixtures are reported. Plasma is generated in a rectangular or coaxial microwave cavity in two separate experiments. In both cases, the emission profiles of the Balmer lines did not show excessive broadening as reported by Mills et al [J. Appl. Phys. 92, 7008 (2002)]. copyright 2004 American Institute of Physics. [J215]

"Spectroscopic diagnostics and modeling of Ar /H₂ /C H₄ microwave discharges used for nanocrystalline diamond deposition"

In this paper Ar/H₂/CH₄ microwave discharges used for nanocrystalline diamond chemical vapor deposition in a bell-jar cavity reactor were characterized by both experimental and modeling investigations. Discharges containing 1% CH₄ and H₂ percentages ranging between 2% and 7% were analyzed as a function of the input microwave power under a pressure of 200 mbar. Emission spectroscopy and broadband absorption spectroscopy were carried out in the UV-visible spectral range in order to estimate the gas temperature and the C₂ density within the plasma. Infrared tunable diode laser absorption spectroscopy was achieved in order to measure the mole fractions of carbon-containing species such as CH₄, C₂H₂, and C₂H₆. A thermochemical model was developed and used in order to estimate the discharge composition, the gas temperature, and the average electron energy in the frame of a quasihomogeneous plasma assumption. Experiments and calculations yielded consistent results with respect to plasma temperature and composition. A relatively high gas temperature ranging between 3000 and 4000 K is found for the investigated discharge conditions. The C₂ density estimated from both experiments and modeling are quite high compared with what is generally reported in the literature for the same kind of plasma system. It ranges between 10^{13} and 10^{14} cm^{-3} in the investigated power range. Infrared absorption measurements and model predictions indicate quite low densities of methane and acetylene, while the atomic carbon density calculated by the model ranges between 10^{13} and 10^{15} cm^{-3} . The methane and hydrogen introduced in the feed gas are subject to a strong dissociation, which results in a surprisingly high H-atom population with mole fraction ranging between 0.04 and 0.16. Result analysis shows that the power coupling efficiency would range between 70% and 90%, which may at least explain the relatively high values obtained, as compared with those reported in the literature for similar discharges, for gas temperature and C₂ population. The high H-atom densities obtained in this work would indicate that growing nanocrystalline diamond films would experience a very high etching. Simulation results also confirm that sp species would play a key role in the surface chemistry that governs the diamond growth. [J216]

"Development of a high-current microwave ion source for proton linac application systems"

A microwave hydrogen ion source was developed to improve reliability, and to increase operation time of proton linac application systems. The ion source needs no filament in the discharge chamber, which leads to better reliability and less maintenance time. The developed source produced a maximum hydrogen ion beam current of 70 mA (high current density of 360 mA/cm², beam energy of 30 keV) with a 5 mm diam extraction aperture and 1.2 kW microwave power. The proton fraction was increased with an increase in rf power and reached around

90% at 1 kW. Measured 90% beam normalized emittance was 0.4 pi mm mrad. Rise times of rf power and beam current to 90% of the final values were about 30 and 35 ns, respectively, at a pulse operation mode with 400 ns pulse width and 100 Hz repetition rate. The dynamic range of beam currents was enlarged (3-63 mA) in the pulse mode with a modified rf wave form to assist ignition of microwave discharge. These performance parameters will be desirable for pulse operation accelerator applications like proton therapy systems. A long time operation stability (150 h) was confirmed with a beam current of 51 mA; change in the current was 2%. copyright 2004 American Institute of Physics. [J217]

"H-ion production in electron cyclotron resonance driven multicusp volume source"

We have used the existing magnetic multicusp configuration of the large volume H-source Camembert III to confine the plasma created by seven elementary multidipolar electron cyclotron resonance (ECR) sources, operating at 2.45 GHz. We varied the pressure from 1 to 4 mTorr, while the total power of the microwave generator was varied between 500 W and 1 kW. We studied the plasma created by this system and measured the various plasma parameters, including the density and temperature of the negative hydrogen ions which are compared to the data obtained in a chamber with elementary ECR sources without multicusp magnetic confinement. The electron temperature is lower than that obtained with similar elementary sources in the absence of the magnetic multicusp field. We found that at pressures in the range from 2 to 4 mTorr and microwave power of up to 1 kW, the electron temperature is optimal for H-ion production (0.6-0.8 eV). This could indicate that the multicusp configuration effectively traps the fast electrons produced by the ECR discharge. copyright 2004 American Institute of Physics. [J218]

"Diagnosis of plasmas in compact ECR ion source equipped with permanent magnet"

A compact electron cyclotron resonance (ECR) ion source equipped with permanent Nd₂Fe₁₄B magnets for mass spectrometry is presented, and the plasma density and electron temperature of the generated plasma are characterized using a Langmuir probe. The compact ion source is only 22.5 mm in internal diameter (1 in. tube), and 56 mm in length, and operates at high microwave frequencies of 7-10 GHz. A permanent ring magnet is introduced to establish a dispersive magnetic field in the ECR zone, and the effect of the position of the magnet is investigated. The plasmas are generated at low pressures of 10-150 mPa, at which the electron temperature and plasma density vary in the range 1-9 eV and 10¹⁶-10¹⁷ m⁻³. From an investigation of the effects of input power, pressure, and magnet position, mode jumps of the plasma discharge are observed with increasing input power, and the magnet position is found to be crucial to the tuning of the ion source. copyright 2004 American Institute of Physics. [J219]

"Wave cutoff method to measure absolute electron density in cold plasma"

A method for precise measurements of absolute electron density in plasma using wave cutoff is described. This method of measurement uses a network analyzer with radiating and detecting antenna. A microwave signal of 10 kHz-3 GHz frequency is introduced into the plasma from a radiating port of the network analyzer and propagates in the plasma. The transmitted wave is monitored at a distance from a radiating antenna using an antenna connected to the receiving port of the network analyzer. The transmitted wave decays rapidly at a cutoff plasma frequency, which is a direct measure of the absolute electron density. This cutoff method is free of many difficulties often encountered with a Langmuir probe, such as thin film deposition and plasma potential fluctuation. The cutoff probe can also measure the spatial distribution of the electron density. The measurement technique is analyzed theoretically and experimentally, demonstrated in density measurements of an inductively coupled radio-frequency plasma, and is compared with the double probe and a plasma oscillation methods. [J220]

"Single sideband modulator, a key component of Tore-Supra heterodyne reflectometers"

Although single sideband modulation offers a simple solution to active heterodyne devices and is common in devices working over 150 GHz, it has been scarcely used for reflectometers. For a few years, large bandwidth (12-20 GHz), high performance single sideband modulators (SSBM) have been available. For higher frequency application, a sideband rejection around -25 dB seems necessary to ensure that the image sideband amplitude remains low after a frequency multiplier. A SSBM provided by Miteq Company presents high enough rejection levels to be assembled with frequency multipliers. Based on this SSBM, we developed a simple microwave scheme suitable for all Tore-Supra reflectometers-from 50 to 155 GHz, dedicated either to density profile reconstruction or to density fluctuation measurements. Compared to the double sideband modulator previously used, SSBM offers higher signal to noise ratio and enables fixed frequency measurements, paving the way for new measurement techniques. [J221]

"Simple structure holey-plate ion source"

A high-efficiency, lightweight, and low-cost microwave ion source, created and sustained by evanescent waves emitted from a parallel-plate type source with a holey-plate has been studied. This source is called a holey-plate (HP) ion source. The microwaves at 2.45 GHz propagate inside the parallel-plate structure and then are converted into an evanescent mode through the use of a HP with 3-mm-diam holes. The plate dimensions are 100 mm \times 140 mm and are separated by 10 mm. In these experiments, the entire unit of the parallel plate is placed in a vacuum chamber. Dense plasma is produced only on the HP. A 78 mm \times 108 mm argon ion beam is extracted from the HP using a single grid with 3-mm-diam holes. The ion current densities are in excess of 1.2 mA/cm² at an extraction voltage of 500 V. copyright 2004 American Institute of Physics. [J222]

"Imaging of ECR plasmas with a pinhole x-ray camera"

X-ray plasma images were made at the 14.5 GHz electron cyclotron resonance ion source of ATOMKI using a pinhole and a high resolution CCD camera. This method has good spatial resolution as well as the capability of postprocessed energy filtering of the images. During the measurements low and high charge state Ar, Xe, and Fe plasmas were produced with simultaneous beam extraction. Full-size and selected region images were recorded and analyzed. Full-size x-ray images show the spatial positions of different sources of x rays (bremsstrahlung, characteristic lines of plasma and wall ions) within low-charged ECRIS plasmas. Images of selected plasma regions (extraction slit, magnet pole, magnet gap) offer a better understanding of the effect of important tuning parameters (bias disk voltage, gas mixing, microwave power, magnetic field strength, etc.) commonly used to produce highly charged plasmas and beams. copyright 2004 American Institute of Physics. [J223]

"A new plasma potential measurement instrument for plasma ion sources"

A very efficient and fast instrument to measure the plasma potential of ion sources has been developed at the Department of Physics, University of Jyväskylä (JYFL). The operating principle of this novel instrument is to apply a decelerating voltage into a mesh located in the beamline of the ion source. The plasma potential is determined by measuring the current at the grounded electrode situated behind the mesh as a function of the voltage. In this article, we will introduce the instrument and the first results. In the experiments, the instrument was connected to the beamline of the JYFL 6.4 GHz electron cyclotron resonance ion source. The plasma potential was measured with different source conditions and it was observed to vary between 30-65 V. The plasma potential tended to increase as the microwave power, or the gas feed rate, was increased. These results are consistent with earlier observations and estimations. It was also noticed that the value of the plasma potential changed when the negative voltage applied to the biased disk at the injection of the ion source was varied. Complementary to optical plasma diagnostics, such an instrument can be used as a very efficient tool to get a precise relationship between plasma conditions and extracted beams. [J224]

"Application of microwave reflectometry to register Alfvén wave resonances in the TCABR tokamak"

Application of microwave reflectometry to study Alfvén wave resonances in the TCABR tokamak is described. A microwave reflectometer was used to register plasma density oscillations driven by the excited Alfvén waves, under the condition of the spectrum scanned by a controlled plasma density rise. It is shown that when the position of the local Alfvén resonance r_A , which is defined by the relation $\omega = k \parallel (r_A) C_A(r_A)$, is close to the plasma zone where the microwave signal is reflected, the high-frequency modulation of the output signal of the reflectometer at the rf generator frequency increases. This method can give information about the localization of the rf power deposition zone in Alfvén wave plasma heating and current drive experiments. It also allows finding the plasma current profile in the region of the rf power deposition. copyright 2004 American Institute of Physics. [J225]

"Simultaneous microwave imaging system for density and temperature fluctuation measurements on TEXTOR (invited)"

Diagnostic systems for fluctuation measurements in plasmas are, of necessity, evolving from simple one-dimensional (1D) systems to multidimensional systems due to the complexity of the magnetohydrodynamics (MHD) and turbulence physics of plasmas as illustrated by advanced numerical simulations. Using the recent significant advancements in millimeter wave imaging technology, microwave imaging reflectometry (MIR) and electron cyclotron emission imaging (ECEI), simultaneously measuring density and temperature fluctuations, have been developed for Toroidal EXperiment for Technology Oriented Research (TEXTOR). The MIR system was installed on Textor and the experiment was performed in September, 2003. Subsequent MIR campaigns have yielded poloidally resolved spectra and assessments of poloidal velocity. The 2D ECE imaging system (with

a total of 128 channels), installed on TEXTOR in December, 2003, successfully captured the first true 2D images of Tefluctuations of $m=1$ oscillations ("sawteeth") near the $q = 1$ surface. [J226]

"Compact microwave imaging system to measure spatial distribution of plasma density"

We have developed an advanced microwave interferometric system operating in the Kband (18-27GHz) with the use of a fan-shaped microwave based on a heterodyne detection system for measuring the spatial distribution of the plasma density. In order to make a simple, low-cost, and compact microwave interferometer with better spatial resolution, a microwave scattering technique by a microstrip antenna array is employed. Experimental results show that the imaging system with the microstrip antenna array can have finer spatial resolution than one with the diode antenna array and reconstruct a good spatially resolved image of the finite size dielectric phantoms placed between the horn antenna and the micro strip antenna array. The precise two-dimensional electron density distribution of the cylindrical plasma produced by an electron cyclotron resonance has been observed. As a result, the present imaging system is more suitable for a two- or three-dimensional display of the objects or stationary plasmas and it is possible to realize a compact microwave imaging system. [J227]

"Instrument reflections and scene amplitude modulation in a polychromatic microwave quadrature interferometer"

A polychromatic microwave quadrature interferometer has been characterized using several laboratory plasmas. Reflections between the transmitter and the receiver have been observed, and the effects of including reflection terms in the data reduction equation have been examined. An error analysis which includes the reflections, modulation of the scene beam amplitude by the plasma, and simultaneous measurements at two frequencies has been applied to the empirical database, and the results are summarized. For reflection amplitudes around 10%, the reflection terms were found to reduce the calculated error bars for electron density measurements by about a factor of 2. The impact of amplitude modulation is also quantified. In the complete analysis, the mean error bar for high-density measurements is 7.5%, and the mean phase shift error for low-density measurements is 1.2° . [J228]

"Diode laser microwave induced plasma cavity ringdown spectrometer: Performance and perspective"

Recent studies combining an atmospheric-pressure plasma source (inductively coupled plasma or microwave induced plasma) with cavity ringdown spectroscopy (plasma-CRDS) have indicated significant promise for ultra-sensitive elemental measurements. Initial plasma-CRDS efforts employed an inductively coupled plasma as the atomization source and a pulsed laser system as the light source. In an effort to improve the portability and reduce the cost of the system for application purposes, we have modified our approach to include a compact microwave induced plasma and a continuous wave diode laser. A technique for controlling the coupling of the continuous wave laser to the ringdown cavity has been implemented using a standard power combiner. No acousto-optic modulator or cavity modulation is required. To test the system performance, diluted standard solutions of strontium (Sr) were introduced into the plasma by an in-house fabricated sampling device combined with an ultrasonic nebulizer. SrOH radicals were generated in the plasma and detected using both a pulsed laser system and a diode laser via a narrow band transition near 680 nm. The experimental results obtained using both light sources are compared and used for system characterization. The ringdown baseline noise and the detection limit for Sr are determined for the current experimental configuration. The results indicate that a plasma-CRDS instrument constructed using diode lasers and a compact microwave induced plasma can serve as a small, portable, and sensitive analytical tool. copyright 2004 American Institute of Physics. [J229]

"Abatement of perfluorinated compounds using microwave plasmas at atmospheric pressure"

Microwave plasmas sustained at atmospheric pressure, for instance by electromagnetic surface waves, can be efficiently used to abate greenhouse-effect gases such as perfluorinated compounds. As a working example, we study the destruction and removal efficiency (DRE) of SF₆ at concentrations ranging from 0.1% to 2.4% of the total gas flow where N₂, utilized as a purge gas, is the carrier gas. O₂ is added to the mixture at a fixed ratio of 1.2-1.5 times the concentration of SF₆ to ensure full oxidation of the SF₆ fragments, providing thereby scrubbable by-products. Fourier-transform infrared spectroscopy has been utilized for identification of the by-products and quantification of the residual concentration of SF₆. Optical emission spectroscopy was employed to determine the gas temperature of the nitrogen plasma. In terms of operating parameters, the DRE is found to increase with increasing microwave power and decrease with increasing gas flow rate and discharge tube radius. Increasing the microwave power, in the case of a surface-wave discharge, or decreasing the gas flow rate increases the residence time of the molecules to be processed, hence, the observed DRE increase. In contrast, increasing the tube radius or the gas-flow rate increases the degree of radial contraction of the discharge and, therefore, the

plasma-free space close to the tube wall: this comparatively colder region favors the reformation of the fragmented SF₆ molecules, and enlarging it lowers the destruction rate. DRE values higher than 95% have been achieved at a microwave power of 6 kW with 2.4% SF₆ in N₂ flow rates up to 30 standard l/min. copyright 2003 American Institute of Physics. [J230]

"Characterization of BCl₃/N₂ plasmas"

Optical emission spectroscopy, quadrupole mass spectrometry, and electron density measurements were used to study the effect of the percentage of N₂ on the characteristics of BCl₃/N₂ plasmas and their resulting etch processes. The etch rate of GaAs increased from 80 E/min in pure BCl₃ to over 1000 E/min in a 40:60 BCl₃:N₂ mixture (15 mTorr, 50 W, 20 sccm). The optical emission intensities of both molecular and atomic chlorine exhibited maxima near 30% N₂, and an argon actinometer indicated a large increase in argon emission as a function of the increase in N₂ percentage. Microwave measurements indicated that the average electron density increased only slightly with an increase in nitrogen percentage up to 60% N₂. Mass spectrometric analysis of the plasmas showed that both the dissociation of BCl₃ and the production of molecular chlorine were significantly enhanced by the addition of N₂. These results suggest that an increase in the electron temperature as a result of electron attachment heating (and possibly energy transfer from N₂ metastables) is responsible for the increased dissociation and enhanced production of etch species. copyright 2003 American Institute of Physics. [J231]

"Two-dimensional self-consistent microwave argon plasma simulations with experimental verification"

Optical emission spectroscopy (OES), absorption measurements, and thermal energy rate analysis were used in tandem with numerical models to characterize microwave argon plasmas. A WAVEMAT (model MPDR-3135) microwave diamond deposition system was used to generate argon plasmas at 5 Torr. Three excited state number densities (4p, 5p, and 5d) were obtained from the OES measurements, and a fourth excited state number density (4s) was obtained from the absorption measurements. Further, power absorbed in the substrate was monitored. A self-consistent two-dimensional argon model coupled with an electromagnetic field model and a 25-level two-dimensional (2D)-collisional-radiative model (CRM) was developed and validated with the experimental measurements. The 2D model provides the gas and electron temperature distributions, and the electron, ion, and 4s state number densities, which are then iteratively fed into the electromagnetic and CRM models. Both the numerically predicted thermal energy rates and excited state densities agreed, within the experimental and numerical uncertainties, with the experimental results. copyright 2003 American Institute of Physics. [J232]

"Recent advancements in microwave imaging plasma diagnostics"

Significant advances in microwave and millimeter wave technology over the past decade have enabled the development of a new generation of imaging diagnostics for current and envisioned magnetic fusion devices. Prominent among these are microwave electron cyclotron emission imaging, microwave phase imaging interferometers, imaging microwave scattering, and microwave imaging reflectometer systems for imaging Te and ne fluctuations (both turbulent and coherent) and profiles (including transport barriers) on toroidal devices such as tokamaks, spherical tori, and stellarators. The diagnostic technology is reviewed, and typical diagnostic systems are analyzed. Representative experimental results obtained with these novel diagnostic systems are also presented. copyright 2003 American Institute of Physics. [J233]

"High resolution infrared "vision" of dynamic electron processes in semiconductor devices (abstract)"

Infrared cameras have been traditionally used in semiconductor industry for noncontact measurements of printed circuit boards (PCBs) local overheating. While an effective way to prevent defective PCB application in a "find-problems-before-your-customer-do" manner, this conventional static (25-50 frames/s) and small spatial resolution (100 μm) approach is incapable, in principle, of explaining the physical reason for the PCB failure. What follows in this report is the demonstration of an IR camera based new approach in high-resolution dynamic study of electron processes responsible for single device performance. More specifically, time resolved two-dimensional visualization of current carrier drift and diffusion processes across the device base that happen in microsecond scale is of prime concern in the work. Thus, contrary to the conventional visualization-through-heating measurements, objective is mapping of electron processes in a device base through negative and positive luminescence (provoked by band-to-band electron transitions) and nonequilibrium thermal emission (provoked by intraband electron transitions) studies inside the region in which current flows. Therefore, the parameters of interest are not only a device thermal mass and thermal conductance, but also free carrier lifetime,

surface recombination velocity, diffusion length, and contact properties. The micro-mapping system developed consists of reflective type IR microscope coaxially attached to calibrated scanning IR thermal imaging cameras (3-5 and 8-12 μm spectral ranges, HgCdTe cooled photodetectors, scene spatial resolution of some 20 μm , minimum time resolved interval of 10 μs , and temperature resolution of about 0.5 $^{\circ}\text{C}$ at 30 $^{\circ}\text{C}$). Data acquisition and image processing (emissivity equalization, noise reduction by image averaging, and external triggering) are computer controlled. Parallel video channel equipped with a CCD camera permits easy positioning and focusing of 141 mm² object along the system optical axis. To motivate this diagnostics superiority, small area light emitting diodes and stripe lasers, light and microwave modulators, thermoelectric generators, and coolers were tested with respect to impact made on visualizing of uniformity of current and heat flows, as well as their divergence in space and time. copyright 2003 American Institute of Physics. [J234]

"Measurement of magnetic field pitch angle using motional Stark effect spectroscopy in the compact helical system"

A spectroscopy system, which consists of a zigzag charge coupled device and ferroelectric liquid crystal cells, has been developed to measure magnetic field pitch angles. The magnetic field pitch angle is derived from the polarization angle of sigma and pi components in the H α line measured with polarization sensitive spectroscopy. By using the spectroscopy system, the location of zero pitch angle is measured to shift outboard due to the Pfirsch-Schluter current by 28 ± 16 mm. This shift is consistent with that predicted by an equilibrium code. copyright 2003 American Institute of Physics. [J235]

"Correlation reflectometry for turbulence and magnetic field measurements in fusion plasmas (invited)"

For the interpretation of correlation reflectometry data a fast two-dimensional full wave code in which realistic plasma geometries are used has been developed. Results of this code are compared with experiments from which turbulence correlation lengths and fluctuation levels are extracted with statistical optics methods. It is shown that in general the measured reflectometer correlation length is not equal to the turbulence correlation length. The code is also used to study the possibility of O-X correlation reflectometry in FIRE for the determination of the local magnetic field strength. It was found that this is only possible at very low fluctuation levels. copyright 2003 American Institute of Physics. [J236]

"Electron cyclotron emission imaging on a large helical device"

In this article, we describe the electron cyclotron emission (ECE) imaging system applied to the Large Helical Device (LHD) at the National Institute for Fusion Science. The imaging system consists of focusing optics installed inside the vacuum chamber of LHD and planer-type detectors fabricated by monolithic microwave integrated circuit technology. The detector consists of the integration of a bowtie antenna, a down-converting mixer using a Schottky barrier diode, and heterojunction bipolar transistors (HBTs) on a GaAs substrate. The HBTs work as an intermediate frequency (IF) amplifier with a 10 GHz bandwidth and a 10 dB voltage gain. The ECE signal and local oscillator beam are irradiated from both sides of the detector. The ECE signals are down-converted at the mixers and the IF signal is fed to a filter bank with center frequencies of 1-8 GHz. The time evolution and the intensity of the ECE signals agree with those obtained by a conventional ECE heterodyne receiver. The cross-correlation spectra of the signals obtained with different IF frequencies (radial correlation) and different detectors (poloidal correlation) are obtained. copyright 2003 American Institute of Physics. [J237]

"Two-dimensional correlation measurements of electron cyclotron emission fluctuations on the stellarator Wendelstein 7-AS"

The miniaturization of receiver arrays permits the arrangement of numerous poloidally staggered radial sightlines of an electron cyclotron emission (ECE) diagnostic for the measurement of the electron temperature and its fluctuations, making two-dimensional (2D) imaging of the electron temperature and its fluctuations caused by plasma turbulence possible. For the stellarator W7-AS, the development of a fully monolithic microwave integrated circuit 150 GHz subharmonic mixer array is under development. As a first step, a 2D ECE system for the measurement of electron temperature fluctuations using four individual horn-reflector arrangements in conjunction with multichannel heterodyne radiometers was installed and set into operation. With Gaussian beam optics and four poloidally staggered sightlines, electron temperature fluctuations could be characterized in radial and poloidal directions simultaneously. First observations in purely electron cyclotron resonance heated stellarator plasmas reveal a broadband drift-wave feature. Earlier experiments showing a decrease of the electron temperature fluctuation level with increasing heating power were confirmed. Additionally, it was revealed, using the 2D ECE correlation radiometer, that an increased velocity shear might account for the decrease of the coherence length and thus for the reduction of the electron temperature fluctuation level.

copyright 2003 American Institute of Physics. [J238]

"Microwave imaging reflectometer for TEXTOR (invited)"

Understanding the behavior of fluctuations in magnetically confined plasmas is essential to the advancement of turbulence-based transport physics. Though microwave reflectometry has proven to be an extremely useful and sensitive tool for measuring small density fluctuations in some circumstances, this technique has been shown to have limited viability for large amplitude, high k_{θ} fluctuations and/or core measurements. To this end, a new instrument based on two-dimensional imaging reflectometry has been developed to measure density fluctuations over an extended plasma region in the TEXTOR tokamak. This technique is made possible by collecting an extended spectrum of reflected waves with large-aperture imaging optics. Details of the imaging reflectometry concept, as well as technical details of the TEXTOR instrument, are presented. Data from proof-of-principle experiments on TEXTOR using a prototype system is presented, as well as results from a systematic off-line study of the advantages and limitations of the imaging reflectometer. copyright 2003 American Institute of Physics. [J239]

"Early quasioptics of near-millimeter and submillimeter waves in IRE-Kharkov, Ukraine: from ideas to the microwave pioneer award"

This paper is about the early quasioptics of near-millimeter and submillimeter waves in IRE-Kharkov (Institute of Radio Physics and Electronics of the National Academy of Sciences of Ukraine) and the development of the hollow dielectric beam-waveguide (HDB) technology and measuring techniques of the near-millimeter and submillimeter wavelength ranges, with main application in hot plasma diagnostics. It presents the details of the development based on the declassified reports and the interviews of Y.M. Kuleshov and another key member of the quasioptics (QO) team, M. S. Yanovski. Y.M. Kuleshov and his team had already accumulated rich experience in developing waveguide measuring devices in the whole millimeter-wave range between 1954 and 1961. In 1994-1996, the research project "Ozero" was carried out with Y.M. Kuleshov as a principal investigator. The aim of the "Ozero" was to explore the feasibility of developing a kit of HDB-based measuring devices in the wavelength range $\lambda = 0.7$ to 1.7 mm. After the finish of "Ozero", in 1968-1971, the next R&D project called "Oliva" was granted by the same directorate of MRI. Its idea was to dwell on and refine the polarization principles in the measuring circuits for $\lambda = 0.5$ - 0.8 mm. HDB was patented only in 1969. Since the 1970s, the activities of the QO department were focused entirely on the development of HDB-based instruments and systems. Here, the major application area was hot plasma diagnostics in new large Tokamaks. They also dwelled in the development of the measuring techniques including reflectometry and polarimetry. Other HDB based systems elaborated in IRE include radars in the 1970-1980s and RCS testing ranges in the 1990s. [J240]

"Plasma frequency measurements for absolute plasma density by means of wave cutoff method"

A method for precise measurements of absolute electron density in the plasma using plasma frequency is developed. A microwave perturbation of a frequency is introduced to plasma from a network analyzer and transmits in the plasma. The transmitting wave at a distance from a radiating antenna is monitored using a spectrum analyzer to scan the perturbing frequency. The transmitting wave rapidly decays by a cutoff at the plasma frequency, which gives the absolute electron density. The transmitting waves of some frequency including plasma frequency are characterized. The measured plasma frequency by this method is coincident with that obtained by the plasma oscillation method. copyright 2003 American Institute of Physics. [J241]

"Comparison of NO titration and fiber optics catalytic probes for determination of neutral oxygen atom concentration in plasmas and postglows"

A comparative study of two different absolute methods NO titration and fiber optics catalytic probe (FOCP) for determination of neutral oxygen atom density is presented. Both methods were simultaneously applied for measurements of O density in a postglow of an Ar/O₂ plasma created by a surfatron microwave generator with the frequency of 2.45 GHz an adjustable output power between 30 and 160 W. It was found that the two methods gave similar results. The advantages of FOCP were found to be as follows: it is a nondestructive method, it enables real time measuring of the O density, it does not require any toxic gas, and it is much faster than NO titration. The advantage of NO titration was found to be the ability to measure O density in a large range of dissociation of oxygen molecules. copyright 2003 American Vacuum Society. [J242]

"Microwave and modulated optical reflectance studies of YBCO thin films"

Planar HTS microwave devices require high quality, homogeneous samples. In this paper, sensitive measurements of the microwave surface impedance of YBCO thin films using coplanar resonators are collated

with modulated optical reflectance (MOR) measurements. MOR provides a powerful noncontact, nondestructive and high resolution means of probing local variations in the quality of thin films at room temperature, and consequently has great potential for diagnostic testing of HTS films prior to microwave device patterning. Microwave and MOR inter-comparisons of four YBCO films patterned into 5.2 and 8 GHz coplanar resonators are presented. Superior global microwave response in the superconducting state, such as low surface impedance and low levels of nonlinearity at enhanced powers, correlate with the magnitude and spatial homogeneity of the room temperature MOR signals. The presence of defects in films is investigated using both techniques. Both large scale single defects and film inhomogeneity can be detected using MOR; however, the spatial resolution of the technique is not sufficient to detect single weak links on a sub-micron scale, whose presence can result in severely degraded microwave resonator performance. [J243]

"Sheet-shaped plasma production using microwave-plasma interaction with ECR region"

New phenomena in producing sheet-shaped plasma under electron cyclotron resonance (ECR) condition have been found and investigated by experiment. Sheet-shaped Ar plasma with density of 10^{18} m^{-3} was successfully obtained at 10-3 torr by using 2.45-GHz microwave with ECR condition. The plasma was generated uniformly and stably in the cross section of 15.5 cm width \times 2.0 cm thickness with the use of waveguide of the rectangular cross section under the quartz window in vacuum. The parameter region of stable sheet-shaped plasma production was made clear by experiments clarifying criteria in parameter map. It was found that the magnetic field strength corresponding to the position and the shape of ECR region was the most effective parameter affecting microwave propagation to control the shape of plasma. However, the uniformity of the sheet-shaped plasma width was poor over the distance of microwave wavelength λ under 1 kW of input power. Therefore, it was concluded that the microwave was absorbed quickly near ECR region and hardly propagates farther than λ to the direction of perpendicular to the magnetic field. The double sheet-shaped plasma was produced at some region and two peaks were relatively shifted to the direction of ECR. Also, the condition of sheet-shaped plasma production was different for helium gas. By the electron density measurement and semi-one-dimensional analysis, the differences of ionization cross section and diffusion coefficient perpendicular to the magnetic fields were important factors for electron density and the shape of sheet plasma. The qualitative interpretation of sheet-shaped plasma production is discussed. [J244]

"CW HI laser based on a stationary inverted Lyman population formed from incandescently heated hydrogen gas with certain Group I catalysts"

Each of the ionization of Rb^+ and cesium and an electron transfer between two K^+ ions (K^+/K^+) provide a reaction with a net enthalpy of an integer multiple of the potential energy of atomic hydrogen, 27.2 eV. The corresponding Group I nitrates provide these reactants as volatilized ions directly or as atoms by undergoing decomposition or reduction to the corresponding metal. The presence of each of the reactants identified as providing an enthalpy of reaction of an integer of that of the potential energy of atomic hydrogen ($n \cdot 27.2 \text{ eV}$) formed a low applied temperature, extremely low-voltage plasma called a resonance transfer (RT)-plasma having strong vacuum ultraviolet (VUV) emission. In contrast, magnesium and aluminum atoms or ions do not ionize at integer multiples of the potential energy of atomic hydrogen. $\text{Mg}(\text{NO}_3)_2$ or $\text{Al}(\text{NO}_3)_3$ did not form a plasma and caused no emission. For further characterization, we recorded the width of the 6563 E Balmer α line on light emitted from RT-plasmas. Significant line broadening of 18, 12, and 12 eV was observed from an RT-plasma of hydrogen with KNO_3 , RbNO_3 , and CsNO_3 , respectively, compared to 3 eV from a hydrogen microwave plasma. These results could not be explained by Stark or thermal broadening or electric field acceleration of charged species since the measured field of the incandescent heater was extremely weak, 1 V/cm, corresponding to a broadening of much less than 1 eV. Rather the source of the excessive line broadening is consistent with that of the observed VUV emission, an energetic reaction caused by a resonance energy transfer between hydrogen atoms and K^+/K^+ , Rb^+ , and cesium, which serve as catalysts. KNO_3 and RbNO_3 formed the most intense plasma. Remarkably, a stationary inverted Lyman population was observed in the case of an RT-plasma formed with potassium and rubidium catalysts. These catalytic reactions may pump a continuous wave HI laser as predicted by laser equations and a collisional radiative model used to determine that the observed overpopulation was above threshold. [J245]

"Comparison of excessive Balmer α line broadening of inductively and capacitively coupled RF, microwave, and glow-discharge hydrogen plasmas with certain catalysts"

From the width of the 656.3-nm Balmer α line emitted from inductively and capacitively coupled radio frequency (RF), microwave, and glow-discharge plasmas, it was found that inductively coupled RF helium-hydrogen and argon-hydrogen plasmas showed extraordinary broadening corresponding to an average hydrogen atom energy of 250-310 and 180-230 eV, respectively, compared to 30-40 and 50-60 eV, respectively, for the corresponding capacitively coupled plasmas. Microwave helium-hydrogen and argon-hydrogen plasmas showed significant

broadening corresponding to an average hydrogen atom energy of 180-210 and 110-130 eV, respectively. The corresponding results from the glow-discharge plasmas were 33-38 and 30-35 eV, respectively, compared to ≈ 4 eV for plasmas of pure hydrogen, neon-hydrogen, and xenon-hydrogen maintained in any of the sources. Similarly, the average electron temperatures T_{e} for helium-hydrogen and argon-hydrogen inductively coupled RF and microwave plasmas were high ($43\,200 \pm 5\%$ K, $18\,600 \pm 5\%$ K, $30\,500 \pm 5\%$ K, and $13\,700 \pm 5\%$ K, respectively); compared to $9300 \pm 5\%$ K, $7300 \pm 5\%$ K, $8000 \pm 5\%$ K, and $6700 \pm 5\%$ K for the corresponding plasmas of xenon-hydrogen and hydrogen alone, respectively. Stark broadening or acceleration of charged species due to high electric fields cannot explain the inductively coupled RF and microwave results since the electron density was low and no high field was present. Rather, a resonant energy transfer mechanism is proposed. [J246]

"Progress toward a practical magnetic field diagnostic for low-field fusion plasmas based on dual mode correlation reflectometry"

Previously, the proof of principle of measurement of magnetic field strength, $|B|$ internal to a plasma by cross correlation of ordinary (O) and extraordinary (X) mode fluctuation reflectometer signals has been demonstrated in a linear plasma device. It was found that dual mode (O-X) reflectometry data could be interpreted by a one-dimensional numerical model to determine $|B|$ in the vicinity of the reflectometer cutoff positions. Radial correlation properties of turbulence are also measured simultaneously with $|B|$. This technique is potentially well suited to measurement of $|B|$ in low-field fusion devices (e.g., $B = 0.6$ T) where standard magnetic field diagnostics are expected to be difficult to implement. However, transfer of this method to toroidal magnetic fusion devices presents a number of potential difficulties such as the effects of magnetic shear, steep density gradients, and limited time for cross correlations. In addition, recent simulations suggest that two-dimensional modeling may be required to interpret experimental data when density fluctuation levels are high. Dual mode correlation reflectometry experiments on the National Spherical Torus Experiment are presented, and progress toward the implementation of this technique as a practical diagnostic is discussed. copyright 2003 American Institute of Physics. [J247]

"Automatic profile reconstruction for millimeter-wave frequency-modulated continuous-wave reflectometry on NSTX"

UCLA operates a set of millimeter-wave/microwave reflectometers on the National Spherical Torus Experiment (NSTX) for routine measurements of electron density profiles and fluctuations. The system has a combined frequency coverage of 12 to 50 GHz (in the bands 12-18, 20-32, and 33-50 GHz) or a corresponding ordinary-mode cutoff range of 1.84×10^{12} to 3.14×10^{13} cm⁻³ to cover both the plasma core and edge. Profile measurements via frequency-modulated continuous-wave operation are typically made in O-mode reflectometry, with sweep times down to 50 μ s over the full band. Automated profile analysis of the reflectometry data is available with limited between-shot analysis and full batch analysis capabilities. The reconstruction algorithm uses complex demodulation with the short-time Fourier transform for signal processing. The unknown portion of the edge profile below the lowest cutoff density is modeled by fitting a family of polynomial density profiles to the experimental data. Uncertainties due to edge profile modeling and comparisons to Thomson scattering measurements are discussed. The reconstructed profiles have documented fast events such as L-H transitions and edge-localized modes in NSTX. copyright 2003 American Institute of Physics. [J248]

"Advances of the density profile reflectometry on TORE SUPRA"

Significant improvements have been achieved in the performances of the broadband reflectometry for the density profile measurements on Tore Supra. The frequency range of the former 50-75 GHz X-mode reflectometer has been extended with an additional device operating between 75 and 110 GHz. Both setups have ultrafast sweeping capabilities allowing full band measurements in 20 μ s. The heterodyne detection and the intermediate frequency system have been upgraded to record beat frequencies up to 100 MHz with a signal to noise ratio of about 40 dB. The in phase and quadrature-type phase detection system (IQ detector) provides sine and cosine components of the received signal for a separate measurement of the phase and the amplitude. A new fast data acquisition system in Versa Module Europa format has been developed. It allows sampling frequency up to 200 MHz with 32 Mo memory capabilities per channel and 10 bit resolution digitizers. Edge profile measurements are now available for a wide range of toroidal magnetic fields (from 3 to 4 T). copyright 2003 American Institute of Physics. [J249]

"Plasma position measurements from ordinary FM-CW reflectometry on ASDEX Upgrade"

Microwave reflectometry has been proposed as an alternative/backup approach to the usual magnetic systems in long pulse operation on the International Thermonuclear Experimental Reactor (ITER) for plasma position and

shape control. This new application of reflectometry must be fully demonstrated in present machines in view of its importance for ITER. First experiments performed in ASDEX Upgrade with frequency modulated continuous wave with reflectometry diagnostic showed that radial variations of the plasma column occurring during preprogrammed horizontal as well as vertical plasma displacements could be followed with sufficient accuracy (~ 1 cm) in phases with approximately constant density. In this article we determine the plasma edge position simultaneously in the inner and outer midplane, of ohmic L-mode density limit and ELMy H-mode discharges in ASDEX Upgrade, both with significant density variations. It is shown that if normalized density layers are selected, at a certain percentage of the average line density, the results from reflectometry are in good agreement with the corresponding data, separatrix position, derived from the magnetics. Further work aiming at the full demonstration of plasma position and shape measurements from reflectometry is discussed. copyright 2003 American Institute of Physics. [J250]

"Electron Bernstein wave emission diagnostic assisted by reflectometry on TST-2 spherical tokamak"

A new electron Bernstein wave emission diagnostic consisting of a heterodyne radiometer and a reflectometer was installed on TST-2. The instrument has a frequency range from 5 to 12 GHz which covers partially the fundamental and fully covers the second and third harmonic emissions. X-mode emission perpendicular to the flux surface, generated by B-X-FX mode-conversion scenario, is measured. The mode-conversion efficiency is calculated using a one-dimensional full-wave code with the density profile obtained simultaneously from the reflectometer, and the electron temperature (T_e) is estimated. The levels corresponding to the 100-150 eV range are measured from the plasma core region, and the mode-conversion efficiency is calculated to be 0.5-0.8, leading to T_e of approximately 200 eV. In addition, it is found that the reflectivity measured by the reflectometer is consistent with the calculated mode-conversion efficiency. This property can be used for a direct measurement of the mode-conversion efficiency. copyright 2003 American Institute of Physics. [J251]

"Time-of-flight refractometry for robust line integral electron density measurements and control in ITER"

A new method of electron density measurements in magnetic confinement plasmas-time-of-flight refractometry (TFR)-is proposed for application in the International Thermonuclear Experimental Reactor (ITER) in order to get robust line integral electron density information. The method provides unambiguous density measurements directly from the measurements of time delay of microwave pulses propagating through the plasma. Generally, both O-and-X probing modes are available for use in the measurements. At ITER conditions ($B \sim 5$ T), X-mode probing in the equatorial plane seems to be attractive for application due to transparency of ITER plasma for electromagnetic emission between lower and upper cutoffs at approximately 60-105 GHz frequency band. When these relatively low frequencies are used for measurements, both electron cyclotron resonance absorption and first mirror problems should be avoided. Also, relatively simple implementation of the access to plasma and comparatively low sensitivity to vibrations and misalignment are expected. General approach to TFR is given in the article. The choice of probing frequencies of TFR for ITER has been conducted. Estimations of expected time delays for different density profiles have been performed. Parameters of TFR prototype used on the T-11M tokamak and results obtained are discussed. A conclusion of sufficiency of recently attained accuracy of the measurements for TFR application on large tokamaks has been done. Some ways of improving the measurement accuracy have been proposed and tested. Advantages and problems of TFR application are discussed. copyright 2003 American Institute of Physics. [J252]

"X-mode pulsed radar reflectometer for density fluctuation measurements on LHD"

A four channel pulsed radar reflectometer system has been installed on the Large Helical Device (LHD). The complicated magnetic structure in LHD causes mode conversion and/or polarization rotation of the microwaves. Pulsed radar reflectometry is a suitable reflectometric technique, because it measures the delay time of the reflected wave, not the phase, and X-mode and O-mode polarized waves can be distinguished. By using X-mode operation of the pulsed radar reflectometer so that each pulse width is about 2 ns, and the repetition rate is up to 200 kHz, the critical density where the microwave is reflected is about $1.4 \times 10^{16} \text{ m}^{-3}$. Also it is found that the static natural island affects the X-mode reflectometric measurements. copyright 2003 American Institute of Physics. [J253]

"Improved reflectometer electron density profile measurements on DIII-D"

Details are presented of recent improvements to hardware and analysis code components of the DIII-D density profile reflectometer system. The improvements to the hardware increased the system signal-to-noise ratio and reduced spurious reflections. An improved automated method is developed to accurately determine the zero

density plasma start position. With these improvements the uncertainty in the zero density plasma start position is reduced from 7 to 2 mm, the position uncertainty with a fixed mirror target is reduced from 4 to 2 mm, and the time resolution is improved to 10 ns (previously 100 ns). copyright 2003 American Institute of Physics. [J254]

"Application of fast reflectometer density profile measurements to investigate plasma instabilities in DIII-D"

The high spatial (2 mm depending upon plasma conditions) and temporal (10 ns) resolution possible with the DIII-D solid state profile reflectometer system makes it possible to investigate profile modifications associated with plasma instabilities. In order to take full advantage of this fast sweep and high resolution capability, multiple issues had to be addressed, including fast data acquisition, large data acquisition memory depth, improved signal to noise, accurate profile start location, and finally fast accurate automatic data analysis. Improvements in all these areas make the profile reflectometer ready for plasma instability studies. In a demonstration of this capability, fast, high spatial resolution reflectometer measurements have been successfully used to investigate the edge harmonic oscillation (EHO) in the quiescent double barrier regime, as well as the edge localized modes (ELMs) on DIII-D. It is found that the scrape-off layer density profile is modulated at the EHO fundamental frequency. The edge density profile evolution is also tracked during ELMs, showing that the density profile expands to the vessel wall at the onset of Type 1 ELMs. copyright 2003 American Institute of Physics. [J255]

"Design of a single-channel millimeter-wave interferometer system for Korea Superconducting Tokamak Advanced Research"

A simple single-channel horizontal millimeter-wave interferometer has been designed for plasma electron density measurements on the Korea Superconducting Tokamak Advanced Research (KSTAR). To measure line integrated plasma densities of 241019 m⁻² in the initial phase of the KSTAR, Gunn oscillator frequency of 280 GHz has been chosen to optimize errors due to both vibration on the beam path and refraction in the plasma. To reduce the free propagation length of the probing beam and to obtain small beam width on the vacuum windows, a retractable cassette system for deep positioning of the diagnostic system has been designed, where microwave parts are located as close as possible to the tokamak with a shielding box. A beam focusing system with concave reflecting mirrors has been designed on the cassette and on the inner wall of the tokamak to reduce beam losses and to minimize beam width in the plasma. The estimated total transmission loss is about 25 dB, and beam widths are reduced significantly in the range of 20-50 mm. copyright 2003 American Institute of Physics. [J256]

"Ultrashort-pulse reflectometry for steady-state plasmas"

An ultrashort-pulse reflectometry (USRM) has been applied to the inductively coupled steady-state plasma (ICP) for density profile measurement. A reflected wave from ICP is directly recorded into a digitizing sampling scope and is analyzed by the signal record analysis (SRA) method. From repetition of the measurement, we have obtained the time evolution of the density profile. In order to apply the USRM and SRA method to high density plasmas such as core region of the Large Helical Device plasma, generation of the pulse with higher frequency up to 90 GHz is essential. We have utilized a frequency upconverter and an active doubler for this purpose. We confirmed the generation of the upconverted pulse in the range of 60-90 GHz and the second-harmonic frequency in the range of 26-40 GHz. Time of flight measurements have been preliminarily performed with a metal target. copyright 2003 American Institute of Physics. [J257]

"Ultrashort pulse reflectometry for density profile and fluctuation measurements on SSPX"

A broadband, multichannel ultrashort pulse reflectometry (USPR) diagnostic on the Sustained Spheromak Physics eXperiment device has recently undergone a number of system upgrades, which has resulted in significant improvements in the signal-to-noise ratio of the USPR signals and a dramatic reduction in the number of "lost signals" in which the amplitude of the reflected wave form drops below detection threshold. This has greatly enhanced the ability of USPR to study relatively fast density profile modifications, and allows the simultaneous monitoring of multiple density layers with as short as a 3 ns pulse repetition rate. This article provides details of the upgraded USPR system together with density profiles and fluctuation data. copyright 2003 American Institute of Physics. [J258]

"Design of an X-mode fast-scanning reflectometry for edge density profile measurement on HT-7 tokamak"

An amplitude modulation reflectometry system with fast-scanning microwave source is designed for edge density

profile measurement on the HT-7 superconducting tokamak ($R_0=1.22$ m, $a=0.28$ m, $B_t:1.8-2.3$ T, plasma pulses of 1-20 s). The reflectometer launches microwave power from a very fast-scanning backward wave oscillator in 53-78 GHz to probe the plasma and receive the reflection by the density cutoff layer. It is an extraordinary mode reflectometer, which can measure the edge density profiles in normalized radius r/a from scrape-off layer up to 0.5 when $B_t=2.2$ T, $n_{e0}=3.4 \times 10^{19}$ m⁻³ in typical HT-7 operation parameters. The microwave amplitude modulation frequency is 200 MHz. A 2 MHz reference signal and the probing signal are obtained by mixing a 198 MHz local oscillator power with the demodulated microwave signals. Phase comparison is then accomplished at 2 MHz by I/Q phase detector. The scanning time over the full band of 53-78 GHz is about 0.5 ms. The reflectometry will fill in the space left by the five-chord interferometer, which measures in the core plasma region and the Langmuir probes, which work in the scrape-off layer; especially the reflectometry is used to study the lower hybrid wave coupling into plasmas for the current drive and the radio frequency wave coupling problems for heating on HT-7. The reflectometry is also considered to be useful on the future HT-7U superconducting tokamak. copyright 2003 American Institute of Physics. [J259]

"Plasma parameters of diffusion-controlled microwave discharges in surface-wave fields"

Results from diagnostics of diffusion-controlled stationary gas discharges maintained in the field of propagating surface waves are presented in this study. The set of the plasma parameters obtained includes: 1) the plasma density n_i , averaged over the discharge cross section; and its axial profile $n_i(z)$; 2) the electron-neutral elastic collision frequency ν ; 3) the parameter μ , which describes the radial profile of the plasma density; 4) the parameter Θ , the power absorbed on average by an electron, and its axial variation $\Theta(z)$; 5) the electron temperature $T_e(z)$; and 6) the gas temperature T_g . The mechanisms of electron heating and discharge self-consistency are discussed [J260]

"Experimental validation of a linear model for data reduction in chirp-pulse microwave CT"

Chirp-pulse microwave computerized tomography (CP-MCT) is an imaging modality developed at the Department of Biocybernetics, University of Niigata (Niigata, Japan), which intends to reduce the microwave-tomography problem to an X-ray-like situation. We have recently shown that data acquisition in CP-MCT can be described in terms of a linear model derived from scattering theory. In this paper, we validate this model by showing that the theoretically computed response function is in good agreement with the one obtained from a regularized multiple deconvolution of three data sets measured with the prototype of CP-MCT. Furthermore, the reliability of the model as far as image restoration is concerned, is tested in the case of space-invariant conditions by considering the reconstruction of simple on-axis cylindrical phantoms. [J261]

"Pulsed inductive microwave magnetometer"

We describe the apparatus, software, and measurement procedures for a pulsed inductive microwave magnetometer (PIMM). PIMM can measure the dynamical properties of materials used in recording heads for magnetic storage applications, and it can be used as a general magnetodynamics diagnostic tool. PIMM uses a coplanar waveguide as both a source of fast pulsed magnetic fields and as an inductive flux sensor. Magnetic field pulses are provided by a 10 V, 55 ps risetime pulse generator; a 20 GHz digital sampling oscilloscope is used to acquire the fast pulse data; and orthogonal Helmholtz pairs provide the bias and saturating fields required for the measurement. The system can measure dynamical behavior as a function of several variables, including applied magnetic bias field, magnetic pulsed field amplitude and width, and sample orientation. Using a fast Fourier transform, PIMM can determine the frequency dependence of the complex magnetic permeability, as well as the step and impulse responses of the magnetic system. Data from 50 nm Ni-Fe and rare-earth-doped Ni-Fe thin films are presented. [J262]

"Wireless house calls: using communications technology for health care and monitoring"

Recent advances in telecommunications and information technologies have enabled various novel applications in health care and monitoring to address the needs of elderly and chronic patients. As wireless technology becomes more ubiquitous and affordable, applications, such as video-telephony over POTS, will gradually migrate towards third-generation wireless systems. We can also expect to see low-cost miniature wireless circuitry merging with sensor technologies to create a wide range of minimally invasive continuous health-monitoring systems. In some cases, wireless signals alone can be interpreted to monitor vital signs. These techniques promise to greatly improve the cost and convenience associated with long-term outpatient monitoring, and could potentially extend monitoring to the broader healthy population for preventative diagnostics and alerts. [J263]

"Two-dimensional optical emission imaging of a XeCl discharge in a microwave resonant cavity"

Optical emission of a XeCl excimer discharge, within a 1.2-cm diameter quartz discharge tube, excited by 2.45-GHz microwaves in an Asmus resonant cavity, operating in the TM₀₁₂ cavity mode, has been imaged onto a two-dimensional (2-D) charge-coupled device (CCD) camera. Spatial imaging of the discharge provides information on the heating regions of the cylindrical plasma as well as the contraction of the plasma diameter with increasing pressure. This technique also provides a real-time diagnostic for production of ultra-violet (UV) emission using a UV bandpass filter [J264]

"Microwave emission from plasmas produced by magnetically confined-electron beams"

Microwave emission, in the x-band frequency range (8.2-12.4 GHz), from a thin, large, rectangular sheet plasma has been measured. The plasma electron density was such that the plasma frequency was within or just above this frequency range. The plasma was immersed in an external magnetic field from a set of Helmholtz coils. The magnetic field was oriented parallel to the electric field between the anode ground plane and a cylindrical, hollow cathode. The spectrum of the emitted noise was measured for both ordinary mode (P to B) and extraordinary mode (to B) polarization in the x-band. The emission was strongest at high harmonics of the electron cyclotron frequency. Mechanisms that might produce this noise and its potential use as a diagnostic tool are discussed [J265]

"Passive high-power microwave components"

This review discusses the present state-of-the-art of passive high-power microwave components for applications in microwave systems for RF plasma generation and heating, plasma diagnostics, plasma and microwave materials processing, spectroscopy, communication, radar ranging and imaging, and for drivers of next generation high-field-gradient electron-positron linear colliders. The paper reports on high-power components for overmoded high-power transmission systems such as smooth-wall waveguides, HE₁₁ hybrid mode waveguides and quasi-optical TEM₀₀ beam waveguides. These include various types of mode converters, polarizers, cross-section tapers, bends, mode selective filters, pulse compressors, DC-breaks, directional couplers, beam combiners and dividers, vacuum windows, and instruments for mode analysis. Problems of ohmic attenuation and unwanted conversion to parasitic modes are discussed in detail and rules for alignment requirements are given. In the case of waveguide transmission, this review mainly concentrates on circular waveguide components but also deals with rectangular waveguide. [J266]

"Initial studies of a long-pulse relativistic backward-wave oscillator utilizing a disk cathode"

One of the major issues in high-power microwave device operation is pulse shortening, which often limits microwave pulses to less than 100 ns. This has been the focus of many studies on the long-pulse backward-wave oscillator (BWO) at the University of New Mexico. Previous diagnostics have indicated that significant plasma is produced by a graphite knife-edge or "cookie cutter" geometry cathode. This plasma caused the beam to expand radially to match the dimensions of the cutoff neck upon entrance into the slow-wave structure. This effect led to an impedance collapse at which point the microwave production ceased. In recent studies by Loza and colleagues, they have produced intense annular relativistic electron beams that maintain a stable cross section for 1- μ s duration utilizing a disk cathode. Whereas the beams produced by Loza and colleagues were not used in microwave sources, we have incorporated such a disk cathode in a long-pulse relativistic BWO to study its effect on pulse shortening. This simple solution has led to an increase in pulse length and radiated microwave power up to a factor of two as compared to the "cookie cutter" cathode. [J267]

"Enthalpy-probe diagnostics of an atmospheric-pressure unleaded petrol exhaust-gas microwave-induced plasma"

An unleaded petrol exhaust-gas microwave-induced plasma (MIP) at atmospheric pressure was generated in a TE₁₀₁ resonant-mode cavity. The microwave discharges were generated at three incident microwave power levels: 500 W, 700 W, and 1500 W. An enthalpy probe was used to characterize the exhaust-gas MIP discharge, yielding values of enthalpy, velocity, and heavy-particle temperature along the microwave-discharge axis. The heavy-particle temperature was found to be 710 K, 940 K, and 1065 K, with velocities of 140 m s⁻¹, 148 m s⁻¹, and 155 m s⁻¹, at the exit plane of the discharge tube for an exhaust-gas flow rate of 3.5 l min⁻¹ at 500 W, 700 W, and 1500 W respectively. The assumption of local thermodynamic equilibrium is required in the calculation of temperature and velocity in the microwave discharge from the enthalpy-probe data. In microwave-induced plasmas, the electron temperature is significantly higher than the heavy-particle temperature. We present arguments that indicate that the calculated heavy-particle temperature and velocity values are nevertheless accurate. [J268]

"Not your mother's mammography [Jbreast cancer detection]"

Breast cancer accounts for nearly one of every three cancers diagnosed in US women. While great strides have been made in early detection, the conventional method of mammography is not failproof it has trouble imaging dense tissue, it may show suspicious areas where no malignancy exists, and radiologists interpreting the images can miss up to 15 percent of cancers. It's also uncomfortable, requiring each breast to be compressed between plastic plates, which can lead to bruising. Susan Hagness wants to change all that. An assistant professor of electrical engineering at the University of Wisconsin-Madison, she is pioneering a novel detection technique that uses ultrawideband microwaves to image even the tiniest malignant tumors in the breast. Breast tumors and normal tissue show much more contrast at microwave frequencies than at the X-ray frequencies used for mammograms. Microwaves are also nonionizing, and the technique requires no breast compression. In Susan Hagness' search for a better way to detect breast cancer, she gets her students involved, too. Such efforts have paid off: her courses consistently receive high marks on student evaluations. [J269]

"Time-domain reconstruction for thermoacoustic tomography in a spherical geometry"

Reconstruction-based microwave-induced thermoacoustic tomography in a spherical configuration is presented. Thermoacoustic waves from biological tissue samples excited by microwave pulses are measured by a wide-band unfocused ultrasonic transducer, which is set on a spherical surface enclosing the sample. Sufficient data are acquired from different directions to reconstruct the microwave absorption distribution. An exact reconstruction solution is derived and approximated to a modified backprojection algorithm. Experiments demonstrate that the reconstructed images agree well with the original samples. The spatial resolution of the system reaches 0.5 mm. [J270]

"Exact frequency-domain reconstruction for thermoacoustic tomography. I. Planar geometry"

We report an exact and fast Fourier-domain reconstruction algorithm for thermoacoustic tomography in a planar configuration assuming thermal confinement and constant acoustic speed. The effects of the finite size of the detector and the finite length of the excitation pulse are explicitly included in the reconstruction algorithm. The algorithm is numerically and experimentally verified. We also demonstrate that the blurring caused by the finite size of the detector surface is the primary limiting factor on the resolution and that it can be compensated for by deconvolution. [J271]

"Exact frequency-domain reconstruction for thermoacoustic tomography. II. Cylindrical geometry"

For pt. I see *ibid.*, vol. 21, no. 7, p. 823-8 (2002). Microwave-induced thermoacoustic tomography (TAT) in a cylindrical configuration is developed to image biological tissue. Thermoacoustic signals are acquired by scanning a flat ultrasonic transducer. Using a new expansion of a spherical wave in cylindrical coordinates, we apply the Fourier and Hankel transforms to TAT and obtain an exact frequency-domain reconstruction method. The effect of discrete spatial sampling on image quality is analyzed. An aliasing-proof reconstruction method is proposed. Numerical and experimental results are included. [J272]

"Mechanism of C₂ hydrocarbon formation from methane in a pulsed microwave plasma"

Methane dissociation, followed by the formation of C₂hydrocarbons, in a pulsed microwave discharge in methane was investigated by mass spectrometry and optical emission spectroscopy (OES). Long microwave pulses (200 μ s) are characterized by a pronounced dehydrogenation, but have a disadvantage in the saturation of the methane conversion at relatively low values, due to methane depletion toward the end of the pulse. For shorter pulses, the conversion degree increases approximately linearly as a function of energy input, and a maximum conversion of 90% with 80% selectivity toward acetylene was obtained for 60 μ s pulses at 1 kHz repetition frequency. A further decrease of the pulse duration (20 μ s) at higher frequency, in order to ensure a similar energy input, resulted in a decrease in conversion and dehydrogenation. The explanation of the effect of the pulse duration is based on information provided by optical emission spectroscopy of active species generated in the discharge. Atomic hydrogen, formed by methane dissociation, was found to play an essential role in methane plasma chemistry. A qualitative estimation of the variation of H atom concentration with operating conditions was done by actinometry, since time-resolved OES provides evidence that atomic hydrogen is mainly formed in the ground state and dissociative excitation can be neglected. In addition to the concentration of atomic hydrogen, the second key parameter is the gas temperature. It was determined from the relative intensity distribution in the rotational structure of the (0,0) C₂Swan band and of the (2,2) H₂Fulcher-alpha band. Gas temperatures between 1500 and 2500 K were determined for the present discharge conditions. The hydrogen abstraction-by hydrogen atoms, favored at high temperature, is responsible for the high methane conversion and low energy requirement achieved (9-10 eV/molecule) and for the distribution of the reaction products. copyright 2002 American Institute of Physics. [J273]

"Charged species dynamics in an inductively coupled Ar/SF₆ plasma discharge"

The chemistry of high-density SF₆ plasma discharges is not well characterized. In this article, a combination of computational modeling and experimental diagnostics has been utilized to understand charged species dynamics in an inductively coupled Ar/SF₆ plasma discharge. The model is based on the two-dimensional Hybrid Plasma Equipment Model with a detailed plasma chemical mechanism for Ar/SF₆. In the experiments, absolute electron density and total negative ion density have been measured using microwave interferometry and laser photodetachment, respectively. In addition, we have also utilized prior measurements of mass and energy resolved ion fluxes by Goyette et al [J. Vac. Sci. Technol. A 19, 1294 (2001)]. Computational results show that all SF_x⁺ (x=0-5) ions are present in the plasma discharge. Important negative ions include SF₆⁻, SF₅⁻, and F⁻. Electron and positive ion densities increase with coil power due to enhanced ionization. However, negative ion densities decrease with coil power as the main negative ion precursor, SF₆, is lost through neutral dissociation. An increase in SF₆ concentration in the Ar/SF₆ gas mixture decreases electron density due to enhanced electron loss through (dissociative) attachment, which enhances negative ion densities. RF bias power does not have an appreciable impact on the ion and electron densities for the parameter range of interest. Experiments show that electron density decreases with gas pressure while the total negative ion density increases up to 25 mTorr. This is due to a decrease in electron temperature, which enhances electron loss through (dissociative) attachment. Although the model is able to capture most of the experimentally observed trends, there are discrepancies regarding the impact of gas pressure on electron density and relative flux of large positive ions. copyright 2002 American Institute of Physics. [J274]

"Langmuir probe diagnostic studies of pulsed hydrogen plasmas in planar microwave reactors"

Langmuir probe techniques have been used to study time and spatially resolved electron densities and electron temperatures in pulse-modulated hydrogen discharges in two different planar microwave reactors (f_{microwave}=2.45 GHz, t_{pulse}=1 ms). The reactors are (i) a standing-wave radiative slotted waveguide reactor and (ii) a modified traveling-wave radiative slotted waveguide reactor, which generate relatively large plasmas over areas from about 350 to 500 cm². The plasma properties of these reactor types are of particular interest as they have been used for basic research and for plasma processing; for example, for surface treatment and layer deposition. In the present study the pressures and microwave powers in the reactors were varied between 33 and 55 Pa and 600 and 3600 W, respectively. In regions with high electromagnetic fields, shielded Langmuir probes were used to avoid disturbances of the probe characteristic. Close to the microwave windows of the reactors both the electron density and the electron temperature showed strong inhomogeneities. In the standing-wave reactor the inhomogeneity was found to be spatially modulated by the position of the slots. The maximum value of the electron temperature was about 10 eV, and the electron density varied between 0.2 and 14 × 10¹¹ cm⁻³. The steady-state electron temperature in a discharge pulse was reached within a few tens of microseconds, whereas the electron density needed some hundreds of microseconds to reach a steady state. Depending on the reactor the electron density reached a maximum between 80 and 200 μs after the beginning of the pulse. copyright 2002 American Institute of Physics. [J275]

"Electromagnetic and absorption properties of some microwave absorbers"

Electromagnetic properties of a thermoplastic natural rubber (TPNR), a lithium-nickel-zinc (Li-Ni-Zn) ferrite and a TPNR-ferrite composite subjected to transverse electromagnetic (TEM) wave propagation were investigated. The incorporation of the ferrite into the matrix of the TPNR was found to reduce the dielectric loss but the magnetic loss increased. The absorption characteristics of all the samples subjected to a normal incidence of TEM wave were investigated based on a model of a single-layered plane wave absorber backed by a perfect conductor. It is evident from a computer simulation that the ferrite is a narrowband absorber, whereas the polymeric samples show broadband absorption characteristics. Minimal reflection of the microwave power or matching condition occurs when the thickness of the absorbers approximates an odd number multiple of a quarter of the propagating wavelength. This is discussed as due to cancellation of the incident and reflected waves at the surface of the absorbers. The Li-Ni-Zn ferrite exhibits another matching condition at low frequency when the magnitude of the complex relative dielectric permittivity (ϵ^*) equals that of the complex relative magnetic permeability (μ^*). The specular absorber method provides a simple theoretical graphic aid for determining the absorption characteristics and the location of the matching conditions in the frequency domain. The result for the ferrite sample was tested and confirmed directly from terminated one-port measurements. copyright 2002 American Institute of Physics. [J276]

"Solid-state laser induced microwave effects"

Intense laser radiation that is intensity modulated at microwave frequencies produces microwave radiation from a variety of solid-state materials that is band limited by the bandwidth of the laser modulation. An experimental investigation is summarized that provides data on the wavelength, laser intensity, laser modulation frequency,

angular distribution, and, in some cases, electric field dependence on the microwave radiation that is produced. When the wavelength of the laser is sufficiently short such that electrons are promoted from the valence to the conduction band, it is clear that the radiation results from the dipole layer radiation resulting from these electrons accelerated in the electric field produced by band bending at the surface or in the PN junction of devices. There appear to be other mechanisms operative in materials such as Ge and ponderomotive forces seem likely. Also poorly understood at this time is the radiation from materials such as ZnS which has a cubic dependence on the incident laser intensity. It is suspected that nonlinear optical effects may be responsible. Although this article only presents experimental results for modulated Q-switched Nd:yttrium-aluminum-garnet laser systems, the authors have obtained entirely consistent results using other laser systems and these results are not presented for the sake of brevity. The production of laser induced microwave effects appears to be a relatively ubiquitous effect in many materials that may provide a useful solid-state diagnostic tool (with improved understanding) or probe of a material's electromagnetic properties. copyright 2002 American Institute of Physics. [J277]

"Applications of RF/microwaves in medicine"

Medical applications of RF/microwaves are highlighted in this paper. The emphasis is placed on newer emerging diagnostic and therapeutic applications, such as microwave breast cancer detection, and treatment with localized high power used in ablation of the heart, and liver, benign prostate hypertrophy, angioplasty, and others. A very brief outline of biological effects of RF/microwaves and associated issues is given as background to the applications [J278]

"Microwave industry outlook-wireless communications in healthcare"

Concomitant advances in communications and medical technology have led to increasing deployment of telemedicine systems and services around the world. The goals of these systems are to increase the accessibility of professional caregivers, increase the quality of care to patients, and to increase the focus on preventative medicine through early intervention, all while reducing the overall cost of healthcare. Current pilot programs are beginning to show that these goals are achievable, warranting continued investment in telemedicine technologies [J279]

"Cathode and anode plasmas in short-pulse explosive field emission cathodes"

Explosive field emission cathodes have been a subject of research for a number of years. These cathodes offer high current densities and total current without requiring a heater for the production of electrons. Generally these cathodes consist of some structure with a series of tips or metal-dielectric regions in which a large electric field enhancement can occur. A cathode plasma is then formed from these discharge points that then supplies the electrons necessary for space charge limited emission. This article reports on a series of optical measurements in which the cathode and anode plasmas of explosive field emission cathodes are observed. Three types of cathodes are investigated. These types are a polymer velvet cathode, a metal-dielectric cathode, and a tufted carbon fiber cathode in which the fibers have been coated with a cesium iodide salt. Cesium iodide coated carbon fiber cathodes have shown a great deal of promise for various field emitter applications. From these high speed photos, the evolution of the plasmas on both cathode and anode can be qualitatively ascertained. Experimentally we find that not only does cathode plasma behavior depend on the type of cathode, but the anode plasma behavior does also. Further, we find that the best performing cathode shows the most rapid plasma formation on both anode and cathode, yet without a rapid plasma expansion across the anode-cathode gap. copyright 2002 American Institute of Physics. [J280]

"Radial contraction of microwave-sustained plasma columns at atmospheric pressure"

Plasma columns sustained at high enough gas pressures undergo radial contraction as manifested by their glow not entirely filling the radial cross-section of the discharge tube. This phenomenon has been reported with direct current, radio frequency, and microwave discharges. However, its modeling is still incomplete, in particular for rf and microwave discharges, a situation attributed to a lack of experimental data. To fill this gap, we took advantage of the extreme flexibility in terms of field frequency, tube diameter and gas nature of surface-wave sustained discharges to achieve a parametric study of this phenomenon. Special attention was paid to filamentation, specific to rf and microwave discharges, which is the breaking of a single channel of plasma into two or more smaller filaments as a result of the skin effect. We used emission spectroscopy as the main diagnostic means. Electron density was obtained from Stark broadening of the H β line, while molecular-band spectra emitted by the OH radical and the N $_2^+$ molecule were employed to determine the discharge gas temperature, leading to its radial distribution upon performing Abel inversion. For a given tube radius, contraction is shown to increase with decreasing thermal conductivity of the discharge. As a result, He and N $_2$ discharges are the least contracted, while contraction increases with increasing atomic mass of noble gases. Of all these

discharges, the N₂ discharge appears to be the closest to local thermodynamic equilibrium. copyright 2002 American Institute of Physics. [J281]

"On a variational approach to the extraction of quadratures from broadband reflectometry signals"

A variational method is employed to retrieve the phase from broadband reflectometry signals. The method yields the so-called in-phase and quadrature components of a signal (the signal quadratures in short), by stipulating that these should have the smallest possible amount of functional variation, whereby the signal carrier frequency is also recovered as a by-product. The variational approach is based on the reasonable assumption that, for given data, the quadratures are expected to be as slow as possible, as they contain the slow modulations of amplitude and phase, while rapid variations are accounted for by the carrier frequency. The advantages and shortcomings of the variational method are discussed, and a pertinent comparison with the analytic signal—recently proposed as a means to extract the phase from broadband reflectometry signals—is also carried out. The application of the variational method to the reflectometry problem is shown to yield results that are similar to those obtained via the analytic signal. The difference is not significant, especially if detailed measurements are not required, but only averaged ones. copyright 2002 American Institute of Physics. [J282]

"Energy distribution of the compact microwave ion source for extremely low voltage ion extraction"

The energy distribution of the ion beam extracted from the compact microwave ion source for extremely low voltage ion extraction was measured with Ar and CO as a discharge gas. The energy distribution was measured by the retarding field method, and changes with respect to the change in gas pressure were observed. The obtained data were arranged by the peak energy and the energy spread. For both gases, the peak energy and the energy spread decreased with an increase in the gas pressure. The energy spread of approximately 5 eV with the peak energy of 15 eV were obtained for Ar gas at the pressure of 10⁻² Pa. For CO gas, the peak energy was higher than Ar and approximately 20 eV. The energy spread was 6 eV at the pressure of 10⁻² Pa. These values agreed with the peak energy and energy spread that were estimated previously from the mass spectra analysis. Since the ion source was designed to be used in the researches of low energy ion-solid interaction, these characteristics satisfy the requirements for this purpose. copyright 2002 American Institute of Physics. [J283]

"A gold film detector for radial profile measurement of plasma density by using a gold neutral beam probe"

A gold film detector was developed in order to measure the plasma density profile by use of the gold neutral beam probe. The detector is a kind of neutral beam detector composed of a rectangular entrance collimator, two sets of grid plates, a gold thin film, a quartz backing, and a microcarbon coated copper plate. The secondary electrons emitted from the gold film were utilized for the neutral beam detection. The yield curves of the secondary electrons were measured as a function of the incident angle and electron energy in both cases of the gold neutral probing beam and ultraviolet ray injection. Time evolution of the plasma line density was measured by adjusting the incident angle and adding a beam chopping method. The result was in good agreement with the line density measured by a microwave interferometer. It was found that this film detector was quite useful in the viewpoint of simultaneous measurements of the electrostatic potential and plasma density profiles. copyright 2002 American Institute of Physics. [J284]

"Imaging system for low-density plasma by heterodyne interferometer with fan beam microwave"

A microwave imaging system based on a heterodyne interferometer has been developed to measure the spatial distribution of the plasma density without introducing any direct disturbance to the plasma by employing a diode array scattering technique. The imaging system with the use of a fan beam microwave for a radar system demonstrates the principle of the technique by placing finite-size dielectric phantoms instead of the plasma between the horn antenna and the diode antenna array. Experimental results show that very good image of the objects can be reconstructed and the system is equivalent to popularly known multichannel imaging system. As a result, it is possible to make simple, low-cost, and compact microwave interferometer for measuring the spatial distribution of the plasma density. copyright 2002 American Institute of Physics. [J285]

"Microwave medical devices"

This article describes several new microwave medical devices that either were or are being developed at MMTc, Inc. in cooperation with the following institutions: Celsion Corporation, Columbia, Maryland (microwave balloon catheters); Montefiore Medical Center (MMC), Bronx, New York (microwave balloon catheters, dual microwave antennas, and microwave poration); and the University of California at San Francisco (conformal array antennas). The individuals who developed these devices have previously published patents and articles that

contain most of the material presented here. All of the medical devices described depend on the ability of microwaves to deeply penetrate into living tissues. The depth to which microwaves can penetrate tissues is primarily a function of the dielectric properties of the tissues and of the frequency of the microwaves. In general, the lower the water content of the tissue, the deeper a wave at a given frequency can penetrate. Also, at the frequencies of interest, the lower the frequency, the deeper is the depth of penetration into tissues with given water content [J286]

"Metalorganic precursor decomposition and oxidation mechanisms in plasma-enhanced ZrO₂ deposition"

We investigated the gas phase reaction mechanisms in the ZrO₂-deposition plasma using zirconium tert-butoxide (ZTB) as a metalorganic precursor, Ar as a carrier of the ZTB vapor, and O₂ as an oxidant using quadrupole mass spectrometry (QMS). Zirconium containing ions including Zr⁺, ZrO⁺, ZrO₂H⁺, ZrO₃H⁺, and ZrO₄H⁺ were clearly observed in the plasma, and ions of higher zirconium oxidation states become progressively favored at higher O₂-to-ZTB carrying Ar flow rate ratio (O₂/Ar), increased chamber pressure, and decreased microwave power. The average oxidation state calculated from the partition of ZrO_xH_y⁺ varied from 0.5 to 2.1 in the process range covering O₂/Ar of 0 to 4, pressure of 5 to 40 mTorr, and power of 150 to 700 W. Based on the QMS analyses, we proposed two main opposing reaction paths responsible for the complex gas phase reactions, i.e., serial dissociations and serial oxidations. The increase in the electron temperature and density resulted in the shift of ZrO_xH_y⁺ to lower oxidation states by enhancing the dissociation of Zr-O bond and by depleting oxygen through gas phase reactions. The repartitioning of the ZrO_xH_y⁺ species was also contributed by their different Zr-O dissociation energies. To ascertain the effect of various process variables, we monitored the time evolutions of O₂⁺ and ZrO_xH_y⁺ intensities as we abruptly change a process variable: the chemical effect (O₂/Ar) led to gradual changes in their intensities, whereas physical effects (pressure and power) caused an abrupt step change in accordance with an instant response of the plasma electrons. copyright 2002 American Institute of Physics. [J287]

"Surface dependent electron and negative ion density in SF₆/argon gas mixtures"

Electron and negative ion densities were measured in an inductively driven plasma containing mixtures of SF₆ and Argon. The electron and negative ion density were measured as functions of the induction coil power, pressure, bias power, and SF₆/argon ratio. To investigate the influence of surface material, the rf biased electrode was covered with a silicon wafer or a fused silica (SiO₂) wafer. Line integrated electron density was determined using a microwave interferometer, and absolute negative ion densities in the center of plasma were inferred using laser photodetachment spectroscopy. Voltage and current at the induction coil and rf biased electrode were also measured for both surfaces as functions of induction coil power, pressure, rf bias, and SF₆/argon ratio. For the range of induction powers, pressures, and bias powers investigated, the electron density had a maximum of $5.4 \times 10^{12} \text{ cm}^{-2}$ (line-integrated) or approximately $5.4 \times 10^{11} \text{ cm}^{-3}$. Over this same range the negative ion density had a maximum of $2.4 \times 10^{11} \text{ cm}^{-3}$, and was always less than the electron density. For most conditions, the negative ion density above the oxide surface was a factor of 5 to 10 larger than the density above the silicon surface. In contrast, the electron density above the oxide surface was equal to or slightly higher than the density above the silicon surface. Surface dependent changes in the induction coil and rf bias voltage and current were also observed. copyright 2002 American Institute of Physics. [J288]

"Probe diagnostics of high pressure microwave discharge in helium"

A method for the determination of electron temperature and plasma density in high pressure helium plasmas is established using numerical results of the continuum probe model by Cohen [Phys. Fluids 6, 1492 (1963)]. Simple algebraic functions are derived to approximate the probe characteristics of high pressure plasmas calculated by Cohen and are applied to use iterative procedures for the determination of plasma parameters. The proposed fitting technique has allowed one to obtain reasonable plasma parameters even for the probe characteristics strongly affected by large secondary electron emission currents from the probe. Fitting of the ion saturation current may possibly be used to estimate the ion temperature, provided that the electron temperature and plasma density are known. Finally high pressure helium microwave discharges have been produced by moderate microwave power of 400 W and investigated by the present method. copyright 2002 American Institute of Physics. [J289]

"Plasma diagnostics in large area plasma processing system"

A series of plasma diagnostic have been carried out in our large area plasma processing system which is based on a modulated electron-beam produced plasma. These discharges were created in both electrically conducting and insulated vacuum chambers operated in 30-120 mTorr of pure gases (argon, oxygen, and nitrogen).

Langmuir probes, microwave transmission, mass spectrometry, and external current sensors show robust discharges were made over fairly wide parameter ranges resulting in plasma densities of $1\text{--}4 \times 10^{11} \text{ cm}^{-3}$ and temperature ranging from 0.2 eV for the molecular gases and 1.4 eV for argon. The effects of various experimental techniques, parameters, and contamination issues are discussed in detail. copyright 2001 American Vacuum Society. [J290]

"Influence of the different operations of gas in the large microwave plasmas"

The study of discharge performance was performed for argon, nitrogen, and the $\text{H}_2\text{--C}_2\text{H}_5\text{OH}$ gas mixture in a power range from 250 to 1000 W, and a pressure range from 10 to 1000 Pa. With argon, a surface wave at the plasma-quartz interface can be excited above 250 W. The surface wave modes can be identified as $m=4$ and $m=6$ with pressures of 10 and 230 Pa. With nitrogen, surface waves propagate in two or more modes superposed with a different value of m below the pressure of 133 Pa. In contrast to the above gases, the $\text{H}_2\text{--C}_2\text{H}_5\text{OH}$ gas mixture showed no surface wave generation for power levels up to 1000 W; only a hemisphere plasma with a diameter of 8 cm was observed just above the substrate. The plasma, having a diameter of 160 mm, is uniform below the pressure of 133 Pa in nitrogen discharges, but the plasma density is lower than in argon discharges. The radial distributions of electron density in the quartz tube also prove the existence of surface waves for argon and nitrogen. In addition, the axial distributions of electron density prove that the traveling and standing surface waves can be excited by argon discharges in each case: with or without the short plunger at the top of the setup. copyright 2001 American Vacuum Society. [J291]

"Process development for small-area GaN/AlGaN heterojunction bipolar transistors"

A self-aligned fabrication process for small emitter contact area (2.4 mcm^2) GaN/AlGaN heterojunction bipolar transistor is described. The process features dielectric-spacer sidewalls, low damage dry etching, and selected-area regrowth of GaAs(C) on the base contact. The junction current-voltage (I-V) characteristics were evaluated at various stages of the process sequence and provided an excellent diagnostic for monitoring the effect of plasma processes such as chemical vapor deposition or etching. A comparison is given with large emitter-area ($1.96 \times 10^3 \text{ mcm}^2$) devices fabricated on the same material. The small-area devices are attractive for microwave power switching applications provided a high-yield process can be developed. copyright 2001 American Vacuum Society. [J292]

"Ultrahigh-rate plasma jet chemical etching of silicon"

A very high-rate chemical dry etching technique based on the plasma jet principle is presented. In this system a gas mixture of $\text{Ar/SF}_6/\text{O}_2$ is fed into the vacuum system through a nozzle. In the vicinity of the nozzle a microwave-excited plasma jet is formed. Reactive radicals created in the plasma jet flow onto the workpiece surface which is located downstream from the plasma jet. Volume etch rates in the order of $50 \text{ mm}^3/\text{min}$ can be achieved. The dependence of the etch rate on the gas mixture and ambient pressure as well as surface temperature has been determined. Reactive species could be identified by means of optical emission spectroscopy. copyright 2001 American Vacuum Society. [J293]

"Spatial distributions of the absolute CF and CF₂ radical densities in high-density plasma employing low global warming potential fluorocarbon gases and precursors for film formation"

Behaviors of gas species in electron cyclotron resonance (ECR) plasmas employing low global warming potential fluorocarbon gases of hexafluorobutadiene (C_4F_6) and hexafluoropropene (C_3F_6) with unsaturated carbon bonds together with the conventional octafluorocyclobutane ($\text{c-C}_4\text{F}_8$) are investigated. The spatial distributions of the absolute CF and CF_2 radical densities are measured by combining the single-path infrared diode laser absorption spectroscopy and laser-induced fluorescence techniques. CF_2 radicals have hollow-type distributions at all conditions in the ECR plasma reactor. However, the spatial distribution of the CF radical density differs greatly from that of the CF_2 radical density. Behaviors of carbon atoms measured by vacuum ultraviolet absorption spectroscopy disagree with those of CF and CF_2 radical densities. The behaviors of ion and fluorine species and the gas pressure in the plasma have been also evaluated. Fluorocarbon films with low dielectric constant of about 3.0 are deposited at a high rate of 600 nm/min at high microwave powers in C_3F_6 and C_4F_6 plasmas. The distribution of deposition rates of the film on the 8 in. Si substrate shows hill-type distributions, which are quite different from the spatial distributions of CF and CF_2 radical densities. Therefore, CF and CF_2 radicals do not directly contribute greatly to the growth of fluorocarbon films in these plasmas. The behaviors of C atom densities indicate the similar tendency to those of deposition rates of films. On the basis of systematically measured results of species in the plasma and film deposition rate on Si wafer, it is clarified that the C atom and polymeric species contribute dominantly to the formation of films at a high rate in low-pressure and high-density fluorocarbon plasmas. copyright 2001 American Vacuum Society. [J294]

"Computational modeling of three-dimensional microwave tomography of breast cancer"

The microwave tomographic approach is proposed to detect and image breast cancers. Taking into account the big difference in dielectrical properties between normal and malignant tissues, the authors have proposed using the microwave tomographic method to image a human breast. Because of the anatomical features of the objects, this case has to be referred to the tomography with a limited angle of observation. As a result of computer experiments the authors have established that multiview cylindrical configurations are able to provide microwave tomograms of the breast with a small size tumor inside. Using the gradient method, the authors have developed a computer code to create images of the three-dimensional objects in dielectrical properties on microwave frequencies. [J295]

"2000 Medical Imaging Conference (MIC)"

The following topics were dealt with: detectors and camera technology (including: a pixellated semiconductor gamma camera; virtual PMTs); PET instrumentation (including: collimated coincidence point sources; an LSO scintillator array); SPECT instrumentation (including: a quasi-monochromatic CT system; scintillation cameras); image analysis and processing (including: 3D image reconstruction; absorbed dose imaging and profiling); miniature radiation cameras (including: an axillary region PET system; small animal SPECT) [J296]

"Active-amplifier-array diagnostics using high-resolution electrooptic field mapping"

Several Ka-band spatial-amplifier power combiners and their free-space feeds were characterized using a high-resolution extreme-near-field electrooptic measurement technique. The two-dimensional electric-field amplitude and phase maps obtained from several arrays are presented. The usefulness of the technique for diagnostic purposes during the design and prototyping stages of the active arrays is discussed. In particular, the electrooptic maps were shown to be valuable for making improvements in the bias line design in one case, and for isolating faulty unit cells in another case [J297]

"Quartz-crystal microbalance study for characterizing atomic oxygen in plasma ash tools"

This article discusses the measurement of atomic oxygen (AO) concentrations in an oxygen discharge using a quartz-crystal microbalance (QCM). This is a device that has been previously used for monitoring thin-film deposition, among several other applications. The sensor consists of a silver-coated quartz crystal that oscillates at its specific resonant frequency (typically, at about 6 MHz), which is dependent on the mass of the crystal. When exposed to AO, the silver oxidizes rapidly, resulting in a change in its mass, and a consequent change in this frequency. The frequency change is measured with a counter, and when plotted versus time, it may be fit to a standard diffusion-limited oxide-growth model. This model is then used to determine the specific AO flux to the crystal, and by inference, to the wafer. Initial results of QCM measurements in the FusionGemini Plasma Asher (GPL™-standard downstream microwave asher) and FusionGemini Enhanced Strip (GES™-fluorine compatible enhanced strip asher) are presented in this article. The results indicate AO densities of the order of 10^{12} cm⁻³ on the wafer. There is a marked increase in AO concentration with addition of nitrogen into the plasma, and a decrease in AO concentration with increasing pressure at constant flow. Effects of increasing the total plasma volume in the enhanced strip tool on AO production are discussed. copyright 2001 American Vacuum Society. [J298]

"Measurement of ion temperatures in a large-diameter electron cyclotron resonance plasma"

The ion temperature in a large-diameter electron cyclotron resonance plasma is measured using high-resolution optical emission spectroscopy, and the correlation between the ion temperature and fluctuations observed near the chamber wall is investigated. Furthermore, the effect of multicusped fields on the ion temperature is examined. The ion temperature and the amplitude of ion saturation current fluctuations are found to decrease when multicusped fields are applied. The ion temperature and fluctuations increase with increasing incident microwave powers from 2.0 to 2.5 kW, indicating that the ion temperature is correlated with the fluctuation amplitude. The measurement of the ion saturation current fluctuation and floating potential fluctuation suggests that the fluctuations are excited by flute instability. copyright 2001 American Institute of Physics. [J299]

"Microwave image reconstruction utilizing log-magnitude and unwrapped phase to improve high-contrast object recovery"

Reconstructing images of large high-contrast objects with microwave methods has proved difficult. Successful images have generally been obtained by using a priori information to constrain the image reconstruction to recover the correct electromagnetic property distribution. In these situations, the measured electric field phases

as a function of receiver position around the periphery of the imaging field-of-view vary rapidly often undergoing changes of greater than π radians especially when the object contrast and illumination frequency increase. Here, the authors introduce a modified form of a Maxwell equation model-based image reconstruction algorithm which directly incorporates log-magnitude and phase of the measured electric field data. By doing so, measured phase variation can be unwrapped and distributed over more than one Riemann sheet in the complex plane. Simulation studies and microwave imaging experiments demonstrate that significant image quality enhancements occur with this approach for large high-contrast objects. Simple strategies for visualizing and unwrapping phase values as a function of the transmitter and receiver positions within our microwave imaging array are described. Metrics of the degree of phase variation expressed in terms of the amount and extent of phase wrapping are defined and found to be figures-of-merit which estimate when it is critical to deploy the new image reconstruction approach. In these cases, the new algorithm recovers high-quality images without resorting to the use of a priori information on object contrast and/or size as previously required. [J300]

"Electron temperature measurement in a slot antenna 2.45 GHz microwave plasma source"

The electron temperature in a low-pressure microwave electron cyclotron resonance slot antenna produced plasma is obtained. The upper excited atomic level populations have been measured through atomic emission spectroscopy. It has been shown that the Corona balance provides a good description of such levels and, based on this fact, a simple argon collisional-radiative model has been used in the temperature determination. copyright 2001 American Vacuum Society. [J301]

"Analytical simulation of microwave reflectometry of a plasma cylinder"

An analytical solution of a time-dependent two-dimensional (2D) full-wave equation is obtained for the case of microwave propagation in a plasma with axial symmetry. The 2D structure of the electromagnetic wave in a nonmagnetized plasma (or an ordinary wave in a magnetized plasma) is studied for the general case of arbitrary time dependence of the incident wave emitted by the horn. The solutions cover the cases of conventional microwave reflectometry as well as the ultrashort pulse reflectometry of fusion and processing plasma. Analytical expressions can be further applied to study plasma density fluctuations as well as effects of plasma curvature and multidimensionality. The 2D plasma cylinder model is deemed by the authors to be more realistic as compared to the one-dimensional plasma slab model previously employed in all the analytical and most numerical treatments since the plasma in the fusion toroidal devices, mirror machines, and plasma processing chambers can be considered axially symmetric on the scale relevant to microwave reflectometry. copyright 2001 American Institute of Physics. [J302]

"New diagnostics for physics studies on TEXTOR-94 (invited)"

Recently the Dutch, Belgian, and North-Rhine Westphalian Fusion Institutes have consolidated their fusion research on the medium-sized tokamak TEXTOR-94 in the so-called Trilateral Euregio Cluster. To aid the new physics program of TEC, a large number of advanced core diagnostics has recently been implemented. In this article we will discuss the reasoning that has led to the choices of the various diagnostics. Furthermore, we will briefly describe the new diagnostics systems. copyright 2001 American Institute of Physics. [J303]

"Microwave interferometer for steady-state plasmas"

Standard single frequency, "fringe-counting," microwave interferometers are of limited use for steady-state plasma experiments. We have constructed a swept frequency microwave interferometer, similar to a classic zebra-stripe interferometer, optimized for electron density measurements in steady-state plasma experiments. The key element in the system is a frequency doubled YIG oscillator capable of sweeping from 20 to 40 GHz. As the source frequency is swept, the sum of the reference and plasma leg signals exhibits a series of beats. Both the frequency shift and phase shift of the beat pattern due to the addition of plasma in one leg of the interferometer is used to determine the line-integrated electron density. copyright 2001 American Institute of Physics. [J304]

"Microwave reflectometry for turbulence studies on ASDEX Upgrade"

We study the evolution of turbulence at several radial plasma locations in the Axially Symmetric Divertor Experiment (ASDEX) Upgrade tokamak, using microwave reflectometry. We analyze two types of scenarios: H-mode plasmas with improved performance and plasmas with electron cyclotron resonance heating modulation. Profound modifications of the turbulence spectra, occurring at specific plasma regions, have been found in both cases, indicating the relation between turbulence changes and confinement. The results demonstrate the ability of the reflectometry system on ASDEX Upgrade to make localized measurements. Mapping the radial distribution of turbulence can help us to understand the links between plasma rotation, shear, E \times B flows, and the plasma

turbulence behavior. copyright 2001 American Institute of Physics. [J305]

"Extreme broadband multichannel ECE radiometer with "zoom" device"

A new radiometer has been built up for the W7-AS stellarator which consists of a frontend with an extreme broadband mixer, two intermediate frequency (IF) parts with 16 channels each and a novel additional 16 filter section with variable IF. The system was designed with the future W7-X in mind. All settings can therefore be remotely changed. This "W7-X" system is integrated into the electron cyclotron emission (ECE) systems at W7-AS. EC radiation is collected using elliptical mirrors in Gaussian optics. W7-AS results will be shown. The "zoom" device is installed at DIII-D at the moment; first results are also shown. copyright 2001 American Institute of Physics. [J306]

"Application of millimeter-wave imaging system to LHD"

Millimeter-wave imaging systems in the frequency range of 70-140 GHz have been developed for diagnostics of magnetically confined plasmas. The 70 GHz imaging system successfully measures time evolutions of both radial and axial profiles of line density and electron cyclotron emission (ECE) in a tandem mirror. The imaging system is being installed in Large Helical Device (LHD) at the National Institute for Fusion Science. In order to cover the frequency range of the second harmonic ECE on LHD, a new detector using monolithic microwave integrated circuit technology has been designed and fabricated. The detector consists of the integration of a receiving antenna, a down-converting mixer diode, and an intermediate frequency amplifier on a GaAs substrate chip. The heterodyne response up to 10 GHz was confirmed at 70-140 GHz. The optical system consisting of an ellipsoidal mirror and a flat mirror was designed by using a ray-tracing code and evaluated experimentally at 140 GHz. copyright 2001 American Institute of Physics. [J307]

"Plasma diagnostics for the sustained spheromak physics experiment"

In this article we present an overview of the plasma diagnostics operating or planned for the sustained spheromak physics experiment device now operating at Lawrence Livermore National Laboratory. A set of 46 wall-mounted magnetic probes provide the essential data necessary for magnetic reconstruction of the Taylor relaxed state. Rogowski coils measure currents induced in the flux conserver. A CO₂ laser interferometer is used to measure electron line density. Spectroscopic measurements include an absolutely-calibrated spectrometer recording extended domain spectrometer for obtaining time-integrated visible ultraviolet spectra and two time-resolved vacuum monochrometers for studying the time evolution of two separate emission lines. Another time-integrated spectrometer records spectra in the visible range. Filtered silicon photodiode bolometers provide total power measurements, and a 16 channel photodiode spatial array gives radial emission profiles. Two-dimensional imaging of the plasma and helicity injector is provided by gated television cameras and associated image-processing software. An array of fiber-coupled photodetectors with H alpha filters view across the midplane and in the injector region to measure neutral hydrogen concentrations. Several novel diagnostics are being fielded including a transient internal probe (TIP) and an ultrashort-pulse reflectometer (USPR) microwave reflectometer. The TIP probe fires a very high velocity optical bullet through the plasma and will provide fairly nonperturbative internal magnetic field and current measurements to compare with an equilibrium code model fitted to wall-mounted probes. The USPR is being designed to study edge density and turbulent fluctuations. A multipoint Thomson scattering system is currently being installed to give radial temperature and density profiles. copyright 2001 American Institute of Physics. [J308]

"Diagnostics of inductively coupled chlorine plasmas: Measurement of electron and total positive ion densities"

This work is part of a broader study that creates a set of experimentally measured chlorine plasma parameters (electron and gas temperatures, electron energy distribution function, electron density, densities of ion fractions, and total ion density). This set is obtained over a broad range of operating conditions (1-20 mTorr, 5-1000 W) of an inductively coupled plasma. In this part, we present the electron (n_e) and total positive ion ($n_i = n_{Cl^{2+}} + n_{Cl^{+}}$) densities. n_e and n_i were measured with a Langmuir probe across the diameter or in the middle of the reactor. Line integrated values of n_e were independently obtained with microwave interferometry, and converted into the spatially resolved data using the Langmuir probe n_e profiles. Finally, a method is presented for measuring relative positive ion densities, based on optical emission at 7504 Å from trace amounts of Ar. copyright 2001 American Institute of Physics. [J309]

"Energy coupling efficiency of a hydrogen microwave plasma reactor"

Zero-dimensional and two-dimensional plasma models and optical emission spectroscopy are used in tandem to investigate the power coupling efficiency for a pure hydrogen microwave plasma. The zero-dimensional model

accounts for the vibrational kinetics of H₂, the chemistry of H₂ and H excited states, and the kinetics of ground-state species. The set of species conservation equations are then coupled to the electron Boltzmann equation (to account for the non-Maxwellian electron energy distribution function) and the total energy equation for solution. The two-dimensional model makes use of a simpler thermochemical description of the plasma. The chemistry is described with nine species and thirty chemical reactions. Three energy modes are considered to describe the plasma's thermal nonequilibrium, and Maxwellian distribution functions for kinetic and vibrational modes are assumed. The non-Maxwellian nature of the electron energy distribution function is separately accounted for. Experimentally, the absolute line emission intensity is utilized to obtain number densities of up to five hydrogen excited states using the following transitions: H α (6563 E), H β (4861 E), H γ (4340 E), H δ (4102 E), and H ϵ (3970 E). The first three transitions were used for a 38 Torr, 1000 W hydrogen discharge, and all five transitions were used for a 121 Torr, 4000 W hydrogen discharge. The absolute continuum emission from the plasma was compared to numerical predictions. The comparison of the numerical and experimental data indicates that 90%-100% of the input power is deposited in the plasma and that both the line and continuum emission match within a factor of 3, with the exception of the high energy excited states for the 4000 W plasma. A control volume heat transfer analysis validates the energy coupling. copyright 2001 American Institute of Physics. [J310]

"Surface recombination of hydrogen atoms studied by a pulsed plasma excitation technique"

The H atom lifetime in a low pressure hydrogen microwave plasma was measured using a pulse induced fluorescence technique. This technique is compared to results obtained by a laser spectroscopy technique. We first demonstrate the validity of the method and then deduce H atom lifetime pressure dependence. The H atom surface loss probability on fused silica was also deduced from our measurements. We show that this coefficient is not constant in the time afterglow but decreases almost by one order of magnitude (from 2.3×10^{-3} to 2.1×10^{-4}) during the first milliseconds. These results are explained using recent experimental and theoretical works concerning atom-surface interaction in low temperature plasmas. copyright 2001 American Institute of Physics. [J311]

"Electron density and recombination rate measurements in CO-seeded optically pumped plasmas"

Electron production rate and electron density in cold optically pumped CO-Ar and CO-N₂ plasmas in the presence of small amounts of O₂ and NO have been measured using a Thomson discharge probe and microwave attenuation. Nonequilibrium ionization in the plasmas is produced by an associative ionization mechanism in collisions of highly vibrationally excited CO molecules. It is shown that adding small amounts of O₂ or NO (50-100 mTorr) to the baseline gas mixtures at P=100 torr results in an increase of the electron density by up to a factor of 20-40 (from $n_e = 10^{10} \text{ cm}^{-3}$ to $n_e = (1.5-3.0) \times 10^{11} \text{ cm}^{-3}$). This occurs while the electron production rate either decreases (as in the presence of O₂) or remains nearly constant within a factor of 2 (as in the presence of NO). It is also shown that the electron-ion recombination rates inferred from these measurements decrease by two to three orders of magnitude compared to their baseline values (with no additives in the cell), down to $\beta = 1.5 \times 10^{-8} \text{ cm}^3/\text{sw}$ with 50-100 mTorr of oxygen or nitric oxide added to the baseline CO-Ar mixture, and $\beta = (2 \text{ to } 3) \times 10^{-7} \text{ cm}^3/\text{sw}$ with 75-100 mTorr of O₂ or N₂O added to the baseline CO-N₂ mixture. The overall electron-ion removal rates in the presence of equal amounts of O₂ or NO additives turn out to be very close, which shows that the effect of electron attachment to oxygen at these conditions is negligible. These results suggest a novel method of electron density control in cold laser-sustained steady-state plasmas and open a possibility of sustaining stable high-pressure nonequilibrium plasmas at high electron densities and low plasma power budget. copyright 2001 American Institute of Physics. [J312]

"Low temperature diamond growth using CO₂/CH₄ plasmas: Molecular beam mass spectrometry and computer simulation investigations"

Microwave plasma enhanced chemical vapor deposition has been used to grow diamond films at substrate temperatures down to 435 °C using CO₂/CH₄ gas mixtures. An Arrhenius plot of growth rate as a function of substrate temperature yields a value for the activation energy for the growth step of 28 kJ mol⁻¹. This is lower than that measured previously for CH₄/H₂ systems and hints at a different gas-surface chemistry when using CH₄/CO₂ plasmas. Molecular beam mass spectrometry has been used to measure simultaneously the concentrations of the dominant gas phase species present during growth, for a wide range of plasma gas mixtures (0%-80% CH₄, balance CO₂). The CHEMKIN computer package has also been used to simulate the experimental results in order to gain insight into the major reactions occurring within the microwave plasma. The calculated trends for all species agree well with the experimental observations. Using these data, the model for the gas phase chemistry can be reduced to only four overall reactions. Our findings suggest that CH₃ radicals are likely to be the key growth species when using CO₂/CH₄ plasmas and provide a qualitative explanation for the narrow concentration window for diamond growth. copyright 2001 American Institute of Physics. [J313]

"Characteristics of an electronically tunable surface-coil-type resonator for L-band electron paramagnetic resonance spectroscopy"

This note describes considerable additional information on the key parameters of an electronically tunable surface-coil-type resonator for L-band continuous-wave electron paramagnetic resonance (EPR) spectroscopy [Hirata et al, J. Magn. Reson. 142, 159 (2000)]. For the 1.1 GHz prototype tunable surface coil (10.6 mm in diameter), the measured efficiency for generating the rf magnetic field is $77 \mu T/W^{1/2}$. The unloaded quality factor of the tunable surface coil is in the range of 260-310. In absence of an EPR sample, 57% of the magnetic energy in the system is stored in the parallel coaxial line, 16% in the surface coil, and a half of the energy is dissipated in the parallel coaxial line. The energy dissipation for the surface coil occurs mainly through radiation (25% of the total energy dissipation). The level of the second harmonic in the reflected microwaves generated by the tunable surface coil was measured. The varactor diodes used in the matching and tuning circuits are the dominant source of the second harmonic. copyright 2001 American Institute of Physics. [J314]

"Plasma diagnostics at electron cyclotron resonance ion sources by injection of laser ablated fluxes of metal atoms"

Short pulses of neutral particles generated by laser ablation of metal targets have been injected into the Frankfurt 14 GHz electron cyclotron resonance (ECR) ion source. Rise/fall times of pulses of highly charged ions of Cd and Mg were registered as a function of microwave power and gas pressure. From a comparison of the measured data to numerical simulations, values of the electron density and the temperature in the ECR plasma were estimated to be about $0.75 \times 10^{12} \text{ cm}^{-3}$ and a few keV. The effective electron temperature increases with increasing microwave power and decreases with increasing gas pressure. The electron density is only a weak function of the microwave power, but increases significantly with the gas pressure. In the Ar/O₂ gas-mixing mode of operation, an improved confinement of lowly charged ions was observed. copyright 2001 American Institute of Physics. [J315]

"Mass spectrometric studies of a CH₄/H₂ microwave plasma under diamond deposition conditions"

We report on mass spectroscopic measurements of species originating from a microwave (MW) discharge plasma under simulated diamond deposition conditions. The plasma is produced in a 30 W MW flow tube through which flows a gas mixture of about 1% methane admixed in hydrogen. Plasma composition was investigated as a function of gas component ratio by Li⁺-ion attachment mass spectrometry. C, C₂, C₂H, C₂H₂, and C₂H₄, together with the free-radical species of C₂H₃ and C₂H₅, were observed on the mass spectra as Li⁺-ion adducts. Atomic carbon was the most abundant species, suggesting an important role for atomic carbons in diamond film growth. copyright 2001 American Institute of Physics. [J316]

"Characterization of electron and negative ion densities in fluorocarbon containing inductively driven plasmas"

Electron and negative ion densities were measured in inductively coupled discharges containing C₄F₈. In addition, the identity of the negative ions in C₂F₆, CHF₃, and C₄F₈ containing discharges was investigated with a photodetachment experiment utilizing a microwave resonant cavity structure. To investigate the influence of surface material, the rf-biased electrode was covered with a silicon wafer or a fused silica (SiO₂) wafer. Line-integrated electron density was determined using a microwave interferometer, and absolute negative ion densities in the center of the plasma were inferred using laser photodetachment spectroscopy. Voltage and current at the induction coil and rf-biased electrode were also measured for both surfaces as functions of induction coil power, pressure, and rf bias. For the range of induction powers, pressures, and bias power investigated, the electron density peaked at $6 \times 10^{12} \text{ cm}^{-2}$ (line integrated), or approximately $6 \times 10^{11} \text{ cm}^{-3}$. The negative ion density peaked at approximately $2.2 \times 10^{11} \text{ cm}^{-3}$. In most cases, the trends in the electron and negative ion densities were independent of the wafer material. However, a maximum in the negative ion density as a function of induction coil power was observed above a silicon wafer. The maximum is attributed to a power-dependent change in the density of one or more of the potential negative ion precursor species. A microwave resonant cavity structure was developed to identify the negative ions using laser photodetachment spectroscopy. The technique was demonstrated for inductively coupled discharges containing C₄F₈, C₂F₆, and CHF₃. Scanning the laser wavelength over the range of the F-photodetachment energy indicated that while the dominant negative ion appeared to be F⁻, weak evidence for other molecular negative ions was observed. Unlike traditional microwave cavity techniques, this method offers the possibility of spatial resolution. copyright 2001 American Institute of Physics. [J317]

"Advances in quasioptical grid array technology for millimeter-wave plasma imaging diagnostics"

Quasioptical grid array technologies can provide low cost, wide bandwidth sources supplying 100-500 mW power levels needed for reflectometric and electron cyclotron imaging of fusion plasmas. Broadband quasioptical overmoded waveguide frequency multiplier grid array systems have been designed, simulated, fabricated, and are under test with a goal of providing Watt level output powers from 50 to 200 GHz. Both 148, one-dimensional and 444, two-dimensional phased antenna arrays utilizing Schottky varactor loaded transmission lines have been designed, simulated, fabricated, and are being tested. Microelectromechanical systems have been designed and fabricated on silicon wafers with traditional integrated circuit processing techniques, resulting in devices with physical dimensions on the order of a few tens of microns. copyright 2001 American Institute of Physics. [J318]

"Implementation of reflectometry as a standard density profile diagnostic on DIII-D"

The profile reflectometer system on the DIII-D tokamak has been significantly upgraded in order to improve time coverage, data quality, and profile availability. The performance of the reflectometer system, which utilizes continuous frequency modulated (FMCW) radar techniques, has been improved as follows: First, a new PC-based data acquisition system has been installed, providing higher data sampling rates and larger memory depth. The higher sampling rate enables use of faster frequency sweeps of the FMCW microwave source, improving time resolution, and increasing profile accuracy. The larger memory depth enables longer data records, so that profiles can now be obtained throughout 5 s discharges at 100 Hz profile measurement rates, while continuous sampling at 10 MHz is available for 1 s for high time resolution physics studies. Second, an initial automated between-shots profile analysis capability is now available. Third, availability of the profiles to end users has been significantly improved. copyright 2001 American Institute of Physics. [J319]

"Microwave reflectometry for turbulence studies on ASDEX upgrade (abstract)"

The reflectometry system installed in the tokamak ASDEX Upgrade has 11 channels primarily aimed at profile measurements and two dedicated channels operating at fixed frequency to study density fluctuations. The channels used for profile measurements can also be operated at fixed frequency. In this article we describe the potential of the system to study important characteristics of the plasma turbulence, from combined fixed frequency and profile measurements (to localize the reflecting layers). The numerical tools used to treat fixed frequency data are briefly described. Using a set of similar discharges and the ability of the microwave reflectometry system to probe simultaneously different layers with several channels, we obtain the time evolution of the integrated power spectra of the different signals versus the minor radius of the plasma. In plasma with H-mode edge and internal transport barrier we could identify a zone at the plasma core and another at the edge with reduced fluctuation levels, coinciding with the increase of central electron temperature and the L-H transition, respectively. Before each barrier is established, the turbulence is observed to decrease at the lower frequency range and is enhanced at the higher frequencies. In modulation electron cyclotron resonance heating experiments similar modifications in turbulence spectra are observed and may be correlated with the modulation period. copyright 2001 American Institute of Physics. [J320]

"Pulsed radar reflectometry on the LHD"

Pulsed radar reflectometry is a suitable reflectometric technique with which to study the effect of strong magnetic shear for the polarization of microwaves in the Large Helical Device. Because pulsed radar reflectometry measures the delay time of the reflected wave, not the phase, X-mode and O-mode polarized waves can be distinguished. At a preliminary stage of X-mode operation it is found that the position of the ergodic edge layer is steady in spite of the increased density in the core region when a neutral beam is injected. If the electron density does not reach the critical cutoff density, the pulsed radar system could be used as a delayometer. The measured delayometer signal is almost in agreement with the numerical calculation under the assumption that polarization of the wave propagated into the plasma is decided at the edge region. copyright 2001 American Institute of Physics. [J321]

"Doppler reflectometry for the investigation of propagating density perturbations"

In a Doppler reflectometry experiment the line of sight is chosen to be nonperpendicular with respect to the reflecting layer. This type of diagnostic is able to probe density perturbations with the wave number in the reflecting layer selected by the tilt angle. The propagation velocity of the perturbations is calculated from the Doppler shift of the returning microwave signal whereas its intensity contains information about the perturbation amplitude. The diagnostic capability of Doppler reflectometry is demonstrated at the W7-AS stellarator using an antenna system with variable tilt angle. The measured values of the propagation velocity of density perturbations and its radial dependence are in good agreement with the E_c velocity of the plasma obtained from

spectroscopy. Transient states can be followed with a temporal resolution less than 50 μ s. Therefore Doppler reflectometry allows one to test the interdependence of sheared flow and turbulence on that timescale. copyright 2001 American Institute of Physics. [J322]

"Performance of the microwave reflectometry diagnostic for density profile measurements on ASDEX Upgrade"

The broadband reflectometry system on ASDEX Upgrade is now routinely providing electron density profiles with a minimum temporal spacing of 30 μ s. The plasma is probed from zero density to $n_e=6.64 \times 10^{19}$ m⁻³ at the low field side with combined O and X modes, and from $n_e=0.318 \times 10^{19}$ to $n_e=6.64 \times 10^{19}$ m⁻³ at the high field side using O mode. Here we analyze the performance of the diagnostic for profile measurements taking into account its design options and the experimental results obtained in a wide range of plasma regimes. We address several questions, in particular the measuring range of the antennas and the range of density gradients. It is shown that it is possible to obtain a detailed evolution of the density profile and density gradient even in the presence of turbulence, providing that sufficient data can be extracted from the plasma. The radial movements of the plasma can be measured with great accuracy, which is especially important for the use of reflectometry for plasma position control, as is proposed for the International Thermonuclear Experimental Reactor. The experimental results demonstrate that the frequency modulation of a continuous wave reflectometry system on ASDEX Upgrade can provide reliable and accurate density profile measurements at both sides of the plasma with automatic analysis. copyright 2001 American Institute of Physics. [J323]

"Dual mode (ordinary-extraordinary) correlation reflectometry for magnetic field and turbulence measurements (invited)"

Dual mode [ordinary-extraordinary (O-X)] correlation reflectometry has the potential advantage of being able to determine magnetic field strength, $|B_z|$, simultaneously with correlation properties of turbulence (e.g., radial correlation length, coherency, power spectra, etc.). Controlled dual mode correlation reflectometry experiments, conducted in the Large Plasma Device at UCLA, are presented. The purpose of these experiments was (1) to demonstrate the proof of principle of $|B_z|$ measurement, and (2) to make detailed comparisons between dual mode and single mode (O-O, X-X) reflectometer, and Langmuir probe radial correlation measurements. It is shown that, in these experiments, $|B_z|$ can be determined from O-X correlation measurements, interpreted via a one-dimensional numerical model. In addition, good agreement is found between correlation lengths (within 10%-15%), coherency, and power spectra measured by O-X, O-O, and X-X reflectometry, and a Langmuir probe array. copyright 2001 American Institute of Physics. [J324]

"Assessment of density profile automatic evaluation from broadband reflectometry data"

Automatic evaluation of electron density profiles from frequency modulated continuous wave (FM-CW) broadband microwave reflectometry on ASDEX Upgrade has been achieved in all plasma regimes combining a high performance system and advanced analysis tools. The results presented demonstrate the capability of the system to resolve the abrupt gradient changes occurring in the edge region during the L-H transition and in the presence of edge localized modes (ELMs). The temporal evolution of the density gradient could be obtained extending from the ohmic and L phases to the ELM H phase. A new data analysis method that uses sets of consecutive sweeps to extract the group delay is also presented and its use versus single sweep analysis is discussed. It is shown that local perturbations may appear and disappear during the sweep time reinforcing the need to obtain redundant data in very short time intervals and apply rejection/averaging techniques. copyright 2001 American Institute of Physics. [J325]

"Simulation of reflectometry density changes using a 2D full-wave code"

Broadband reflectometry is used to obtain density profiles in fusion plasmas using waves reflected at different plasma layers. The reflected signal can be severely affected by plasma fluctuations and/or fast density changes. In order to understand the plasma response, a finite difference time domain two-dimensional full wave code was developed. The code was used to study typical situations of fusion plasmas where important profile movements occur: when a rotating magnetic island is present and during an ELM. The numerical results are in good agreement with experimental results obtained in ASDEX and ASDEX Upgrade in the situations above. Our study demonstrates that contributions from the plasma movements are important and should be taken into account to obtain accurate profile measurements. copyright 2001 American Institute of Physics. [J326]

"Measurement of cross-polarization scattering using ultrashort pulse microwaves"

A numerical simulation of cross-polarization scattering (CPS) was performed by using frequency dependent finite

difference time domain [(FD)2TD]method. In the CPS process, an incident ordinary (extraordinary) wave is converted to an extraordinary (ordinary) wave by magnetic fluctuations in a plasma. It is confirmed in the simulation that an incident wave propagates in an anisotropic dispersive media properly. The relation between scattered electric field and magnetic fluctuations is also obtained. copyright 2001 American Institute of Physics. [J327]

"Collective microwave scattering diagnostic on the H-1 heliac"

A multichannel microwave scattering diagnostic has been developed and installed on the H-1 heliac. The purpose of the new diagnostic is to study small-scale plasma fluctuations in H-1, which are believed to be responsible for the loss of particles and energy from the plasma. The diagnostic is a 132 GHz, four-channel superheterodyne system. The transmitter and receiver antennas (consisting of horns and focusing bispherical mirrors) are located inside the vacuum vessel of H-1. A radial resolution of $\Delta r/a = 0.2$ is achieved. The scattering volume is positioned in the density gradient region at $r/a = 0.6$. At present, the system is aligned to measure fluctuations in the poloidal wave number range from approximately 10 to 25 cm⁻¹. The use of the heterodyne detection system allows the fluctuation propagation direction to be determined. The low frequency bandwidth of the system is 1 MHz. The instrument sensitivity is about $P_s/P_i = 10^{-6}$. copyright 2001 American Institute of Physics. [J328]

"Millimeter-wave imaging array development for microwave reflectometry and ECE imaging"

Millimeter-wave imaging arrays employing slot bow-tie (SBT) antenna elements and GaAs Schottky diodes have previously been successfully developed and utilized in electron cyclotron emission imaging systems, which have proven to be an important new plasma diagnostic technique for measuring plasma electron temperature profiles and fluctuations. More recently, there has been interest in applying similar arrays for reflectometric imaging. Here, the design of SBT antennas for proof-of-principle millimeter-wave imaging reflectometry receiver arrays for use on Torus Experiment for Technology Oriented Research is presented. These low-cost, 14-channel Schottky mixer diode arrays, designed at 85 GHz, have been developed for measuring plasma electron density fluctuation profiles, which are expected to solve the long standing issue of ambiguity in the interpretation of reflectometric data. The final layout of the array is shown, together with details and experimental results of single SBT antennas. copyright 2001 American Institute of Physics. [J329]

"Three-dimensional fluctuation imaging diagnostic for TEXTOR (abstract)"

After more than 4 decades of fusion research, plasma transport in tokamaks remains an outstanding issue. The standard hypothesis, that the observed anomalous transport is caused by small scale turbulence, is consistent with experimental observations, but it is neither based on a self-consistent theory of plasma turbulence nor on an exhaustive set of turbulence measurements. One of the major obstacles to the development of a satisfactory anomalous transport theory is the inability of standard fluctuation diagnostics to provide the full spectrum of turbulent fluctuations. The result is a nearly complete reliance on numerical simulations. Unfortunately, in spite of the enormous capabilities of today's computers, this is extremely unsatisfactory since any theory or simulation of plasma turbulence can only be driven by direct experimental observations. The first step in achieving such data was the highly successful UC Davis Electron Cyclotron Emission (ECE) Imaging system, which was first developed for use on the TEXT-U tokamak and later modified for use on the Rijnhuizen Tokamak Project tokamak. Here, correlation techniques are applied to spatially resolved second harmonic ECE signals to provide detailed information about the microturbulence associated with Te fluctuations. The present work extends this work by developing a similar technique for spatially resolved ne fluctuations via microwave imaging reflectometry. The result is a diagnostic capable of the simultaneous measurement of both Te and ne fluctuations (both turbulent and coherent) and profiles on toroidal devices such as tokamaks and stellarators. A 16 channel ECE imaging system has recently been installed on the Torus Experiment for Technology Oriented Research (TEXTOR) tokamak. A prototype millimeter wave imaging reflectometry system will be installed on TEXTOR in July-2000, which will operate in Vband (50-75 GHz) and reflect from the X-mode cutoff. Data collected with this system will be utilized in the design of the full three-dimensional (3D) imaging system, which is scheduled for installation on TEXTOR in April 2001. System details and laboratory characterization results of the prototype reflectometric imaging system will be presented, along with a preliminary design for the full 3D system. copyright 2001 American Institute of Physics. [J330]

"The ten-channel pulsed radar reflectometer at the TEXTOR-94 tokamak"

A new ten-channel pulsed radar reflectometer has been taken into operation at the Torus Experiment for Technology Oriented Research-94. The system will be used simultaneously as a density profile and as a density fluctuation diagnostic. Ten density layers from 0.44 to 0.19 m can be probed simultaneously at 2 MHz.

The design of the diagnostic has undergone some changes, to improve reliability of the system. Examples of time delay measurements are shown. These examples illustrate the fluctuation capabilities of the diagnostic at high time resolution, as well as the response of the different channels to density profile changes. copyright 2001 American Institute of Physics. [J331]

"Ultrashort pulse reflectometry for electron density profile measurements on SSPX"

A broadband ultrashort pulse reflectometry (USPR) diagnostic has been developed for measuring electron density profiles of the sustained spheromak physics experiment (SSPX) device. In USPR, an extremely short pulse or chirped wave form is propagated which contains a broad range of frequency components spanning the desired plasma density profile (or a significant fraction thereof). Upon reflection, each frequency component in the incident waveform reflects from a different spatial location (density layer) in the plasma, thus spreading out the reflected wave packet in time. By simultaneously collecting double-pass time delay data at many distinct frequencies, the time delay data may then be inverted to generate plasma density profiles using a single source and a single set of measurements. On SSPX, wideband mixers are utilized to up- and downconvert 6-18 GHz chirp signals to millimeter-wave frequencies (33-158 GHz) to form a 48 channel O-mode reflectometer system. In this article we describe details of the new USPR system installed on the SSPX device and provide preliminary time-of-flight results. copyright 2001 American Institute of Physics. [J332]

"Millimeter-wave reflectometry for electron density profile and fluctuation measurements on NSTX"

A millimeter-wave reflectometry system for electron density profile and fluctuation measurements is being developed and installed on the National Spherical Torus Experiment. The initial frequency coverage will be in the bands 12-18, 20-32, and 33-50 GHz, provided by frequency-tunable solid-state sources. These frequencies correspond to O-mode cutoff densities ranging from 1.84×10^{12} to $3.14 \times 10^{13} \text{ cm}^{-3}$, which will span both the plasma core ($\rho = r/a \approx 0.8$) and edge ($\rho \approx 0.8$) regions. Operated as a broadband swept-frequency (frequency-modulated continuous-wave) reflectometer, the diagnostic is expected to provide routine (shot-to-shot) time- ($\leq 50 \mu\text{s}$) and spatially resolved ($\approx 1 \text{ cm}$) density profiles. The previous hardware can be easily reconfigured as a fixed-frequency reflectometer for density fluctuation measurements. The combination of measurements would be valuable for studying phenomena such as possible L- to H-mode transitions and edge-localized modes. copyright 2001 American Institute of Physics. [J333]

"Two-dimensional full-wave simulation of microwave reflectometry on Alcator C-Mod"

A new two-dimensional full-wave code has been developed to simulate ordinary (O) mode reflectometry signals caused by plasma density fluctuations. The code uses the finite-difference time-domain method with a perfectly matched layer absorption boundary to solve Maxwell's equations. Huygens wave sources are incorporated to generate Gaussian beams. The code has been used to simulate the reflectometer measurement of the quasicohherent mode (60-250 kHz) associated with enhanced D-alpha (EDA) H modes in the Alcator C-Mod tokamak. It is found that an analysis of the realistic experimental layout is essential for the quantitative interpretation of the mode amplitude. copyright 2001 American Institute of Physics. [J334]

СПИСОК ЛИТЕРАТУРЫ

- J1. Cataldo A. Broadband Reflectometry for Diagnostics and Monitoring Applications. / Cataldo A., De Benedetto E. // IEEE Sensors Journal. - 2011. - Vol. 11, No. 2. - P. 451-459. ↑
- J2. Zhili Zhang. Quantitative Microplasma Electron Number Density Measurement by Coherent Microwave Rayleigh Scattering. IEEE Transactions on Plasma Science. - 2011. - Vol. 39, No. 1. - P. 593-595. ↑
- J3. Henriques J. Microwave N₂-Ar plasma torch. II. Experiment and comparison with theory. / Henriques J., Tatarova E., Dias F. M., Ferreira C. M. // Journal of Applied Physics. - 2011. - Vol. 109, No. 2. - P. 023302-023302-8. ↑
- J4. Ruchko L. F. Registration of Alfvén resonances in TCABR tokamak by the scanning reflectometer at sideband frequencies. / Ruchko L. F., Elfimov A. G., Teixeira C. M., Elizondo J. I., Sanada E., Galvao R. M. O., Manso M. E., Silva A. // Review of Scientific Instruments. - 2011. - Vol. 82, No. 2. - P. 023504-023504-4. ↑

- J5. Srivastava N. Determination of OH Radicals in an Atmospheric Pressure Helium Microwave Plasma Jet. / Srivastava N., Chuji Wang. // IEEE Transactions on Plasma Science. - 2011. - Vol. 39, No. 3. - P. 918-924. ↑
- J6. Shashurin A. Temporary-resolved measurement of electron density in small atmospheric plasmas. / Shashurin A., Shneider M. N., Dogariu A., Miles R. B., Keidar M. // Applied Physics Letters. - 2010. - Vol. 96, No. 17. - P. 171502-171502-3. ↑
- J7. Maksymov I.S. Approach to Spectral Measurements of a Millimeter-Wave-Band Relativistic Magnetron. / Maksymov I.S., Magda I.I., Ustyantsev M.A., Churyumov G.I. // IEEE Transactions on Plasma Science. - 2010. - Vol. 38, No. 5. - P. 1086-1090. ↑
- J8. O'Halloran M. Quasi-Multistatic MIST Beamforming for the Early Detection of Breast Cancer. / O'Halloran M., Jones E., Glavin M. // IEEE Transactions on Biomedical Engineering. - 2010. - Vol. 57, No. 4. - P. 830-840. ↑
- J9. Jamison S. P. fewUpconversion of a relativistic Coulomb field terahertz pulse to the near infrared. / Jamison S. P., Berden G., Phillips P. J., Gillespie W. A., MacLeod A. M. // Applied Physics Letters. - 2010. - Vol. 96, No. 23. - P. 231114-231114-3. ↑
- J10. Curley G. A. Surface loss rates of H and Cl radicals in an inductively coupled plasma etcher derived from time-resolved electron density and optical emission measurements. / Curley G. A., Gatilova L., Guilet S., Bouchoule S., Gogna G. S., Sirse N., Karkari S., Booth J. P. // and Films Journal of Vacuum Science & Technology A: Vacuum, Surfaces. - 2010. - Vol. 28, No. 2. - P. 360-372. ↑
- J11. Weihua Jiang. Time-Frequency Analysis of Virtual-Cathode Oscillator. IEEE Transactions on Plasma Science. - 2010. - Vol. 38, No. 6. - P. 1325-1328. ↑
- J12. Noland J. Measurement of radial and axial high energy x-ray spectra in electron cyclotron resonance ion source plasmas. / Noland J., Benitez J. Y., Leitner D., Lyneis C., Verboncoeur J. // Review of Scientific Instruments. - 2010. - Vol. 81, No. 2. - P. 02A308-02A308-3. ↑
- J13. Torres J. Multiple diagnostics in a high-pressure hydrogen microwave plasma torch. / Torres J., van der Mullen J. J. A. M., Gamero A., Sola A. // Applied Physics Letters. - 2010. - Vol. 96, No. 5. - P. 051501-051501-3. ↑
- J14. Mashal A. Toward Carbon-Nanotube-Based Theranostic Agents for Microwave Detection and Treatment of Breast Cancer: Enhanced Dielectric and Heating Response of Tissue-Mimicking Materials. / Mashal A., Sitharaman B., Xu Li, Avti P.K., Sahakian A.V., Booske J.H., Hagness S.C. // IEEE Transactions on Biomedical Engineering. - 2010. - Vol. 57, No. 8. - P. 1831-1834. ↑
- J15. Gitlin M. S. Time-resolved imaging of millimeter waves using visible continuum from the positive column of a Cs-Xe dc discharge. / Gitlin M. S., Golovanov V. V., Spivakov A. G., Tsvetkov A. I., Zelenogorskiy V. V. // Journal of Applied Physics. - 2010. - Vol. 107, No. 6. - P. 063301-063301-11. ↑
- J16. Villegas F.J. A Phenomenological Investigation of Anomalous Performance in Flex Coaxial Cables. / Villegas F.J., Adams M., Thompson P., Jackson C. // IEEE Transactions on Microwave Theory and Techniques. - 2010. - Vol. 58, No. 4. - P. 1003-1011. ↑
- J17. Tokuzawa T. Multifrequency channel microwave reflectometer with frequency hopping operation for density fluctuation measurements in Large Helical Device. / Tokuzawa T., Ejiri A., Kawahata K. // Review of Scientific Instruments. - 2010. - Vol. 81, No. 10. - P. 10D906-10D906-4. ↑
- J18. Qing Zhang. Characteristics of Microwave Plasma Torch at Atmospheric Pressure. / Qing Zhang, Guixin Zhang, Shumin Wang, Liming Wang, Na Huo. // IEEE Transactions on Plasma Science. - 2010. - Vol. 38, No. 11. - P. 3197-3200. ↑
- J19. Lei L. A synthetic diagnostic for the evaluation of new microwave imaging reflectometry diagnostics for DIII-D and KSTAR. / Lei L., Tobias B., Domier C. W., Luhmann N. C., Kramer G. J., Valeo E. J., Lee W., Yun G. S., Park H. K. // Review of Scientific Instruments. - 2010. - Vol. 81, No. 10. - P. 10D904-10D904-3. ↑
- J20. Bashirullah R. Wireless Implants. IEEE Microwave Magazine. - 2010. - Vol. 11, No. 7. - P. S14-S23. ↑
- J21. Happel T. On the role of spectral resolution in velocity shear layer measurements by Doppler

reflectometry. / Happel T., Blanco E., Estrada T. // Review of Scientific Instruments. - 2010. - Vol. 81, No. 10. - P. 10D901-10D901-3. ↑

J22. Gorbunov A. V. Development of laser induced fluorescence diagnostic for measuring the parameters of plasma containing rare gas species. / Gorbunov A. V., Molodtsov N. A., Moskalenko I. V., Shcheglov D. A. // Review of Scientific Instruments. - 2010. - Vol. 81, No. 10. - P. 10D712-10D712-4. ↑

J23. Miura N. Argon Microplasma Diagnostics by Diode Laser Absorption. / Miura N., Jun Xue, Hopwood J.A. // IEEE Transactions on Plasma Science. - 2010. - Vol. 38, No. 9. - P. 2458-2464. ↑

J24. Ashtari A. Using a priori Information for Regularization in Breast Microwave Image Reconstruction. / Ashtari A., Noghianian S., Sabouni A., Aronsson J., Thomas G., Pistorius S. // IEEE Transactions on Biomedical Engineering. - 2010. - Vol. 57, No. 9. - P. 2197-2208. ↑

J25. Heuraux S. Simulations on the Role of the Resonance of the Probing Wave on Reflectometry Measurements in Fluctuating Plasmas. / Heuraux S., Gusakov E., Popov A.Yu., da Silva F., Irzak M. // IEEE Transactions on Plasma Science. - 2010. - Vol. 38, No. 9. - P. 2150-2158. ↑

J26. Diem S. J. Optimization studies of the ITER low field side reflectometer. / Diem S. J., Wilgen J. B., Bigelow T. S., Hanson G. R., Harvey R. W., Smirnov A. P. // Review of Scientific Instruments. - 2010. - Vol. 81, No. 10. - P. 10D914-10D914-3. ↑

J27. Yoshinaga T. Simultaneous projection and detection system of four different frequencies for microwave imaging reflectometry in Large Helical Device. / Yoshinaga T., Nagayama Y., Kuwahara D., Tsuchiya H., Yamaguchi S., Kogi Y., Tsuji-lio S., Mase A. // Review of Scientific Instruments. - 2010. - Vol. 81, No. 10. - P. 10D915-10D915-4. ↑

J28. Kubota S. A Ka-band tunable direct-conversion correlation reflectometer for NSTX. / Kubota S., Peebles W. A., Nguyen X. V., Crocker N. A., Roquemore A. L., Holoman T., Guttadora L., Kaita R. // Review of Scientific Instruments. - 2010. - Vol. 81, No. 10. - P. 10D917-10D917-4. ↑

J29. Park H. K. Microwave imaging reflectometry studies for turbulence diagnostics on KSTAR. / Park H. K., Hong I., Kim M., Yun G. S., Lee W., Kim J., Tobias B., Domier C. W., Luhmann N. C., Kim K. W. // Review of Scientific Instruments. - 2010. - Vol. 81, No. 10. - P. 10D933-10D933-3. ↑

J30. Zhang D. Design criteria of the bolometer diagnostic for steady-state operation of the W7-X stellarator. / Zhang D., Burhenn R., Koenig R., Giannone L., Grodzki P. A., Klein B., Grosser K., Baldzuhn J., Ewert K., Erckmann V., Hirsch M., Laqua H. P., Oosterbeek J. W. // Review of Scientific Instruments. - 2010. - Vol. 81, No. 10. - P. 10E134-10E134-4. ↑

J31. Novac B. M. A Tesla-pulse forming line-plasma opening switch pulsed power generator. / Novac B. M., Kumar R., Smith I. R. // Review of Scientific Instruments. - 2010. - Vol. 81, No. 10. - P. 104704-104704-9. ↑

J32. Kuwahara D. Development of electron cyclotron emission imaging system on Large Helical Device. / Kuwahara D., Tsuji-lio S., Nagayama Y., Yoshinaga T., Tsuchiya H., Sugito S., Yamaguchi S., Kogi Y., Akaki K., Mase A. // Review of Scientific Instruments. - 2010. - Vol. 81, No. 10. - P. 10D919-10D919-3. ↑

J33. Lee W. Comparative study between the reflective optics and lens based system for microwave imaging system on KSTAR. / Lee W., Yun G. S., Nam Y., Hong I., Kim J. B., Park H. K., Tobias B., Liang T., Domier C. W., Luhmann N. C. // Review of Scientific Instruments. - 2010. - Vol. 81, No. 10. - P. 10D932-10D932-3. ↑

J34. Kong X. Antenna development for high field plasma imaging. / Kong X., Domier C. W., Luhmann N. C. // Review of Scientific Instruments. - 2010. - Vol. 81, No. 10. - P. 10D923-10D923-3. ↑

J35. Tatarova E. Microwave air plasma source at atmospheric pressure: Experiment and theory. / Tatarova E., Dias F. M., Felizardo E., Henriques J., Pinheiro M. J., Ferreira C. M., Gordiets B. // Journal of Applied Physics. - 2010. - Vol. 108, No. 12. - P. 123305-123305-18. ↑

J36. Abbosh A. Strain Imaging of the Breast by Compression Microwave Imaging. / Abbosh A., Crozier S. // IEEE Antennas and Wireless Propagation Letters. - 2010. - Vol. 9, {no data available}. - P. 1229-1232. ↑

J37. Farhang Hossein. Report on MSMW'2010 and TERATECH'2010. / Farhang Hossein, Yanovsky Felix J. //

IEEE Antennas and Propagation Magazine. - 2010. - Vol. 52, No. 5. - P. 158-162. ↑

J38. Meneses Luis. New frequency translation technique for FM-CW reflectometry. / Meneses Luis, Cupido Luis, Manso M. E., JET-EFDA Contributors. // Review of Scientific Instruments. - 2010. - Vol. 81, No. 10. - P. 10D924-10D924-3. ↑

J39. Kramer-Flecken A. Correlation reflectometry at TEXTOR. / Kramer-Flecken A., Soldatov S., Vowinkel B., Muller P. // Review of Scientific Instruments. - 2010. - Vol. 81, No. 11. - P. 113502-113502-7. ↑

J40. Siefert Nicholas S. Electrical double layers at shock fronts in glow discharges and afterglows. Journal of Applied Physics. - 2010. - Vol. 108, No. 12. - P. 123304-123304-11. ↑

J41. Gries T. Diagnostics and modeling of CH₄-CO₂ plasmas for nanosmooth diamond deposition: Comparison to experimental data. / Gries T., Vandenbulcke L., de Persis S., Aubry O., Delfau J. L. // Journal of Vacuum Science & Technology B: Microelectronics and Nanometer Structures. - 2009. - Vol. 27, No. 5. - P. 2309-2320. ↑

J42. Schumacher U. Spectroscopic Analysis of Microwave-Generated Plasmas. / Schumacher U., Stirn R., Ene A.B., Hirsch K., Leins M., Lindner P., Schulz A., Walker M. // IEEE Transactions on Plasma Science. - 2009. - Vol. 37, No. 9. - P. 1836-1842. ↑

J43. Krile J.T. Short-Pulse High-Power Microwave Surface Flashover at 3 GHz. / Krile J.T., McQuage L., Edmiston G.F., Walter J., Neuber A.A. // IEEE Transactions on Plasma Science. - 2009. - Vol. 37, No. 11. - P. 2139-2145. ↑

J44. Torshin Yu. Initiation and propagation of the negative leader in transformer oil under impulse voltage. IEEE Transactions on Dielectrics and Electrical Insulation. - 2009. - Vol. 16, No. 6. - P. 1536-1542. ↑

J45. Zhang Qing. Measurement of the electron density in a microwave plasma torch at atmospheric pressure. / Zhang Qing, Zhang Guixin, Wang Liming, Wang Xinxin, Wang Shumin, Chen Yan. // Applied Physics Letters. - 2009. - Vol. 95, No. 20. - P. 201502-201502-3. ↑

J46. Limin Li. Effects of CsI Coating of Carbon Fiber Cathodes on the Microwave Emission From a Triode Virtual Cathode Oscillator. / Limin Li, Lie Liu, Jianchun Wen, Yonggui Liu. // IEEE Transactions on Plasma Science. - 2009. - Vol. 37, No. 1. - P. 15-22. ↑

J47. Porteanu H.-E. Low-Power Microwave Plasma Conductivity. / Porteanu H.-E., Kuhn S., Gesche R. // IEEE Transactions on Plasma Science. - 2009. - Vol. 37, No. 1. - P. 44-49. ↑

J48. Neidman Y. Diagnostic of phased arrays with faulty elements using the mutual coupling method. / Neidman Y., Shavit R., Bronshtein A. // IET Microwaves, Antennas & Propagation. - 2009. - Vol. 3, No. 2. - P. 235-241. ↑

J49. Gregorio J. Design of a Microwave Microplasma Source at Atmospheric Pressure. / Gregorio J., Leroy O., Leprince P., Alves L.L., Boisse-Laporte C. // IEEE Transactions on Plasma Science. - 2009. - Vol. 37, No. 6. - P. 797-808. ↑

J50. Catarinucci L. A Cost-Effective UHF RFID Tag for Transmission of Generic Sensor Data in Wireless Sensor Networks. / Catarinucci L., Colella R., Tarricone L. // IEEE Transactions on Microwave Theory and Techniques. - 2009. - Vol. 57, No. 5. - P. 1291-1296. ↑

J51. Zhu Li-Guo. Spatial nonuniformity of electron energy in a microwave atmospheric-pressure microplasma. / Zhu Li-Guo, Zhang Zhi-Bo, Zhu Xi-Ming, Pu Yi-Kang, Li Ze-Ren. // Applied Physics Letters. - 2009. - Vol. 94, No. 15. - P. 151502-151502-3. ↑

J52. Shashurin A. Temporal behavior of cold atmospheric plasma jet. / Shashurin A., Shneider M. N., Dogariu A., Miles R. B., Keidar M. // Applied Physics Letters. - 2009. - Vol. 94, No. 23. - P. 231504-231504-3. ↑


J53. Yuji T. Optical Emission Characteristics of Atmospheric-Pressure Nonequilibrium Microwave Discharge and High-Frequency DC Pulse Discharge Plasma Jets. / Yuji T., Fujii S., Mungkung N., Akatsuka H. // IEEE Transactions on Plasma Science. - 2009. - Vol. 37, No. 6. - P. 839-845. ↑


↑


- J54.** Hae Young Choi. Development of New X-Ray Source Based on Carbon Nanotube Field Emission and Application to the Non Destructive Imaging Technology. / Hae Young Choi, Chae Hwa Shon, Jong Uk Kim. // IEEE Transactions on Nuclear Science. - 2009. - Vol. 56, No. 3. - P. 1297-1300. ↑
- J55.** Boxer Alexander C. Multichannel microwave interferometer for the levitated dipole experiment. / Boxer Alexander C., Garnier Darren T., Mauel Michael E. // Review of Scientific Instruments. - 2009. - Vol. 80, No. 4. - P. 043502-043502-4. ↑
- J56.** Dawson Elizabeth A. A system to investigate the remediation of organic vapors using microwave-induced plasma with fluidized carbon granules. / Dawson Elizabeth A., Parkes Gareth M. B., Bond Gary, Mao Runjie. // Review of Scientific Instruments. - 2009. - Vol. 80, No. 3. - P. 034102-034102-5. ↑
- J57.** Zhu Li-Guo. Chromatic-free spatially resolved optical emission spectroscopy diagnostics for microplasma. / Zhu Li-Guo, Chen Wen-Cong, Zhu Xi-Ming, Pu Yi-Kang, Li Ze-Ren. // Review of Scientific Instruments. - 2009. - Vol. 80, No. 2. - P. 023105-023105-4. ↑
- J58.** Yatsuka Eiichi. Radio-frequency electromagnetic field measurements for direct detection of electron Bernstein waves in a torus plasma. / Yatsuka Eiichi, Kinjo Kiyotake, Morikawa Junji, Ogawa Yuichi. // Review of Scientific Instruments. - 2009. - Vol. 80, No. 2. - P. 023505-023505-6. ↑
- J59.** Lechte C. Investigation of the Scattering Efficiency in Doppler Reflectometry by Two-Dimensional Full-Wave Simulations. IEEE Transactions on Plasma Science. - 2009. - Vol. 37, No. 6. - P. 1099-1103. ↑
- J60.** Brai Maria. Electronic paramagnetic resonance power saturation of wooden samples. / Brai Maria, Longo Anna, Maccotta Antonella, Marrale Maurizio. // Journal of Applied Physics. - 2009. - Vol. 105, No. 9. - P. 094913-094913-8. ↑
- J61.** Higashiguchi Takeshi. Short pulse, high power microwave radiation source with a laser-induced sheet plasma mirror. / Higashiguchi Takeshi, Yugami Noboru. // Journal of Applied Physics. - 2009. - Vol. 105, No. 9. - P. 093301-093301-4. ↑
- J62.** Ogata Ken. Characterizations of strip-line microwave micro atmospheric plasma and its application to neutralization. / Ogata Ken, Terashima Kazuo. // Journal of Applied Physics. - 2009. - Vol. 106, No. 2. - P. 023301-023301-6. ↑
- J63.** Happel T. Doppler reflectometer system in the stellarator TJ-II. / Happel T., Estrada T., Blanco E., Tribaldos V., Cappa A., Bustos A. // Review of Scientific Instruments. - 2009. - Vol. 80, No. 7. - P. 073502-073502-8. ↑
- J64.** Tarasova A. V. Measurements of plasma potential in high-pressure microwave plasmas. / Tarasova A. V., Podder N. K., Clothiaux E. J. // Review of Scientific Instruments. - 2009. - Vol. 80, No. 4. - P. 043506-043506-5. ↑
- J65.** Hemawan Kadek W. Compact microwave re-entrant cavity applicator for plasma-assisted combustion. / Hemawan Kadek W., Wichman Indrek S., Lee Tonghun, Grotjohn Timothy A., Asmussen Jes. // Review of Scientific Instruments. - 2009. - Vol. 80, No. 5. - P. 053507-053507-9. ↑
- J66.** Ma Jie. Validating optical emission spectroscopy as a diagnostic of microwave activated CH₄/Ar/H₂ plasmas used for diamond chemical vapor deposition. / Ma Jie, Ashfold Michael N. R., Mankelevich Yuri A. // Journal of Applied Physics. - 2009. - Vol. 105, No. 4. - P. 043302-043302-12. ↑
- J67.** Padhi S.K. Measured Antenna Response of a Proposed Microwave Tomography System Using an Efficient 3-D FDTD Model. / Padhi S.K., Fhager A., Persson M., Howard J. // IEEE Antennas and Wireless Propagation Letters. - 2008. - Vol. 7, {no data available}. - P. 689-692. ↑
- J68.** Nam Sang Ki. Effect of microwave frequency on breakdown and electron energy distribution function using a global model. / Nam Sang Ki, Verboncoeur John P. // Applied Physics Letters. - 2008. - Vol. 93, No. 15. - P. 151504-151504-3. ↑
- J69.** Xu Xu. Visual phenomena of surface plasmon polaritons at the dielectric-plasma interface. / Xu Xu, Liu Feng, Zhou Qianhong, Liang Bo, Liang Yizi, Liang Rongqing. // Applied Physics Letters. - 2008. - Vol. 92, No. 1. - P. 011501-011501-3. ↑


- J70.** Shiffler Don. Materials characteristics and surface morphology of a cesium iodide coated carbon velvet cathode. / Shiffler Don, Heidger Susan, Cartwright Keith, Vaia Rich, Liptak David, Price Gary, LaCour Matthew, Golby Ken. // Journal of Applied Physics. - 2008. - Vol. 103, No. 1. - P. 013302-013302-6. ↑
- J71.** Karkari S. K. Direct measurement of spatial electron density oscillations in a dual frequency capacitive plasma. / Karkari S. K., Ellingboe A. R., Gaman C. // Applied Physics Letters. - 2008. - Vol. 93, No. 7. - P. 071501-071501-3. ↑
- J72.** Bliokh Yu. P. Probe measurements in a nonstationary plasma. / Bliokh Yu. P., Brodsky Yu. L., Chashka Kh. B., Felsteiner J., Slutsker Ya. Z. // Journal of Applied Physics. - 2008. - Vol. 103, No. 5. - P. 053303-053303-7. ↑
- J73.** Santosh Babu G. Crystal structure, Raman spectroscopy, far-infrared, and microwave dielectric properties of (1-x)La (MgSn)_{0.5}O₃-xNd (MgSn)_{0.5}O₃ system. / Santosh Babu G., Subramanian V., Murthy V. R. K., Moreira R. L., Lobo R. P. S. M. // Journal of Applied Physics. - 2008. - Vol. 103, No. 8. - P. 084104-084104-7. ↑
- J74.** Jia Haijun. A microwave-induced plasma source: Characterization and application for the fast deposition of crystalline silicon films. / Jia Haijun, Kuraseko Hiroshi, Kondo Michio. // Journal of Applied Physics. - 2008. - Vol. 103, No. 2. - P. 024904-024904-6. ↑
- J75.** Srivastava A. K. Attenuation of microwaves propagating through parallel-plate helium glow discharge at atmospheric pressure. / Srivastava A. K., Prasad G., Atrey P. K., Kumar Vinay. // Journal of Applied Physics. - 2008. - Vol. 103, No. 3. - P. 033302-033302-7. ↑
- J76.** Yamaguchi S. Development of microwave imaging reflectometry in large helical device. / Yamaguchi S., Nagayama Y., Kuwahara D., Yoshinaga T., Shi Z. B., Kogi Y., Mase A. // Review of Scientific Instruments. - 2008. - Vol. 79, No. 10. - P. 10F111-10F111-4. ↑
- J77.** Tokuzawa T. V-band frequency hopping microwave reflectometer in LHD. / Tokuzawa T., Ejiri A., Kawahata K., Tanaka K., Ito Y. // Review of Scientific Instruments. - 2008. - Vol. 79, No. 10. - P. 10F109-10F109-4. ↑
- J78.** Gourdain P.-A. Application of reflectometry power flow for magnetic field pitch angle measurements in tokamak plasmas (invited). / Gourdain P.-A., Peebles W. A. // Review of Scientific Instruments. - 2008. - Vol. 79, No. 10. - P. 10F102-10F102-8. ↑
- J79.** Bechu Stephane. Investigation of H-production by surface interaction of the plasma generated in "Camembert III" reactor via distributed electron cyclotron resonance at 2.45 GHz (abstract). / Bechu Stephane, Bes Alexandre, Lemoine Didier, Pelletier Jacques, Bacal Marthe. // Review of Scientific Instruments. - 2008. - Vol. 79, No. 2. - P. 02A505-02A505-1. ↑
- J80.** Sakamoto Y. Compact 2.45 GHz microwave ion/atom source. / Sakamoto Y., Kasuya T., Wada M., Maeno S. // Review of Scientific Instruments. - 2008. - Vol. 79, No. 2. - P. 02A318-02A318-3. ↑
- J81.** Iraj D. Fast visible imaging of turbulent plasma in TORPEX. / Iraj D., Diallo A., Fasoli A., Furno I., Shibaev S. // Review of Scientific Instruments. - 2008. - Vol. 79, No. 10. - P. 10F508-10F508-4. ↑
- J82.** Yang Juan. Development and research of a coaxial microwave plasma thruster. / Yang Juan, Xu Yingqiao, Tang Jinlan, Mao Genwang, Yang Tielian, Tan Xiaoquen. // Review of Scientific Instruments. - 2008. - Vol. 79, No. 8. - P. 083503-083503-6. ↑
- J83.** Bertschinger G. Dichroic filters to protect milliwatt far-infrared detectors from megawatt ECRH radiation. / Bertschinger G., Endres C. P., Lewen F., Oosterbeek J. W. // Review of Scientific Instruments. - 2008. - Vol. 79, No. 10. - P. 10E709-10E709-4. ↑
- J84.** Marques T. G. Real-time digital heterodyne interferometer for high resolution plasma density measurements at ISTTOK. / Marques T. G., Gouveia A., Pereira T., Fortunato J., Carvalho B. B., Sousa J., Silva C., Fernandes H. // Review of Scientific Instruments. - 2008. - Vol. 79, No. 10. - P. 10E711-10E711-3. ↑
- J85.** Bitter M. Wide-angle point-to-point x-ray imaging with almost arbitrarily large angles of incidence. / Bitter M., Hill K. W., Scott S., Feder R., Ko Jinseok, Ince-Cushman A., Rice J. E. // Review of Scientific Instruments. - 2008. - Vol. 79, No. 10. - P. 10E711-10E711-3. ↑


2008. - Vol. 79, No. 10. - P. 10E927-10E927-3. 


J86. Li Bin. Pulse compression radar reflectometry to measure electron density in plasma with parasitic reflections. / Li Bin, Li Hong, Chen Zhipeng, Luo Chen, Wang Huihui, Geng Song, Feng Lei, Liu Qiuyan, Liu Wandong. // Review of Scientific Instruments. - 2008. - Vol. 79, No. 7. - P. 073504-073504-5. 


J87. Nam Y. U. A 280 GHz single-channel millimeter-wave interferometer system for KSTAR. / Nam Y. U., Lee K. D. // Review of Scientific Instruments. - 2008. - Vol. 79, No. 10. - P. 10E705-10E705-3. 


J88. Yoshikawa M. Radial density profile measurement by using the multichannel microwave interferometer in GAMMA 10. / Yoshikawa M., Matsumoto T., Shima Y., Negishi S., Miyata Y., Mizuguchi M., Imai N., Yoneda Y., Hojo H., Itakura A., Imai T. // Review of Scientific Instruments. - 2008. - Vol. 79, No. 10. - P. 10E706-10E706-3. 


J89. Mordyk S. Investigation of helicon ion source extraction systems. / Mordyk S., Miroshnichenko V., Shulha D., Storizhko V. // Review of Scientific Instruments. - 2008. - Vol. 79, No. 2. - P. 02B707-02B707-4. 


J90. Hidaka Y. Imaging of Atmospheric Air Breakdown Caused by a High-Power 110-GHz Pulsed Gaussian Beam. / Hidaka Y., Choi E.M., Mastovsky I., Shapiro M.A., Sirigiri J.R., Temkin R.J. // IEEE Transactions on Plasma Science. - 2008. - Vol. 36, No. 4. - P. 936-937. 


J91. Lestinska L. Atmospheric Pressure Nitrogen Microwave Plasma. / Lestinska L., Foltin V., Machala Z. // IEEE Transactions on Plasma Science. - 2008. - Vol. 36, No. 4. - P. 962-963. 


J92. Redo-Sanchez A. Terahertz Science and Technology Trends. / Redo-Sanchez A., Xi-Cheng Zhang. // IEEE Journal of Selected Topics in Quantum Electronics. - 2008. - Vol. 14, No. 2. - P. 260-269. 


J93. Gupta S.B. The Potential of Pulsed Underwater Streamer Discharges as a Disinfection Technique. / Gupta S.B., Bluhm H. // IEEE Transactions on Plasma Science. - 2008. - Vol. 36, No. 4. - P. 1621-1632. 


J94. de Rodriguez M.E. 3-D-Microwave Breast Tumor Detection: Study of System Performance. / de Rodriguez M.E., Vera-Isasa M., del Rio V.S. // IEEE Transactions on Biomedical Engineering. - 2008. - Vol. 55, No. 12. - P. 2772-2777. 


J95. Thiyagarajan M. Experimental Investigation of 193-nm Laser Breakdown in Air. / Thiyagarajan M., Scharer J.E. // IEEE Transactions on Plasma Science. - 2008. - Vol. 36, No. 5. - P. 2512-2521. 


J96. Karanasiou I.S. Development and Laboratory Testing of a Noninvasive Intracranial Focused Hyperthermia System. / Karanasiou I.S., Karathanasis K.T., Garetsos A., Uzunoglu N.K. // IEEE Transactions on Microwave Theory and Techniques. - 2008. - Vol. 56, No. 9. - P. 2160-2171. 


J97. Baskaran R. Studies on x-ray and UV emissions in electron cyclotron resonance x-ray source. / Baskaran R., Selvakumaran T. S. // Review of Scientific Instruments. - 2008. - Vol. 79, No. 2. - P. 02C702-02C702-3. 

J98. Song H. Stable microwave coaxial cavity plasma system at atmospheric pressure. / Song H., Hong J. M., Lee K. H., Choi J. J. // Review of Scientific Instruments. - 2008. - Vol. 79, No. 5. - P. 054702-054702-5. 

J99. Bardati F. Modeling the Visibility of Breast Malignancy by a Microwave Radiometer. / Bardati F., Iudicello S. // IEEE Transactions on Biomedical Engineering. - 2008. - Vol. 55, No. 1. - P. 214-221. 

J100. Arunachalam K. A Computational Investigation of Microwave Breast Imaging Using Deformable Reflector. / Arunachalam K., Udpa L., Udpa S.S. // IEEE Transactions on Biomedical Engineering. - 2008. - Vol. 55, No. 2. - P. 554-562. 

J101. Yokota Y. Measurement of edge density profiles of Large Helical Device plasmas using an ultrashort-pulse reflectometer. / Yokota Y., Mase A., Kogi Y., Bruskin L. G., Tokuzawa T., Kawahata K. // Review of Scientific Instruments. - 2008. - Vol. 79, No. 5. - P. 056106-056106-3. 

J102. Kunkee D.B. Analysis of the Special Sensor Microwave Imager/Sounder (SSMIS) Fields-of-View on DMSP F16. / Kunkee D.B., Ye Hong, Thompson D.A., Werner M.F., Poe G.A. // IEEE Transactions on Geoscience and Remote Sensing. - 2008. - Vol. 46, No. 4. - P. 934-945. 

J103. Frederickson K. Mitigation of electron attachment to oxygen in high pressure air plasmas by vibrational

excitation. / Frederickson K., Lee W., Palm P., Adamovich I. V., Rich J. W., Lempert W. R. // Journal of Applied Physics. - 2007. - Vol. 101, No. 9. - P. 093302-093302-7. ↑

J104. Sakamoto Takeshi. Spectroscopic study on the vibrational populations of N 2 C 3 Pi and B 3 Pi states in a microwave nitrogen discharge. / Sakamoto Takeshi, Matsuura Haruaki, Akatsuka Hiroshi. // Journal of Applied Physics. - 2007. - Vol. 101, No. 2. - P. 023307-023307-7. ↑

J105. Tatarova E. Spectroscopic determination of H, He, and H 2 temperatures in a large-scale microwave plasma source. / Tatarova E., Dias F. M., Ferreira C. M., Puac N. // Journal of Applied Physics. - 2007. - Vol. 101, No. 6. - P. 063306-063306-8. ↑

J106. An Wladimir. Underwater streamer propagation analyzed from detailed measurements of pressure release. / An Wladimir, Baumung Kurt, Bluhm Hansjoachim. // Journal of Applied Physics. - 2007. - Vol. 101, No. 5. - P. 053302-053302-10. ↑

J107. Takeda Keigo. Diagnostics of surface wave excited Kr /O2 plasma for low-temperature oxidation processes. / Takeda Keigo, Kubota Yoshiki, Takashima Seigo, Hori Masaru, Serdyuchenko Anna, Ito Masafumi, Matsumi Yutaka. // Journal of Applied Physics. - 2007. - Vol. 102, No. 1. - P. 013302-013302-6. ↑

J108. Stopper U. Three-dimensional analysis of microwave generated plasmas with extended planar laser-induced fluorescence. / Stopper U., Lindner P., Schumacher U. // Review of Scientific Instruments. - 2007. - Vol. 78, No. 4. - P. 043508-043508-6. ↑

J109. Karkari S. K. Electron density modulation in an asymmetric bipolar pulsed dc magnetron discharge. / Karkari S. K., Ellingboe A. R., Gaman C., Swindells I., Bradley J. W. // Journal of Applied Physics. - 2007. - Vol. 102, No. 6. - P. 063308-063308-8. ↑

J110. Shneider Mikhail N. Plasma induced by resonance enhanced multiphoton ionization in inert gas. / Shneider Mikhail N., Zhang Zhili, Miles Richard B. // Journal of Applied Physics. - 2007. - Vol. 102, No. 12. - P. 123103-123103-7. ↑

J111. Yamada T. Direct measurement of density oscillation induced by a radio-frequency wave. / Yamada T., Ejiri A., Shimada Y., Oosako T., Tsujimura J., Takase Y., Kasahara H. // Review of Scientific Instruments. - 2007. - Vol. 78, No. 8. - P. 083502-083502-5. ↑

J112. Shi Cheng. Reduction of the Coupling to External Sources and Modes of Propagation by a Nearly Confocal Resonator. / Shi Cheng, Ferrari A., Johnson M., Rydberg A.S., Ziemann V., Ojefors E. // IEEE Transactions on Microwave Theory and Techniques. - 2007. - Vol. 55, No. 10. - P. 2257-2261. ↑

J113. Capozzoli A. Phaseless characterisation of compact antenna test ranges. / Capozzoli A., D'Elia G., Lisenio A. // IET Microwaves, Antennas & Propagation. - 2007. - Vol. 1, No. 4. - P. 860-866. ↑

J114. Vodonos Y.I. Advances in Ground Transmitters for the NASA Deep Space Network. / Vodonos Y.I., Conroy B.L., Losh D.L., Silva A. // Proceedings of the IEEE. - 2007. - Vol. 95, No. 10. - P. 1947-1957. ↑

J115. Bansal R. Microwave surfing-Channeling the voice within. IEEE Microwave Magazine. - 2007. - Vol. 8, No. 5. - P. 20-26. ↑

J116. Khan U.A. Broadband Dielectric Characterization of Tumorous and Nontumorous Breast Tissues. / Khan U.A., Al-Moayed N., Nguyen N., Korolev K.A., Afsar M.N., Naber S.P. // IEEE Transactions on Microwave Theory and Techniques. - 2007. - Vol. 55, No. 12. - P. 2887-2893. ↑

J117. Thumm M. EU Megawatt-Class 140-GHz CW Gyrotron. / Thumm M., Alberti S., Arnold A., Brand P., Braune H., Dammertz G., Erckmann V., Gantenbein G., Giguet E., Heidinger R., Hogge J.-P., Illy S., Kasperek W., Laqua H.P., Legrand F., Leonhardt W., LievinLievin C., Michel G., Neffe G., Piosczyk B., Schmid M., Schworer K., Minh Quang Tran. // IEEE Transactions on Plasma Science. - 2007. - Vol. 35, No. 2. - P. 143-153. ↑

J118. Hopfe V. Atmospheric-Pressure PECVD Coating and Plasma Chemical Etching for Continuous Processing. / Hopfe V., Sheel D.W. // IEEE Transactions on Plasma Science. - 2007. - Vol. 35, No. 2. - P. 204-214. ↑

J119. Park B.-K. Arctangent Demodulation With DC Offset Compensation in Quadrature Doppler Radar

Receiver Systems. / Park B.-K., Boric-Lubecke O., Lubecke V. M. // IEEE Transactions on Microwave Theory and Techniques. - 2007. - Vol. 55, No. 5. - P. 1073-1079. ↑

J120. Lyons C.M. Fabrication of a Nb-Based 180-Degree IF Hybrid for Balanced SIS Mixers. / Lyons C.M., Lichtenberger A.W., Kerr A.R., Lauria E.F., Ziurys L.M. // IEEE Transactions on Applied Superconductivity. - 2007. - Vol. 17, No. 2. - P. 194-197. ↑

J121. Jacobsen S. Active antennas in medical microwave radiometry. / Jacobsen S., Klemetsen O. // Electronics Letters. - 2007. - Vol. 43, No. 11. - P. 606-608. ↑

J122. Nie Liming. Detection of foreign body using fast thermoacoustic tomography with a multielement linear transducer array. / Nie Liming, Xing Da, Yang Diwu, Zeng Lvming, Zhou Quan. // Applied Physics Letters. - 2007. - Vol. 90, No. 17. - P. 174109-174109-3. ↑

J123. Hidaka Y. Performance and analysis of an electron cyclotron resonance plasma cathode. / Hidaka Y., Foster J. E., Getty W. D., Gilgenbach R. M., Lau Y. Y. // and Films Journal of Vacuum Science & Technology A: Vacuum, Surfaces. - 2007. - Vol. 25, No. 4. - P. 781-790. ↑

J124. Hong Yong Cheol. Simulated experiment for elimination of air contaminated with odorous chemical agents by microwave plasma burner. / Hong Yong Cheol, Shin Dong Hun, Uhm Han Sup. // Applied Physics Letters. - 2007. - Vol. 91, No. 16. - P. 161502-161502-3. ↑

J125. Combo A. Upgrade of the data acquisition and control system of the ASDEX upgrade microwave reflectometer. / Combo A., Silva A., Varela P., Manso M., Sousa J., Correia C., Varandas C.A.F. // IEEE Transactions on Nuclear Science. - 2006. - Vol. 53, No. 3. - P. 918-922. ↑

J126. Mehta P. Microwave reflectometry as a novel diagnostic tool for detection of skin cancers. / Mehta P., Chand K., Narayanswamy D., Beetner D.G., Zoughi R., Stoecker W.V. // IEEE Transactions on Instrumentation and Measurement. - 2006. - Vol. 55, No. 4. - P. 1309-1316. ↑

J127. Cross A.W. Guest Editorial Special Issue on Plenary and Invited Papers From ICOPS 2005. / Cross A.W., Kolobov V.I. // IEEE Transactions on Plasma Science. - 2006. - Vol. 34, No. 2. - P. 130-131. ↑

J128. Murray R.C. Microwave diagnostics of a repetitive, short-pulse-sustained, weakly ionized, air plasma under the influence of a magnetic field. / Murray R.C., Zaidi S.H., Macheret S.O., Miles R.B. // IEEE Transactions on Plasma Science. - 2006. - Vol. 34, No. 3. - P. 1004-1012. ↑

J129. Carlsten B.E. Beam Line Design, Beam Alignment Procedure, and Initial Results for the -Band Gain Experiment at Los Alamos. / Carlsten B.E., Earley L.M., Haynes W.B., Krawczyk F.L., Romero F.P., Russell S.J., Smirnova E.I., Zhi-Fu Wang. // IEEE Transactions on Plasma Science. - 2006. - Vol. 34, No. 5. - P. 2393-2403. ↑

J130. Cavalieri D.J. Assessment of EOS Aqua AMSR-E Arctic Sea Ice Concentrations Using Landsat-7 and Airborne Microwave Imagery. / Cavalieri D.J., Markus T., Hall D.K., Gasiewski A.J., Klein M., Ivanoff A. // IEEE Transactions on Geoscience and Remote Sensing. - 2006. - Vol. 44, No. 11. - P. 3057-3069. ↑

J131. Edmiston G. High-Power Microwave Surface Flashover of a Gas-Dielectric Interface at 90–760 torr. / Edmiston G., Krile J., Neuber A., Dickens J., Krompholz H. // IEEE Transactions on Plasma Science. - 2006. - Vol. 34, No. 5. - P. 1782-1788. ↑

J132. Skiff F. Diagnostics of Collisionless Processes in Plasma. IEEE Transactions on Plasma Science. - 2006. - Vol. 34, No. 4. - P. 1548-1552. ↑

J133. Chan Uk Bang. Methane-Augmented Microwave Plasma Burner. / Chan Uk Bang, Yong Cheol Hong, Soon Cheon Cho, Uhm H.S., Won Ju Yi. // IEEE Transactions on Plasma Science. - 2006. - Vol. 34, No. 5. - P. 1751-1756. ↑

J134. Zhao H. Y. Measurements of bremsstrahlung spectra of Lanzhou ECR Ion Source No. 3 (LECR3). / Zhao H. Y., Zhao H. W., Ma X. W., Zhang S. F., Feng W. T., Zhu X. L., Zhang Z. M., He W., Sun L. T., Feng Y. C., Cao Y., Li J. Y., Li X. X., Wang H., Ma B. H. // Review of Scientific Instruments. - 2006. - Vol. 77, No. 3. - P. 03A312-03A312-3. ↑

J135. Leporis M. Electron cyclotron resonance ion source DECRIS-4 for the U400 cyclotron. / Leporis M.,

Bekhterev V., Bogomolov S., Efremov A., Gulbekian G., Kostyukhov Yu., Lebedev A., Loginov V., Yazvitsky N. // Review of Scientific Instruments. - 2006. - Vol. 77, No. 3. - P. 03A301-03A301-3. ↑

J136. Mordyk S. Extraction of single-ion beams from helicon ion source in high plasma density operation mode: Experiment and simulation. / Mordyk S., Miroschnichenko V., Nahorny A., Nahorny D., Shulha D., Storizhko V., Voznyy V. // Review of Scientific Instruments. - 2006. - Vol. 77, No. 3. - P. 03B901-03B901-3. ↑

J137. Combs S. K. Technique for measuring D 2 pellet mass loss through a curved guide tube using two microwave cavity detectors. / Combs S. K., Caughman J. B. O., Wilgen J. B. // Review of Scientific Instruments. - 2006. - Vol. 77, No. 7. - P. 073503-073503-6. ↑

J138. Seo Seong-Heon. In situ frequency calibration technique of FM reflectometer. / Seo Seong-Heon, Lee Dong Ju. // Review of Scientific Instruments. - 2006. - Vol. 77, No. 4. - P. 045103-045103-4. ↑

J139. Yamada Takuma. Application of differential phase method to interferometry. / Yamada Takuma, Ejiri Akira, Shiraiwa Syun'ichi, Takase Yuichi. // Review of Scientific Instruments. - 2006. - Vol. 77, No. 12. - P. 124701-124701-5. ↑

J140. Silva A. Recent improvements of the broadband FMCW reflectometry system for density profile measurements on ASDEX Upgrade. / Silva A., Manso M., Varela P., Cupido L., Meneses L. // Review of Scientific Instruments. - 2006. - Vol. 77, No. 10. - P. 10E932-10E932-4. ↑

J141. Hao Shao. Characterization of modes in coaxial vircator. / Hao Shao, Guozhi Liu, Zhanfeng Yang, Changhua Chen, Zhimin Song, Wenhua Huang. // IEEE Transactions on Plasma Science. - 2006. - Vol. 34, No. 1. - P. 7-13. ↑

J142. Wilgen J. B. Reflectometer sensing of rf waves in front of the high harmonic fast wave antenna on NSTX. / Wilgen J. B., Ryan P. M., Hanson G. R., Swain D. W., Bernabei S. I., Greenough N., DePasquale S., Phillips C. K., Hosea J. C., Wilson J. R. // Review of Scientific Instruments. - 2006. - Vol. 77, No. 10. - P. 10E933-10E933-4. ↑

J143. Murari A. New diagnostic techniques and technologies at JET (invited). / Murari A., Alper B., Bertalot L., Brzozowski J. H., Coad P., Conroy S., De La Luna E., Ericsson G., Esser H. G., Hacquin S., Kaelble J., Kiptily V., Lawson K., O'Mullane M., Philipps V., Sharapov S., Zastrow K.-D. // Review of Scientific Instruments. - 2006. - Vol. 77, No. 10. - P. 10F529-10F529-5. ↑

J144. Ding X. T. New diagnostic systems on HL-2A. / Ding X. T., Zhou Y., Deng Z. C., Xiao W. W., Liu Z. T., Shi Z. B., Yan L. W., Hong W. Y., Yang Q. W. // Review of Scientific Instruments. - 2006. - Vol. 77, No. 10. - P. 10F528-10F528-4. ↑

J145. Blumenthal R. Role of neutral molecule chemistry in electron cyclotron resonance microwave plasmas capable of diamond deposition. / Blumenthal R., Webb S. F. // Journal of Vacuum Science & Technology B: Microelectronics and Nanometer Structures. - 2006. - Vol. 24, No. 2. - P. 643-650. ↑

J146. Hong Yong Cheol. Microwave plasma burner and temperature measurements in its flames. / Hong Yong Cheol, Cho Soon Cheon, Bang Chan Uk, Shin Dong Hun, Kim Jong Hun, Uhm Han Sup, Yi Won Ju. // Applied Physics Letters. - 2006. - Vol. 88, No. 20. - P. 201502-201502-3. ↑

J147. Igami H. Searching for O-X-B mode-conversion window with monitoring of stray microwave radiation in LHD. / Igami H., Kubo S., Laqua H. P., Nagasaki K., Inagaki S., Notake T., Shimozuma T., Yoshimura Y., Mutoh T., LHD Experimental Group. // Review of Scientific Instruments. - 2006. - Vol. 77, No. 10. - P. 10E931-10E931-3. ↑

J148. Yamaguchi S. Microwave imaging reflectometry in LHD. / Yamaguchi S., Nagayama Y., Pavlichenko R., Inagaki S., Kogi Y., Mase A. // Review of Scientific Instruments. - 2006. - Vol. 77, No. 10. - P. 10E930-10E930-4. ↑

J149. Gray T. Fast gas injection as a diagnostic technique for particle confinement time measurements. / Gray T., Kaita R., Majeski R., Spaleta J., Timberlake J. // Review of Scientific Instruments. - 2006. - Vol. 77, No. 10. - P. 10E901-10E901-3. ↑

J150. Siefert Nicholas S. Electron and metastable state interactions in two-step ionization waves. / Siefert

Nicholas S., Sands Brian L., Ganguly Biswa N. // Applied Physics Letters. - 2006. - Vol. 89, No. 1. - P. 011502-011502-3. ↑

J151. Hong Yong Cheol. Atmospheric-pressure hybrid plasma with combination of ac and microwave. / Hong Yong Cheol, Uhm Han Sup. // Applied Physics Letters. - 2006. - Vol. 89, No. 25. - P. 251502-251502-3. ↑

J152. Tokuzawa T. Multichannel ultrashort pulsed radar reflectometer on LHD. / Tokuzawa T., Kawahata K., Tanaka K., LHD Experimental Group. // Review of Scientific Instruments. - 2006. - Vol. 77, No. 10. - P. 10E903-10E903-3. ↑

J153. Yoshikawa M. Electron density fluctuation measurements using a multichannel microwave interferometer in GAMMA 10. / Yoshikawa M., Shima Y., Matsumoto T., Nakahara A., Yanagi N., Itakura A., Hojo H., Kobayashi T., Matama K., Tatematsu Y., Imai T., Kohagura J., Hirata M., Nakashima Y., Cho T. // Review of Scientific Instruments. - 2006. - Vol. 77, No. 10. - P. 10E906-10E906-3. ↑

J154. Kubota S. Ultrafast millimeter-wave frequency-modulated continuous-wave reflectometry for NSTX. / Kubota S., Peebles W. A., Nguyen X. V., Crocker N. A., Roquemore A. L. // Review of Scientific Instruments. - 2006. - Vol. 77, No. 10. - P. 10E926-10E926-3. ↑

J155. Hacquin S. X -mode reflectometry measurements in the JET plasma core region. / Hacquin S., Meneses L., Cupido L., Sharapov S., Alper B., Fessey J., Klein A., Testa D. // Review of Scientific Instruments. - 2006. - Vol. 77, No. 10. - P. 10E925-10E925-3. ↑

J156. Barankova H. Cold atmospheric plasma in nitrogen and air generated by the hybrid plasma source. / Barankova H., Bardos L., Soderstrom D. // and Films Journal of Vacuum Science & Technology A: Vacuum, Surfaces. - 2006. - Vol. 24, No. 4. - P. 1410-1413. ↑

J157. Kuo S. P. Characteristic Study of a Portable Arc Microwave Plasma Torch. / Kuo S. P., Rubinraut M., Popovic S., Bivolaru D. // IEEE Transactions on Plasma Science. - 2006. - Vol. 34, No. 6. - P. 2537-2544. ↑

J158. Zhang Zhili. Microwave diagnostics of laser-induced avalanche ionization in air. / Zhang Zhili, Shneider Mikhail N., Miles Richard B. // Journal of Applied Physics. - 2006. - Vol. 100, No. 7. - P. 074912-074912-6. ↑

J159. Mase Atsushi. Remote experiment of ultrashort-pulse reflectometry for large helical device plasmas. / Mase Atsushi, Yokota Yuya, Uchida Kazuyuki, Kogi Yuichiro, Ito Naoki, Tokuzawa Tokihiko, Kawahata Kazuo, Tanaka Kenji, Nagayama Yoshio, Hojo Hitoshi. // Review of Scientific Instruments. - 2006. - Vol. 77, No. 10. - P. 10E916-10E916-3. ↑

J160. Kraft D. J. Analysis of multifrequency interferometry in a cylindrical plasma. / Kraft D. J., Bengtson Roger D., Breizman B. N., Chavers D. G., Dobson C. C., Jones J. E., Jacobson V. T. // Review of Scientific Instruments. - 2006. - Vol. 77, No. 10. - P. 10E910-10E910-3. ↑

J161. Tanaka K. Homodyne reflectometer for neutral beam injection interlock on large helical device. / Tanaka K., Ejiri A., Ito Y., Kawahata K., Tokuzawa T., Osakabe M., Takeiri Y. // Review of Scientific Instruments. - 2006. - Vol. 77, No. 10. - P. 10E912-10E912-3. ↑

J162. Cavazzana Roberto. Multilayer vacuum window for wide-band microwave plasma diagnostic systems. / Cavazzana Roberto, Moresco Maurizio. // Review of Scientific Instruments. - 2006. - Vol. 77, No. 10. - P. 10E921-10E921-3. ↑

J163. Yanovsky F.J. Retrieval of information about turbulence in rain by using Doppler-polarimetric Radar. / Yanovsky F.J., Russchenberg H.W.J., Unal C.M.H. // IEEE Transactions on Microwave Theory and Techniques. - 2005. - Vol. 53, No. 2. - P. 444-450. ↑

J164. Eungsu Kim. Resonant reradiation of electromagnetic waves by thin conductors with transverse gaps. / Eungsu Kim, Fuks M.I., Kovalev N.F., Schamiloglu E. // IEEE Transactions on Plasma Science. - 2005. - Vol. 33, No. 1. - P. 119-128. ↑

J165. Pogorzelski R.J. A 5-by-5 element coupled oscillator-based phased array. IEEE Transactions on Antennas and Propagation. - 2005. - Vol. 53, No. 4. - P. 1337-1345. ↑

J166. Notake T. Real time polarization monitor developed for high power electron cyclotron resonance heating

and current drive experiments in large helical device. / Notake T., Idei H., Kubo S., Shimozuma T., Yoshimura Y., Kobayashi S., Mizuno Y., Ito S., Takita Y., Ohkubo K., Kasperek W., Watari T., Kumazawa R. // Review of Scientific Instruments. - 2005. - Vol. 76, No. 2. - P. 023504-023504-9. ↑

J167. Seo Seong-Heon. Phase measurement algorithm without phase jump. / Seo Seong-Heon, Park M. K., Lee T. G. // Review of Scientific Instruments. - 2005. - Vol. 76, No. 3. - P. 036104-036104-2. ↑

J168. Alvarez R. The effect of the gas flow-rate on the radial structure of a torch-like helium plasma. / Alvarez R., Quintero M.C., Rodero A. // IEEE Transactions on Plasma Science. - 2005. - Vol. 33, No. 2. - P. 422-423. ↑

J169. Kabouzi Y. Pulsed microwave discharges sustained at atmospheric pressure: study of the contraction and filamentation phenomena. / Kabouzi Y., Moisan M. // IEEE Transactions on Plasma Science. - 2005. - Vol. 33, No. 2. - P. 292-293. ↑

J170. Haas F. A. Electron and ion sheath effects on a microwave "hairpin" probe. / Haas F. A., Al-Kuzee J., Braithwaite N. St. J. // Applied Physics Letters. - 2005. - Vol. 87, No. 20. - P. 201503-201503-3. ↑

J171. Bansal R. Magnetic pull: biological effects or medical applications?. IEEE Microwave Magazine. - 2005. - Vol. 6, No. 4. - P. 54-56. ↑

J172. Alvarez R. Thermal inequilibrium of atmospheric helium microwave plasma produced by an axial injection torch. / Alvarez R., Rodero A., Quintero M. C., Sola A., Gamero A., Ortega D. // Journal of Applied Physics. - 2005. - Vol. 98, No. 9. - P. 093304-093304-10. ↑

J173. Popovic S. Transition from diffuse to filamentary domain in a 9.5 GHz microwave-induced surface discharge. / Popovic S., Exton R. J., Herring G. C. // Applied Physics Letters. - 2005. - Vol. 87, No. 6. - P. 061502-061502-3. ↑

J174. Semenov S.Y. Microwave-tomographic imaging of the high dielectric-contrast objects using different image-reconstruction approaches. / Semenov S.Y., Bulyshev A.E., Abubakar A., Posukh V.G., Sizov Y.E., Souvorov A.E., van den Berg P.M., Williams T.C. // IEEE Transactions on Microwave Theory and Techniques. - 2005. - Vol. 53, No. 7. - P. 2284-2294. ↑

J175. Howlader M.K. Time-resolved measurements of electron number density and collision frequency for a fluorescent lamp plasma using microwave diagnostics. / Howlader M.K., Yunqiang Yang, Roth J.R. // IEEE Transactions on Plasma Science. - 2005. - Vol. 33, No. 3. - P. 1093-1099. ↑

J176. Moehs D.P. Negative hydrogen ion sources for accelerators. / Moehs D.P., Peters J., Sherman J. // IEEE Transactions on Plasma Science. - 2005. - Vol. 33, No. 6. - P. 1786-1798. ↑

J177. Minami K. Microwave Measurement of Decaying Plasma in Liquid Helium. / Minami K., Kojima C., Ohira T., Ishihara O. // IEEE Transactions on Plasma Science. - 2005. - Vol. 33, No. 4. - P. 1324-1331. ↑

J178. Rawlins W. T. Observations of gain on the $I(2P_{1/2} \rightarrow 2P_{3/2})$ transition by energy transfer from $O(2\Delta_g)$ generated by a microwave discharge in a subsonic-flow reactor. / Rawlins W. T., Lee S., Kessler W. J., Davis S. J. // Applied Physics Letters. - 2005. - Vol. 86, No. 5. - P. 051105-051105-3. ↑

J179. Kim Jaeho. 2.45 GHz microwave-excited atmospheric pressure air microplasmas based on microstrip technology. / Kim Jaeho, Terashima Kazuo. // Applied Physics Letters. - 2005. - Vol. 86, No. 19. - P. 191504-191504-3. ↑

J180. Bardos L. Characterization of the cold atmospheric plasma hybrid source. / Bardos L., Barankova H. // and Films Journal of Vacuum Science & Technology A: Vacuum, Surfaces. - 2005. - Vol. 23, No. 4. - P. 933-937. ↑

J181. Nagai Mikio. Properties of atmospheric pressure plasmas with microwave excitations for plasma processing. / Nagai Mikio, Hori Masaru, Goto Toshio. // and Films Journal of Vacuum Science & Technology A: Vacuum, Surfaces. - 2005. - Vol. 23, No. 2. - P. 221-225. ↑

J182. Shneider M. N. Microwave diagnostics of small plasma objects. / Shneider M. N., Miles R. B. // Journal of Applied Physics. - 2005. - Vol. 98, No. 3. - P. 033301-033301-3. ↑

- J183.** Yamakawa Koji. Ultrahigh-speed etching of organic films using microwave-excited nonequilibrium atmospheric-pressure plasma. / Yamakawa Koji, Hori Masaru, Goto Toshio, Den Shoji, Katagiri Toshiro, Kano Hiroyuki. // Journal of Applied Physics. - 2005. - Vol. 98, No. 4. - P. 043311-043311-5. ↑
- J184.** Yamakawa Koji. Etching process of silicon dioxide with nonequilibrium atmospheric pressure plasma. / Yamakawa Koji, Hori Masaru, Goto Toshio, Den Shoji, Katagiri Toshiro, Kano Hiroyuki. // Journal of Applied Physics. - 2005. - Vol. 98, No. 1. - P. 013301-013301-6. ↑
- J185.** Reznik Alexander N. Electrodynamics of microwave near-field probing: Application to medical diagnostics. / Reznik Alexander N., Yurasova Nadezhda V. // Journal of Applied Physics. - 2005. - Vol. 98, No. 11. - P. 114701-114701-9. ↑
- J186.** Munsat T. 2-D imaging of electron temperature in Tokamak plasmas. / Munsat T., Mazzucato E., Park H., Domier C.W., Johnson M., Luhmann N.C. Jr., Wang J., Xia Z., Classen I.G.J., Donne A.J.H., van de Pol M.J. // IEEE Transactions on Plasma Science. - 2005. - Vol. 33, No. 2. - P. 466-467. ↑
- J187.** Koleva I. On line-ratio analysis for helium-argon microwave discharges. / Koleva I., Shivarova A., Makasheva K., Schluter H. // Journal of Applied Physics. - 2005. - Vol. 97, No. 4. - P. 043302-043302-8. ↑
- J188.** Lauer J.L. Control of uniformity of plasma-surface modification inside of small-diameter polyethylene tubing using microplasma diagnostics. / Lauer J.L., Shohet J.L., Albrecht R.M., Esnault S., Malter J.S., von Andrian U.H., Shohet S.B. // IEEE Transactions on Plasma Science. - 2005. - Vol. 33, No. 2. - P. 791-798. ↑
- J189.** Broekaert J.A.C. Microstrip microwave induced plasma on a chip for atomic emission spectral analysis. / Broekaert J.A.C., Siemens V., Bings N.H. // IEEE Transactions on Plasma Science. - 2005. - Vol. 33, No. 2. - P. 560-561. ↑
- J190.** Kuo S.P. Characteristics of an arc-seeded microwave plasma torch. / Kuo S.P., Bivolaru D., Lai H., Lai W., Popovic S., Kessaratikoon P. // IEEE Transactions on Plasma Science. - 2004. - Vol. 32, No. 4. - P. 1734-1741. ↑
- J191.** Siegel P.H. Terahertz technology in biology and medicine. IEEE Transactions on Microwave Theory and Techniques. - 2004. - Vol. 52, No. 10. - P. 2438-2447. ↑
- J192.** Isernia T. New tools and series for forward and inverse scattering problems in lossy media. / Isernia T., Crocco L., D'Urso M. // IEEE Geoscience and Remote Sensing Letters. - 2004. - Vol. 1, No. 4. - P. 327-331. ↑
- J193.** Kikuchi M. Biomedical engineering's contribution to defending the homeland. / Kikuchi M., Ishihara M., Matsui T., Wakisaka H., Ashida H., Sato S., Ishizuka T. // IEEE Engineering in Medicine and Biology Magazine. - 2004. - Vol. 23, No. 1. - P. 175-186. ↑
- J194.** Radzievsky A. Millimeter-wave-induced hypoalgesia in mice: dependence on type of experimental pain. / Radzievsky A., Gordienko O., Cowan A., Alekseev S.I., Ziskin M.C. // IEEE Transactions on Plasma Science. - 2004. - Vol. 32, No. 4. - P. 1634-1643. ↑
- J195.** Nagayama Y. Electron Cyclotron emission diagnostics for helical plasma in the large helical device. / Nagayama Y., Kawahata K., Inagaki S., Morisaki T., Narihara K. // IEEE Transactions on Plasma Science. - 2004. - Vol. 32, No. 4. - P. 1716-1720. ↑
- J196.** Zhong Qing Zhang. Three-dimensional nonlinear image reconstruction for microwave biomedical imaging. / Zhong Qing Zhang, Qing Huo Liu. // IEEE Transactions on Biomedical Engineering. - 2004. - Vol. 51, No. 3. - P. 544-548. ↑
- J197.** Caorsi S. A reconstruction procedure for microwave nondestructive evaluation based on a numerically computed Green's function. / Caorsi S., Massa A., Pastorino M., Randazzo A., Rosani A. // IEEE Transactions on Instrumentation and Measurement. - 2004. - Vol. 53, No. 4. - P. 987-992. ↑
- J198.** Iza F. Rotational, vibrational, and excitation temperatures of a microwave-frequency microplasma. / Iza F., Hopwood J.A. // IEEE Transactions on Plasma Science. - 2004. - Vol. 32, No. 2. - P. 498-504. ↑
- J199.** Huo Y. Modeling of noninvasive microwave characterization of breast tumors. / Huo Y., Bansal R., Zhu Q. // IEEE Transactions on Biomedical Engineering. - 2004. - Vol. 51, No. 7. - P. 1089-1094. ↑

- J200.** Qianqian Fang. Microwave image reconstruction of tissue property dispersion characteristics utilizing multiple-frequency information. / Qianqian Fang, Meaney P.M., Paulsen K.D. // IEEE Transactions on Microwave Theory and Techniques. - 2004. - Vol. 52, No. 8. - P. 1866-1875. ↑
- J201.** Matsui T. A novel method to prevent secondary exposure of medical and rescue personnel to toxic materials under biochemical hazard conditions using microwave radar and infrared thermography. / Matsui T., Hagusawa K., Ishizuka T., Takase B., Ishihara M., Kikuchi M. // IEEE Transactions on Biomedical Engineering. - 2004. - Vol. 51, No. 12. - P. 2184-2188. ↑
- J202.** Shiffler D.A. Emission uniformity and shot-to-shot variation in cold field emission cathodes. / Shiffler D.A., Luginsland J., Ruebush M., LaCour M., Golby K., Cartwright K., Haworth M., Spencer T. // IEEE Transactions on Plasma Science. - 2004. - Vol. 32, No. 3. - P. 1262-1266. ↑
- J203.** Thelen D. Characterization of relaxation-oscillation noise in continuous-wave traveling wave tubes. / Thelen D., Reynolds R., Emerson R., Pearson M., Gilmour A.S. Jr., MacMullen A. // IEEE Transactions on Plasma Science. - 2004. - Vol. 32, No. 3. - P. 1057-1065. ↑
- J204.** Graca S. Upgrade to the control system of the reflectometry diagnostic of ASDEX upgrade. / Graca S., Santos J., Manso M. E., . // Review of Scientific Instruments. - 2004. - Vol. 75, No. 10. - P. 3852-3854. ↑
- J205.** Santos J. Frequency modulation continuous wave reflectometry measurements of plasma position in ASDEX Upgrade ELMy H-mode regimes. / Santos J., Hacquin S., Manso M. // Review of Scientific Instruments. - 2004. - Vol. 75, No. 10. - P. 3855-3858. ↑
- J206.** Cupido L. Frequency hopping millimeter wave reflectometer. / Cupido L., Sanchez J., Estrada T. // Review of Scientific Instruments. - 2004. - Vol. 75, No. 10. - P. 3865-3867. ↑
- J207.** Ignatenko M. Effects of asymmetry and target location on microwave imaging reflectometry. / Ignatenko M., Mase A., Bruskin L. G., Kogi Y., Hojo H. // Review of Scientific Instruments. - 2004. - Vol. 75, No. 10. - P. 3810-3812. ↑
- J208.** Smith D. R. Microwave scattering system design for rho e scale turbulence measurements on NSTX. / Smith D. R., Mazzucato E., Munsat T., Park H., Johnson D., Lin L., Domier C. W., Johnson M., Luhmann N. C. // Review of Scientific Instruments. - 2004. - Vol. 75, No. 10. - P. 3840-3842. ↑
- J209.** Hattori K. Evaluation of tapered slot antennas for use in multichannel reflectometers. / Hattori K., Tsugueda H., Takabatake O., Tobari H., Ando A., Inutake M. // Review of Scientific Instruments. - 2004. - Vol. 75, No. 10. - P. 3843-3845. ↑
- J210.** Hennequin P. Doppler backscattering system for measuring fluctuations and their perpendicular velocity on Tore Supra. / Hennequin P., Honore C., Truc A., Quemeneur A., Lemoine N., Chareau J.-M., Sabot R. // Review of Scientific Instruments. - 2004. - Vol. 75, No. 10. - P. 3881-3883. ↑
- J211.** Lauer J. L. Reduced adhesion of human blood platelets to polyethylene tubing by microplasma surface modification. / Lauer J. L., Shohet J. L., Albrecht R. M., Pratoomtong C., Murugesan R., Esnault S., Malter J. S., von Andrian U. H., Bathke R. D., Shohet S. B. // Journal of Applied Physics. - 2004. - Vol. 96, No. 8. - P. 4539-4546. ↑
- J212.** Leroy O. Determination of titanium temperature and density in a magnetron vapor sputtering device assisted by two microwave coaxial excitation systems. / Leroy O., de Poucques L., Boisse-Laporte C., Ganciu M., Teule-Gay L., Touzeau M. // and Films Journal of Vacuum Science & Technology A: Vacuum, Surfaces. - 2004. - Vol. 22, No. 1. - P. 192-200. ↑
- J213.** Joseph E. A. Investigation and modeling of plasma-wall interactions in inductively coupled fluorocarbon plasmas. / Joseph E. A., Zhou B., Sant S. P., Overzet L. J., Goeckner M. J. // and Films Journal of Vacuum Science & Technology A: Vacuum, Surfaces. - 2004. - Vol. 22, No. 3. - P. 689-697. ↑
- J214.** Kubota Y. Development of an integrated pellet diagnostic system for fueling pellets. / Kubota Y., Yoshikawa M., Nakashima Y., Yamada H., Sakamoto R. // Review of Scientific Instruments. - 2004. - Vol. 75, No. 10. - P. 4228-4230. ↑
- J215.** Jovicevic S. Excessive Balmer line broadening in microwave-induced discharges. / Jovicevic S., Ivkovic

- M., Konjevic N., Popovic S., Vuskovic L. // Journal of Applied Physics. - 2004. - Vol. 95, No. 1. - P. 24-29. ↑
- J216.** Lombardi G. Spectroscopic diagnostics and modeling of Ar /H 2 /C H 4 microwave discharges used for nanocrystalline diamond deposition. / Lombardi G., Hassouni K., Benedic F., Mohasseb F., Ropcke J., Gicquel A. // Journal of Applied Physics. - 2004. - Vol. 96, No. 11. - P. 6739-6751. ↑
- J217.** Tanaka M. Development of a high-current microwave ion source for proton linac application systems. / Tanaka M., Hara S., Hae T., Iga T., Saitou K., Amemiya K., Hiramoto K., Kakiuchi S. // Review of Scientific Instruments. - 2004. - Vol. 75, No. 5. - P. 1894-1896. ↑
- J218.** Ivanov A. A. H-ion production in electron cyclotron resonance driven multicusp volume source. / Ivanov A. A., Rouille C., Bacal M., Arnal Y., Bechu S., Pelletier J. // Review of Scientific Instruments. - 2004. - Vol. 75, No. 5. - P. 1750-1753. ↑
- J219.** Suzuki T. Diagnosis of plasmas in compact ECR ion source equipped with permanent magnet. / Suzuki T., Sawado Y., Iida T., Fujii Y. // Review of Scientific Instruments. - 2004. - Vol. 75, No. 5. - P. 1520-1522. ↑
- J220.** Kim Jung-Hyung. Wave cutoff method to measure absolute electron density in cold plasma. / Kim Jung-Hyung, Choi Sang-Chul, Shin Yong-Hyeon, Chung Kwang-Hwa. // Review of Scientific Instruments. - 2004. - Vol. 75, No. 8. - P. 2706-2710. ↑
- J221.** Sabot R. Single sideband modulator, a key component of Tore-Supra heterodyne reflectometers. / Sabot R., Bottereau C., Chateau J.-M., Claret F., Paume M. // Review of Scientific Instruments. - 2004. - Vol. 75, No. 8. - P. 2656-2659. ↑
- J222.** Yoshida Yoshikazu. Simple structure holey-plate ion source. / Yoshida Yoshikazu, Ogura Hiroshi. // Review of Scientific Instruments. - 2004. - Vol. 75, No. 5. - P. 1897-1899. ↑
- J223.** Biri S. Imaging of ECR plasmas with a pinhole x-ray camera. / Biri S., Valek A., Suta T., Takacs E., Szabo Cs., Hudson L. T., Radics B., Imrek J., Juhasz B., Palinkas J. // Review of Scientific Instruments. - 2004. - Vol. 75, No. 5. - P. 1420-1422. ↑
- J224.** Tarvainen O. A new plasma potential measurement instrument for plasma ion sources. / Tarvainen O., Suominen P., Koivisto H. // Review of Scientific Instruments. - 2004. - Vol. 75, No. 10. - P. 3138-3145. ↑
- J225.** Ruchko L. F. Application of microwave reflectometry to register Alfvén wave resonances in the TCABR tokamak. / Ruchko L. F., Valencia R., Galvao R. M. O., Lerche E. A., Elfimov A. G., Bellintani V., Elizondo J. I., Fagundes A. N., Fonseca A. M. M., Kuznetsov Yu. K., Nascimento I. C., de Sa W. P., Sanada E., da Silva R. P. // Review of Scientific Instruments. - 2004. - Vol. 75, No. 3. - P. 655-660. ↑
- J226.** Park H. Simultaneous microwave imaging system for density and temperature fluctuation measurements on TEXTOR (invited). / Park H., Mazzucato E., Munsat T., Domier C. W., Johnson M., Luhmann N. C., Wang J., Xia Z., Classen I. G. J., Donne A. J. H., van de Pol M. J. // Review of Scientific Instruments. - 2004. - Vol. 75, No. 10. - P. 3787-3792. ↑
- J227.** Ito H. Compact microwave imaging system to measure spatial distribution of plasma density. / Ito H., Oba R., Yugami N., Nishida Y. // Review of Scientific Instruments. - 2004. - Vol. 75, No. 10. - P. 3294-3297. ↑
- J228.** Dobson Chris C. Instrument reflections and scene amplitude modulation in a polychromatic microwave quadrature interferometer. / Dobson Chris C., Jones Jonathan E., Chavers D. Gregory. // Review of Scientific Instruments. - 2004. - Vol. 75, No. 3. - P. 674-683. ↑
- J229.** Wang Chuji. Diode laser microwave induced plasma cavity ringdown spectrometer: Performance and perspective. / Wang Chuji, Koirala Sudip P., Scherrer Susan T., Duan Yixiang, Winstead Christopher B. // Review of Scientific Instruments. - 2004. - Vol. 75, No. 5. - P. 1305-1313. ↑
- J230.** Kabouzi Y. Abatement of perfluorinated compounds using microwave plasmas at atmospheric pressure. / Kabouzi Y., Moisan M., Rostaing J. C., Trassy C., Guerin D., Keroack D., Zakrzewski Z. // Journal of Applied Physics. - 2003. - Vol. 93, No. 12. - P. 9483-9496. ↑
- J231.** Nordheden Karen J. Characterization of BCl 3 /N 2 plasmas. / Nordheden Karen J., Sia Joanne F. // Journal of Applied Physics. - 2003. - Vol. 94, No. 4. - P. 2199-2202. ↑

- J232.** Li Y. Two-dimensional self-consistent microwave argon plasma simulations with experimental verification. / Li Y., Gordon M. H., Roe L. A., Hassouni K., Grotjohn T. // Journal of Applied Physics. - 2003. - Vol. 94, No. 1. - P. 85-95. ↑
- J233.** Park H. Recent advancements in microwave imaging plasma diagnostics. / Park H., Chang C. C., Deng B. H., Domier C. W., Donne A. J. H., Kawahata K., Liang C., Liang X. P., Lu H. J., Luhmann N. C., Mase A., Matsuura H., Mazzucato E., Miura A., Mizuno K., Munsat T., Nagayama Y., van de Pol M. J., Wang J., Xia Z. G., Zhang W-K. // Review of Scientific Instruments. - 2003. - Vol. 74, No. 10. - P. 4239-4262. ↑
- J234.** Malyutenko V. K. High resolution infrared "vision" of dynamic electron processes in semiconductor devices (abstract). Review of Scientific Instruments. - 2003. - Vol. 74, No. 1. - P. 655. ↑
- J235.** Takayama Sadatsugu. Measurement of magnetic field pitch angle using motional Stark effect spectroscopy in the compact helical system. / Takayama Sadatsugu, Ida Katsumi, Okamura Shouichi, Kado Shinichiro. // Review of Scientific Instruments. - 2003. - Vol. 74, No. 1. - P. 73-79. ↑
- J236.** Kramer G. J. Correlation reflectometry for turbulence and magnetic field measurements in fusion plasmas (invited). / Kramer G. J., Nazikian R., Valeo E. // Review of Scientific Instruments. - 2003. - Vol. 74, No. 3. - P. 1421-1425. ↑
- J237.** Mase A. Electron cyclotron emission imaging on a large helical device. / Mase A., Kogi Y., Ohashi M., Ohsako S., Nagayama Y., Kawahata K., Aoi S., Sakata E. // Review of Scientific Instruments. - 2003. - Vol. 74, No. 3. - P. 1445-1448. ↑
- J238.** Baumel S. Two-dimensional correlation measurements of electron cyclotron emission fluctuations on the stellarator Wendelstein 7-AS. / Baumel S., Michel G., HartfuB H. J., Rodriguez-Girones Arbolí M., Hartnagel H. L. // Review of Scientific Instruments. - 2003. - Vol. 74, No. 3. - P. 1441-1444. ↑
- J239.** Munsat T. Microwave imaging reflectometer for TEXTOR (invited). / Munsat T., Mazzucato E., Park H., Deng B. H., Domier C. W., Luhmann N. C., Wang J., Xia Z. G., Donne A. J. H., van de Pol M. // Review of Scientific Instruments. - 2003. - Vol. 74, No. 3. - P. 1426-1432. ↑
- J240.** Tishchenko I.A. Early quasioptics of near-millimeter and submillimeter waves in IRE-Kharkov, Ukraine: from ideas to the microwave pioneer award. / Tishchenko I.A., Noisch A.I. // IEEE Microwave Magazine. - 2003. - Vol. 4, No. 4. - P. 32-44. ↑
- J241.** Kim Jung-Hyung. Plasma frequency measurements for absolute plasma density by means of wave cutoff method. / Kim Jung-Hyung, Seong Dae-Jin, Lim Jong-Yeon, Chung Kwang-Hwa. // Applied Physics Letters. - 2003. - Vol. 83, No. 23. - P. 4725-4727. ↑
- J242.** Mozetic Miran. Comparison of NO titration and fiber optics catalytic probes for determination of neutral oxygen atom concentration in plasmas and postglows. / Mozetic Miran, Ricard Andre, Babic Dusan, Poberaj Igor, Levaton Jacque, Monna Virginie, Cvelbar Uros. // and Films Journal of Vacuum Science & Technology A: Vacuum, Surfaces. - 2003. - Vol. 21, No. 2. - P. 369-374. ↑
- J243.** Huish D.W. Microwave and modulated optical reflectance studies of YBCO thin films. / Huish D.W., Velichko A.V., Lancaster M.J., Abell J.S., Xuming Xiong, Almond D.P., Hyland D., Perry A., Porch A. // IEEE Transactions on Applied Superconductivity. - 2003. - Vol. 13, No. 2. - P. 3638-3642. ↑
- J244.** Yoshida M. Sheet-shaped plasma production using microwave-plasma interaction with ECR region. / Yoshida M., Kajinishi K. // IEEE Transactions on Plasma Science. - 2003. - Vol. 31, No. 1. - P. 40-48. ↑
- J245.** Mills R.L. CW H I laser based on a stationary inverted Lyman population formed from incandescently heated hydrogen gas with certain Group I catalysts. / Mills R.L., Ray P.C., Mayo R.M. // IEEE Transactions on Plasma Science. - 2003. - Vol. 31, No. 2. - P. 236-247. ↑
- J246.** Mills R.L. Comparison of excessive Balmer α line broadening of inductively and capacitively coupled RF, microwave, and glow-discharge hydrogen plasmas with certain catalysts. / Mills R.L., Ray P.C., Nansteel M., Xuemin Chen, Mayo R.M., Jiliang He, Dhandapani B. // IEEE Transactions on Plasma Science. - 2003. - Vol. 31, No. 3. - P. 338-355. ↑
- J247.** Gilmore M. Progress toward a practical magnetic field diagnostic for low-field fusion plasmas based on

dual mode correlation reflectometry. / Gilmore M., Peebles W. A., Kubota S., Nguyen X. V., Ejiri A. // Review of Scientific Instruments. - 2003. - Vol. 74, No. 3. - P. 1469-1472. ↑

J248. Kubota S. Automatic profile reconstruction for millimeter-wave frequency-modulated continuous-wave reflectometry on NSTX. / Kubota S., Peebles W. A., Nguyen X. V., Roquemore A. L. // Review of Scientific Instruments. - 2003. - Vol. 74, No. 3. - P. 1477-1480. ↑

J249. Claret F. Advances of the density profile reflectometry on TORE SUPRA. / Claret F., Bottereau C., Chateau J. M., Sabot R. // Review of Scientific Instruments. - 2003. - Vol. 74, No. 3. - P. 1481-1484. ↑

J250. Santos J. Plasma position measurements from ordinary FM-CW reflectometry on ASDEX Upgrade. / Santos J., Manso M., Varela P., Neuhauser and the J. // Review of Scientific Instruments. - 2003. - Vol. 74, No. 3. - P. 1489-1492. ↑

J251. Shiraiwa S. Electron Bernstein wave emission diagnostic assisted by reflectometry on TST-2 spherical tokamak. / Shiraiwa S., Nagashima Y., Ushigome M., Yamada T., Taniguchi T., Ohara S., Yamagishi K., Kasahara H., Iijima D., Kobori Y., Nishi T., Aramasu M., Ejiri A., Takase Y. // Review of Scientific Instruments. - 2003. - Vol. 74, No. 3. - P. 1453-1456. ↑

J252. Petrov A. A. Time-of-flight refractometry for robust line integral electron density measurements and control in ITER. / Petrov A. A., Petrov V. G. // Review of Scientific Instruments. - 2003. - Vol. 74, No. 3. - P. 1465-1468. ↑

J253. Tokuzawa T. X-mode pulsed radar reflectometer for density fluctuation measurements on LHD. / Tokuzawa T., Kawahata K., Tanaka K., Nagayama Y., Kaneba T., Ejiri A. // Review of Scientific Instruments. - 2003. - Vol. 74, No. 3. - P. 1506-1509. ↑

J254. Wang G. Improved reflectometer electron density profile measurements on DIII-D. / Wang G., Zeng L., Doyle E. J., Rhodes T. L., Peebles W. A. // Review of Scientific Instruments. - 2003. - Vol. 74, No. 3. - P. 1525-1529. ↑

J255. Zeng L. Application of fast reflectometer density profile measurements to investigate plasma instabilities in DIII-D. / Zeng L., Doyle E. J., Rhodes T. L., Wang G., Peebles W. A., Burrell K. H. // Review of Scientific Instruments. - 2003. - Vol. 74, No. 3. - P. 1530-1533. ↑

J256. Nam Y. U. Design of a single-channel millimeter-wave interferometer system for Korea Superconducting Tokamak Advanced Research. / Nam Y. U., Cheon M. S., Kwon M., Hwang Y. S. // Review of Scientific Instruments. - 2003. - Vol. 74, No. 3. - P. 1613-1616. ↑

J257. Kogi Y. Ultrashort-pulse reflectometry for steady-state plasmas. / Kogi Y., Mase A., Ohsako S., Yamamoto A., Yasuda T., Bruskin L. G., Hojo H. // Review of Scientific Instruments. - 2003. - Vol. 74, No. 3. - P. 1510-1513. ↑

J258. Roh Y. Ultrashort pulse reflectometry for density profile and fluctuation measurements on SSPX. / Roh Y., Domier C. W., Luhmann N. C. // Review of Scientific Instruments. - 2003. - Vol. 74, No. 3. - P. 1518-1521. ↑

J259. Zhang S. Y. Design of an X-mode fast-scanning reflectometry for edge density profile measurement on HT-7 tokamak. / Zhang S. Y., Qin G. B., Zhuravlev V., Poznyak V., Ploskirev E. // Review of Scientific Instruments. - 2003. - Vol. 74, No. 3. - P. 1522-1524. ↑

J260. Makasheva K. Plasma parameters of diffusion-controlled microwave discharges in surface-wave fields. / Makasheva K., Shivarova A. // IEEE Transactions on Plasma Science. - 2002. - Vol. 30, No. 1. - P. 384-390. ↑

J261. Miyakawa M. Experimental validation of a linear model for data reduction in chirp-pulse microwave CT. / Miyakawa M., Orikasa K., Bertero M., Boccacci P., Conte F., Piana M. // IEEE Transactions on Medical Imaging. - 2002. - Vol. 21, No. 4. - P. 385-395. ↑

J262. Kos Anthony B. Pulsed inductive microwave magnetometer. / Kos Anthony B., Silva Thomas J., Kabos Pavel. // Review of Scientific Instruments. - 2002. - Vol. 73, No. 10. - P. 3563-3569. ↑

J263. Boric-Lubeke O. Wireless house calls: using communications technology for health care and monitoring. / Boric-Lubeke O., Lubecke V.M. // IEEE Microwave Magazine. - 2002. - Vol. 3, No. 3. - P. 43-48. ↑

- J264.** Anderson S.A. Two-dimensional optical emission imaging of a XeCl discharge in a microwave resonant cavity. / Anderson S.A., Guibord N., Delaney M., Brake M.L. // IEEE Transactions on Plasma Science. - 2002. - Vol. 30, No. 1. - P. 196-197. ↑
- J265.** Murphy D.P. Microwave emission from plasmas produced by magnetically confined-electron beams. / Murphy D.P., Fernsler R.F., Pechacek R.E., Meger R.A. // IEEE Transactions on Plasma Science. - 2002. - Vol. 30, No. 1. - P. 436-441. ↑
- J266.** Thumm M.K. Passive high-power microwave components. / Thumm M.K., Kasperek W. // IEEE Transactions on Plasma Science. - 2002. - Vol. 30, No. 3. - P. 755-786. ↑
- J267.** Hahn K. Initial studies of a long-pulse relativistic backward-wave oscillator utilizing a disk cathode. / Hahn K., Fuks M.I., Schamiloglu E. // IEEE Transactions on Plasma Science. - 2002. - Vol. 30, No. 3. - P. 1112-1119. ↑
- J268.** Destefani C.A. Enthalpy-probe diagnostics of an atmospheric-pressure unleaded petrol exhaust-gas microwave-induced plasma. / Destefani C.A., Murphy A.B., Siores E. // IEEE Transactions on Plasma Science. - 2002. - Vol. 30, No. 4. - P. 1587-1591. ↑
- J269.** Sheppard L.M. Not your mother's mammography [breast cancer detection]. IEEE Spectrum. - 2002. - Vol. 39, No. 10. - P. 56-57. ↑
- J270.** Minghua Xu. Time-domain reconstruction for thermoacoustic tomography in a spherical geometry. / Minghua Xu, Wang L.V. // IEEE Transactions on Medical Imaging. - 2002. - Vol. 21, No. 7. - P. 814-822. ↑
- J271.** Yuan Xu. Exact frequency-domain reconstruction for thermoacoustic tomography. I. Planar geometry. / Yuan Xu, Dazi Feng, Wang L.V. // IEEE Transactions on Medical Imaging. - 2002. - Vol. 21, No. 7. - P. 823-828. ↑
- J272.** Yuan Xu. Exact frequency-domain reconstruction for thermoacoustic tomography. II. Cylindrical geometry. / Yuan Xu, Minghua Xu, Wang L.V. // IEEE Transactions on Medical Imaging. - 2002. - Vol. 21, No. 7. - P. 829-833. ↑
- J273.** Heintze M. Mechanism of C₂ hydrocarbon formation from methane in a pulsed microwave plasma. / Heintze M., Magureanu M., Kettlitz M. // Journal of Applied Physics. - 2002. - Vol. 92, No. 12. - P. 7022-7031. ↑
- J274.** Rauf Shahid. Charged species dynamics in an inductively coupled Ar/SF₆ plasma discharge. / Rauf Shahid, Ventzek Peter L. G., Abraham Ion C., Hebner Gregory A., Woodworth Joseph R. // Journal of Applied Physics. - 2002. - Vol. 92, No. 12. - P. 6998-7007. ↑
- J275.** Rousseau A. Langmuir probe diagnostic studies of pulsed hydrogen plasmas in planar microwave reactors. / Rousseau A., Teboul E., Lang N., Hannemann M., Ropcke J. // Journal of Applied Physics. - 2002. - Vol. 92, No. 7. - P. 3463-3471. ↑
- J276.** Yusoff A. N. Electromagnetic and absorption properties of some microwave absorbers. / Yusoff A. N., Abdullah M. H., Ahmad S. H., Jusoh S. F., Mansor A. A., Hamid S. A. A. // Journal of Applied Physics. - 2002. - Vol. 92, No. 2. - P. 876-882. ↑
- J277.** Carl Leader J. Solid-state laser induced microwave effects. / Carl Leader J., Larson C. E., Treis P. A. // Journal of Applied Physics. - 2002. - Vol. 92, No. 11. - P. 6505-6524. ↑
- J278.** Rosen A. Applications of RF/microwaves in medicine. / Rosen A., Stuchly M.A., Vander Vorst A. // IEEE Transactions on Microwave Theory and Techniques. - 2002. - Vol. 50, No. 3. - P. 963-974. ↑
- J279.** Schepps J. Microwave industry outlook-wireless communications in healthcare. / Schepps J., Rosen A. // IEEE Transactions on Microwave Theory and Techniques. - 2002. - Vol. 50, No. 3. - P. 1044-1045. ↑
- J280.** Shiffler D. Cathode and anode plasmas in short-pulse explosive field emission cathodes. / Shiffler D., Ruebush M., Zagar D., LaCour M., Sena M., Golby K., Haworth M., Umstadtd R. // Journal of Applied Physics. - 2002. - Vol. 91, No. 9. - P. 5599-5603. ↑
- J281.** Kabouzi Y. Radial contraction of microwave-sustained plasma columns at atmospheric pressure. /

Kabouzi Y., Calzada M. D., Moisan M., Tran K. C., Trassy C. // Journal of Applied Physics. - 2002. - Vol. 91, No. 3. - P. 1008-1019. ↑

J282. Figueiredo Antonio C. A. On a variational approach to the extraction of quadratures from broadband reflectometry signals. / Figueiredo Antonio C. A., Bizarro Joao P. S. // Review of Scientific Instruments. - 2002. - Vol. 73, No. 2. - P. 289-297. ↑

J283. Gotoh Y. Energy distribution of the compact microwave ion source for extremely low voltage ion extraction. / Gotoh Y., Nakajima K., Hagiwara T., Tsuji H., Ishikawa J. // Review of Scientific Instruments. - 2002. - Vol. 73, No. 2. - P. 758-760. ↑

J284. Ishii K. A gold film detector for radial profile measurement of plasma density by using a gold neutral beam probe. / Ishii K., Takemura Y., Fueki A., Hagiwara K., Kojima A., Itakura A., Yoshikawa M., Katanuma I., Yatsu K. // Review of Scientific Instruments. - 2002. - Vol. 73, No. 11. - P. 3806-3812. ↑

J285. Ito H. Imaging system for low-density plasma by heterodyne interferometer with fan beam microwave. / Ito H., Yugami N., Nishida Y., Sakai W. // Review of Scientific Instruments. - 2002. - Vol. 73, No. 12. - P. 4229-4231. ↑

J286. Sterzer F. Microwave medical devices. IEEE Microwave Magazine. - 2002. - Vol. 3, No. 1. - P. 65-70. ↑

J287. Cho Byeong-Ok. Metalorganic precursor decomposition and oxidation mechanisms in plasma-enhanced ZrO₂ deposition. / Cho Byeong-Ok, Wang Jianjun, Chang Jane P. // Journal of Applied Physics. - 2002. - Vol. 92, No. 8. - P. 4238-4244. ↑

J288. Hebner G. A. Surface dependent electron and negative ion density in SF₆/argon gas mixtures. / Hebner G. A., Abraham I. C. // Journal of Applied Physics. - 2002. - Vol. 91, No. 12. - P. 9539-9546. ↑

J289. Talukder M. R. Probe diagnostics of high pressure microwave discharge in helium. / Talukder M. R., Korzec D., Kando M. // Journal of Applied Physics. - 2002. - Vol. 91, No. 12. - P. 9529-9538. ↑

J290. Leonhardt D. Plasma diagnostics in large area plasma processing system. / Leonhardt D., Walton S. G., Blackwell D. D., Amatucci W. E., Murphy D. P., Fernsler R. F., Meger R. A. // and Films Journal of Vacuum Science & Technology A: Vacuum, Surfaces. - 2001. - Vol. 19, No. 4. - P. 1367-1373. ↑

J291. Wu Cong-Feng. Influence of the different operations of gas in the large microwave plasmas. / Wu Cong-Feng, Huang Wei-Dong, Zhan Ru-Juan. // and Films Journal of Vacuum Science & Technology A: Vacuum, Surfaces. - 2001. - Vol. 19, No. 2. - P. 503-506. ↑

J292. Lee K. P. Process development for small-area GaN/AlGaIn heterojunction bipolar transistors. / Lee K. P., Zhang A. P., Dang G., Ren F., Han J., Hobson W. S., Lopata J., Abenathy C. R., Pearton S. J., Lee J. W. // and Films Journal of Vacuum Science & Technology A: Vacuum, Surfaces. - 2001. - Vol. 19, No. 4. - P. 1846-1849. ↑

J293. Arnold Th. Ultrahigh-rate plasma jet chemical etching of silicon. / Arnold Th., Boehm G., Schindler A. // and Films Journal of Vacuum Science & Technology A: Vacuum, Surfaces. - 2001. - Vol. 19, No. 5. - P. 2586-2589. ↑

J294. Nakamura Masayuki. Spatial distributions of the absolute CF and CF₂ radical densities in high-density plasma employing low global warming potential fluorocarbon gases and precursors for film formation. / Nakamura Masayuki, Hori Masaru, Goto Toshio, Ito Masafumi, Ishii Nobuo. // and Films Journal of Vacuum Science & Technology A: Vacuum, Surfaces. - 2001. - Vol. 19, No. 5. - P. 2134-2141. ↑

J295. Bulyshev A.E. Computational modeling of three-dimensional microwave tomography of breast cancer. / Bulyshev A.E., Semenov S.Y., Souvorov A.E., Svenson R.H., Nazarov A.G., Sizov Y.E., Tatsis G.P. // IEEE Transactions on Biomedical Engineering. - 2001. - Vol. 48, No. 9. - P. 1053-1056. ↑

J296. {no data available}. 2000 Medical Imaging Conference (MIC). IEEE Transactions on Nuclear Science. - 2001. - Vol. 48, No. 3. - {no data available}. ↑

J297. Yang K. Active-amplifier-array diagnostics using high-resolution electrooptic field mapping. / Yang K., Marshall T., Forman M., Hubert J., Mirth L., Popovic Z., Katehi L.P.B., Whitaker J.F. // IEEE Transactions on Microwave Theory and Techniques. - 2001. - Vol. 49, No. 5. - P. 849-857. ↑

- J298.** Srivastava A. K. Quartz-crystal microbalance study for characterizing atomic oxygen in plasma ash tools. / Srivastava A. K., Sakthivel P. // and Films Journal of Vacuum Science & Technology A: Vacuum, Surfaces. - 2001. - Vol. 19, No. 1. - P. 97-100. ↑
- J299.** Koga Mayuko. Measurement of ion temperatures in a large-diameter electron cyclotron resonance plasma. / Koga Mayuko, Yoshizawa Takenori, Ueda Yoko, Kawai Yoshinobu, Yonesu Akira. // Applied Physics Letters. - 2001. - Vol. 79, No. 19. - P. 3041-3043. ↑
- J300.** Meaney P.M. Microwave image reconstruction utilizing log-magnitude and unwrapped phase to improve high-contrast object recovery. / Meaney P.M., Paulsen K.D., Pogue B.W., Miga M.I. // IEEE Transactions on Medical Imaging. - 2001. - Vol. 20, No. 2. - P. 104-116. ↑
- J301.** Cotrino J. Electron temperature measurement in a slot antenna 2.45 GHz microwave plasma source. / Cotrino J., Palmero A., Rico V., Barranco A., Espinos J. P., Gonzalez-Elise A. R. // Journal of Vacuum Science & Technology B: Microelectronics and Nanometer Structures. - 2001. - Vol. 19, No. 2. - P. 410-414. ↑
- J302.** Bruskin L. G. Analytical simulation of microwave reflectometry of a plasma cylinder. / Bruskin L. G., Mase A. // Review of Scientific Instruments. - 2001. - Vol. 72, No. 11. - P. 4139-4144. ↑
- J303.** Donne A. J. H. New diagnostics for physics studies on TEXTOR-94 (invited). / Donne A. J. H., Jaspers R., Barth C. J., Bindslev H., Elzendoorn B. S. Q., van Gorkom J. C., van der Meiden H. J., Oyevaar T., van de Pol M. J., Udintsev V. S., Widdershoven H. L. M., Biel W., Finken K. H., Kramer-Flecken A., Kreter A., Oosterbeek H., Schweer B., Unterberg B., Deng B. H., Domier C. W., Luhmann N. C., Mazzucato E., Munsat T., Park H., Porte L., Woskov P., Shmaenok L. // Review of Scientific Instruments. - 2001. - Vol. 72, No. 1. - P. 1046-1053. ↑
- J304.** Scime Earl E. Microwave interferometer for steady-state plasmas. / Scime Earl E., Boivin Robert F., Kline John L., Balkey Matthew M. // Review of Scientific Instruments. - 2001. - Vol. 72, No. 3. - P. 1672-1676. ↑
- J305.** Ribeiro T. T. Microwave reflectometry for turbulence studies on ASDEX Upgrade. / Ribeiro T. T., Serra F., Conway G. D., Manso M. E., Ryter F., Cupido L., Kurzan B., Silva A., Suttrop W., Vergamota S. // Review of Scientific Instruments. - 2001. - Vol. 72, No. 2. - P. 1366-1371. ↑
- J306.** Fuchs Ch. Extreme broadband multichannel ECE radiometer with "zoom" device. / Fuchs Ch., Hartfuss H. J. // Review of Scientific Instruments. - 2001. - Vol. 72, No. 1. - P. 383-386. ↑
- J307.** Mase A. Application of millimeter-wave imaging system to LHD. / Mase A., Ohashi M., Yamamoto A., Negishi H., Oyama N., Nagayama Y., Kawahata K., Watabe K., Mizuno K., Matsuura H., Uchida K., Miura A. // Review of Scientific Instruments. - 2001. - Vol. 72, No. 1. - P. 375-378. ↑
- J308.** McLean H. S. Plasma diagnostics for the sustained spheromak physics experiment. / McLean H. S., Ahmed A., Buchenauer D., Den Hartog D., Domier C. W., Hill D. N., Holcomb C., Hooper E. B., Morse E. C., Nagata M., Roh Y., Stallard B., Wood R. D., Woodruff S., Wurden G., Wang Z. // Review of Scientific Instruments. - 2001. - Vol. 72, No. 1. - P. 556-561. ↑
- J309.** Malyshev M. V. Diagnostics of inductively coupled chlorine plasmas: Measurement of electron and total positive ion densities. / Malyshev M. V., Donnelly V. M. // Journal of Applied Physics. - 2001. - Vol. 90, No. 3. - P. 1130-1137. ↑
- J310.** Gordon M. H. Energy coupling efficiency of a hydrogen microwave plasma reactor. / Gordon M. H., Duten X., Hassouni K., Gicquel A. // Journal of Applied Physics. - 2001. - Vol. 89, No. 3. - P. 1544-1549. ↑
- J311.** Rousseau A. Surface recombination of hydrogen atoms studied by a pulsed plasma excitation technique. / Rousseau A., Cartry G., Duten X. // Journal of Applied Physics. - 2001. - Vol. 89, No. 4. - P. 2074-2078. ↑
- J312.** Palm Peter. Electron density and recombination rate measurements in CO-seeded optically pumped plasmas. / Palm Peter, Plonjes Elke, Buoni Matt, Subramaniam Vish V., Adamovich Igor V. // Journal of Applied Physics. - 2001. - Vol. 89, No. 11. - P. 5903-5910. ↑
- J313.** Petherbridge James R. Low temperature diamond growth using CO₂/CH₄ plasmas: Molecular beam mass spectrometry and computer simulation investigations. / Petherbridge James R., May Paul W., Pearce Sean

R. J., Rosser Keith N., Ashfold Michael N. R. // Journal of Applied Physics. - 2001. - Vol. 89, No. 2. - P. 1484-1492. ↑

J314. Hirata Hiroshi. Characteristics of an electronically tunable surface-coil-type resonator for L-band electron paramagnetic resonance spectroscopy. / Hirata Hiroshi, Walczak Tadeusz, Swartz Harold M. // Review of Scientific Instruments. - 2001. - Vol. 72, No. 6. - P. 2839-2841. ↑

J315. Mironov V. Plasma diagnostics at electron cyclotron resonance ion sources by injection of laser ablated fluxes of metal atoms. / Mironov V., Runkel S., Stiebing K. E., Hohn O., Shirkov G., Schmidt-Bocking H., Schempp A. // Review of Scientific Instruments. - 2001. - Vol. 72, No. 5. - P. 2271-2278. ↑

J316. Fujii Toshihiro. Mass spectrometric studies of a CH₄/H₂ microwave plasma under diamond deposition conditions. / Fujii Toshihiro, Kareev Michael. // Journal of Applied Physics. - 2001. - Vol. 89, No. 5. - P. 2543-2546. ↑

J317. Hebner G. A. Characterization of electron and negative ion densities in fluorocarbon containing inductively driven plasmas. / Hebner G. A., Abraham I. C. // Journal of Applied Physics. - 2001. - Vol. 90, No. 10. - P. 4929-4937. ↑

J318. Rosenau S. A. Advances in quasioptical grid array technology for millimeter-wave plasma imaging diagnostics. / Rosenau S. A., Liang C., Chang C.-C., Hsu P. L., Luhmann N. C., Zhang W.-K., Li W.-Y., Domier C. W., Hsia R. P. // Review of Scientific Instruments. - 2001. - Vol. 72, No. 1. - P. 371-374. ↑

J319. Zeng L. Implementation of reflectometry as a standard density profile diagnostic on DIII-D. / Zeng L., Doyle E. J., Luce T. C., Peebles W. A. // Review of Scientific Instruments. - 2001. - Vol. 72, No. 1. - P. 320-323. ↑

J320. Ribeiro T. T. Microwave reflectometry for turbulence studies on ASDEX upgrade (abstract). / Ribeiro T. T., Serra F., Manso M. E., Vergamota S., Cupido L., Silva A., Conway G. D., Ryter F., Suttrop and the W. // Review of Scientific Instruments. - 2001. - Vol. 72, No. 1. - P. 319. ↑

J321. Tokuzawa T. Pulsed radar reflectometry on the LHD. / Tokuzawa T., Kawahata K., Pavlichenko R. O., Tanaka K., Ejiri A. // Review of Scientific Instruments. - 2001. - Vol. 72, No. 1. - P. 328-331. ↑

J322. Hirsch M. Doppler reflectometry for the investigation of propagating density perturbations. / Hirsch M., Holzhauer E., Baldzuhn J., Kurzan B. // Review of Scientific Instruments. - 2001. - Vol. 72, No. 1. - P. 324-327. ↑

J323. Silva A. Performance of the microwave reflectometry diagnostic for density profile measurements on ASDEX Upgrade. / Silva A., Manso M., Vergamota S., Cupido L., Meneses L., Nunes I. // Review of Scientific Instruments. - 2001. - Vol. 72, No. 1. - P. 307-310. ↑

J324. Gilmore M. Dual mode (ordinary-extraordinary) correlation reflectometry for magnetic field and turbulence measurements (invited). / Gilmore M., Peebles W. A., Nguyen X. V. // Review of Scientific Instruments. - 2001. - Vol. 72, No. 1. - P. 293-300. ↑






J325. Varela P. Assessment of density profile automatic evaluation from broadband reflectometry data. / Varela P., Manso M., Vergamota S., Grossmann V., Santos J. // Review of Scientific Instruments. - 2001. - Vol. 72, No. 1. - P. 315-318. ↑

J326. da Silva F. Simulation of reflectometry density changes using a 2D full-wave code. / da Silva F., Manso M., Silva A., . // Review of Scientific Instruments. - 2001. - Vol. 72, No. 1. - P. 311-314. ↑

J327. Kogi Y. Measurement of cross-polarization scattering using ultrashort pulse microwaves. / Kogi Y., Mase A., Hojo H., Itakura A., Ichimura M., Tamano T. // Review of Scientific Instruments. - 2001. - Vol. 72, No. 1. - P. 355-358. ↑

J328. Solomon W. M. Collective microwave scattering diagnostic on the H-1 heliac. / Solomon W. M., Shats M. G., Korneev D., Nagasaki K. // Review of Scientific Instruments. - 2001. - Vol. 72, No. 1. - P. 352-354. ↑

J329. Hsu P. L. Millimeter-wave imaging array development for microwave reflectometry and ECE imaging. / Hsu P. L., Deng B. H., Wang J., Domier C. W., Luhmann N. C. // Review of Scientific Instruments. - 2001. - Vol. 72, No. 1. - P. 364-367. ↑

- J330.** Domier C. W. Three-dimensional fluctuation imaging diagnostic for TEXTOR (abstract). / Domier C. W., Deng B. H., Donn A. J. H., Hsu P. L., Luhmann N. C., Mazzucato E., Park H. K., van de Pol M. J., Wang J. // Review of Scientific Instruments. - 2001. - Vol. 72, No. 1. - P. 363. 
- J331.** van Gorkom J. C. The ten-channel pulsed radar reflectometer at the TEXTOR-94 tokamak. / van Gorkom J. C., van de Pol M. J., Donne A. J. H. // Review of Scientific Instruments. - 2001. - Vol. 72, No. 1. - P. 336-339. 
- J332.** Roh Y. Ultrashort pulse reflectometry for electron density profile measurements on SSPX. / Roh Y., Domier C. W., Luhmann N. C. // Review of Scientific Instruments. - 2001. - Vol. 72, No. 1. - P. 332-335. 
- J333.** Kubota S. Millimeter-wave reflectometry for electron density profile and fluctuation measurements on NSTX. / Kubota S., Nguyen X. V., Peebles W. A., Zeng L., Doyle E. J., Roquemore A. L. // Review of Scientific Instruments. - 2001. - Vol. 72, No. 1. - P. 348-351. 
- J334.** Lin Y. Two-dimensional full-wave simulation of microwave reflectometry on Alcator C-Mod. / Lin Y., Irby J. H., Nazikian R., Marmor E. S., Mazurenko A. // Review of Scientific Instruments. - 2001. - Vol. 72, No. 1. - P. 344-347. 
-

© В.И. Карнышев, 2011

Тематический реферативный сборник сгенерирован в автоматическом режиме
с использованием специализированного программного модуля (ПАО ТУСУР)